MS-1

GPO PRICE $ _____

OTS PRICE(S) $ _____

Hard copy (HC) 4.00

Microfiche (MF) .75

NORTH AMERICAN AVIATION, INC.
SPACE and INFORMATION SYSTEMS DIVISION

Accession No. 04956-65

Contract No. NAS8-11690 SID 65-649

PRE-STRAIN WELD DEVELOPMENT PROGRAM

Final Report

23 April 1965

Prepared by

Saturn S-II Manufacturing

Approved by

A.C. Van Leuven
Director, Saturn S-II Manufacturing

NORTH AMERICAN AVIATION, INC.
SPACE and INFORMATION SYSTEMS DIVISION

FOREWORD

This document is the final report of the Pre-Strain Weld Development Program, performed by the Space and Information Systems Division of North American Aviation, Inc., Downey, California, under Contract NAS8-11690 (dated 30 June 1964), issued by the National Aeronautics and Space Administration, George C. Marshall Space Flight Center, Huntsville, Alabama.

CONTENTS

ILLUSTRATIONS

TABLES

SUMMARY

25245

This report covers a feasibility study performed under Contract NAS8-11690 to improve the quality of 2014-T6 aluminum alloy weldments by application of mechanically or thermally induced pre-loads. Data were obtained on thermal flow patterns as functions of weld head location, reduction of residual stresses as functions of applied pre-load levels and location, and effects of pre-load application on part distortions caused by welding.

In mechanically applied pre-load weld experiments on flat panels, significant reductions were achieved in residual stresses (approximately thirty percent), even at nonoptimized pre-load levels. Substantial reductions in distortions also were achieved. Similar reductions of residual stresses and distortions were observed in weldments performed with applied thermal (shrink-fit) pre-loads.

A mechanics analysis, utilizing a unit cube/parallel strip model, was developed. The analysis shows good agreement between analytically predicted and experimentally observed residual stresses and has promise of becoming a useful tool in predicting pre-load magnitudes and patterns that might be applied in future production of actual parts.

Author

INTRODUCTION

Welding processes as employed in the fabrication of Saturn S-II structures are accompanied with distortions and residual stresses. These distortions are caused primarily by metal shrinkage due to heat applied during the welding cycles. It can be surmised readily that application of pre-loads or pre-strains in a direction opposite to the weld-induced stresses should reduce the magnitude of distortions and residual stresses considerably. The study program reported herein concerns establishment of the feasibility of this practice, bracketing of the parameters involved, development of an applicable mechanics analysis, and conceptual translation of the idea — if shown to be feasible — to Saturn S-II hardware.

In investigations (Reference 1) preceding this program, an empirical approach toward welding under thermally induced shrink-fit pre-load conditions has been explored and found to be effective. A circular disk to be welded into a panel by this technique is made oversize in diameter; then, by chilling in liquid nitrogen at approximately -320 F, it is shrunken to a size that will drop into an opening of nominal diameter in the prepared panel. Expansion occurs as the chilled part returns to room temperature, and the predetermined pre-strain develops between the disk and the panel.

The method was tried with disks and panels of various sizes until the amount of interference between the two parts causing the least distortion after welding was determined. When a sufficient quantity of test parts had been welded to assure repeatability, production-sized prototypes and, eventually, production parts were welded by this technique.

In the investigation conducted during the study program, the method of applying pre-load was extended from shrink-fitting, which is feasible only for configurations in which one detail is surrounded by others, to the use of mechanical means on linear panel weldments. Quantitative measurements of distortion and residual strains were taken on these weldments, as well as on circular, thermally pre-loaded ones. The data, after reduction and analysis, are the basis of valid criteria for evaluation of the potential benefits of pre-load application in welding, and permit estimation of the expected optimum range of pre-load. Evaluation of

experimental results discloses that this optimum range is in the neighborhood of applied pre-loads corresponding to 35 to 40 percent of nominal room temperature yield strength of the parent 2014-T651 aluminum alloy. In this range, pre-load application may easily reduce weld-induced residual stresses by a factor of one-half—30 percent being attainable even at pre-load parameters far from optimum. Pre-load application also affords substantial reduction of warpage.

Despite the promising end results, the experimental program experienced certain difficulties. In particular, delays were encountered because of the following reasons:

An original set of linear panel specimens warped to an undue degree and in a random manner when machined to weld-landed configuration. It was found that the raw material used had an uncertain history; the set had to be rejected and new panels from virgin material prepared.

The main structure of the welding machine destined for the program was found to be inadequate to sustain the anticipated loads with a sufficient safety margin. Several weeks were lost in securing an available tool of adequate capacity; additional time was required in equipping it with the pulling devices to be used in the mechanical pre-strain portion of the program.

Excellent agreement was obtained between experimental results and those predicted by a mechanics analysis employing a unit cube/parallel strip model, thus establishing confidence in analytical predictions based on this model.

Recommended future work includes the following:

1. Refinement of the analytical method by taking into account effects of temperature gradients through the weldment thickness and use of more accurate values for elastic modulus reflecting dependence on stress and strain levels as well as temperature.

2. Rephrasing of mathematical expressions to adapt them to computer programming.

3. Performance of additional weld experiments on mechanically pre-loaded linear panels under conditions permitting application of higher pre-load levels in the relatively uniformly pre-loaded central portion of the specimen, thus isolating pre-load level from possible geometry effects and permitting more definitive conclusions as to optimum pre-load conditions.

4. Verification of mechanics analysis by comparison of analytical predictions with experimental results on additional mechanically pre-loaded linear weldments of different gages.

5. Inclusion of an investigation of angular pre-positioning of weldment details in future weld experiments.

The study was conducted under the direction of N. S. Wilson, Program Manager. Key participating personnel were J. E. Adams, Project Engineer; M. A. Nadler and E. Margitan, experimental investigation; and D. A. Reed, Jr., and Dr. R. Verette, data reduction and mechanics analysis.

PROGRAM PLAN

The basic program plan involved development of the following information.

MATERIAL PROPERTIES

Salient mechanical and thermal properties of Al 2014-T651 aluminum alloy and 2319 aluminum alloy weld filler material were to be established as functions of temperature up to melt. Reasonable information on these properties in the elevated temperature range is not readily available and was considered a necessity for quantitative mechanics analysis.

DETERMINATION OF HEAT FLOW PATTERNS CREATED BY WELDING

Knowledge of the thermal field around the weld head is required for assessment of the elastic and nonelastic deformations that lead to weld shrinkage and distortion. In addition to establishing the thermal distribution pattern for the basic experimental panel weldment configuration (0.250-inch-thick weld land, 0.125-inch-thick web), measurements were made on a thinner weldment (0.160-inch weld land, 0.080-inch web) in order to accumulate background data for general extrapolation purposes.

DETERMINATION OF POSSIBLE BENEFITS OF MECHANICAL PRE-STRAINING OF WELDMENTS

Primary criteria for this purpose were to be relative residual stress levels and distortions compared to zero pre-strain control panels. The original plan called for pre-straining of several panels of two different thicknesses at several pre-load levels in an iteration plan designed to establish the optimum pre-load range level, and to conduct confirmatory repeatability experiments at or near this level. This plan had to be changed, however, for the following reasons:

1. Program funding limitations did not allow the planned number of experiments to be carried out.

2. Load-carrying capability of basic equipment and desired simplicity of attach features (in order to simulate possible simple tooling modifications) did not permit safe straining of the weld

panels in their center third section, where stress is relatively uniform, past 20 percent of nominal yield strength, without danger of equipment failure or tear-out of the panels at the attach point.

A plan which combined information on effects of panel thickness on residual stress, pre-load level versus beneficial effects, and reproducibility was devised in the following manner:

Non-pre-strained Weldments 4 and 5, of different thicknesses, served as controls and permitted assessment of residual stress as function of panel thickness.

Weldments 7, 8, and 9 were pre-strained and welded identically. Pre-strain levels were fairly uniform over the center third of the weldments (approximately 17 percent of nominal yield strength) and rose to approximately 30 percent at 12 inches from the ends of the 72-inch-long panels. This permitted comparison of data from pre-strained weldments with the non-pre-strained controls and enabled conclusions to be drawn on the reproducibility of pre-strain effects and on the effect of pre-strain intensity on residual stress and distortion tendencies. Data from the weldment end section where intensity varies rapidly as a function of distance had to be considered in evaluating the latter.

Evaluation criteria used were comparative deformations and residual stresses and moments derived from strain measurements of back-to-back biaxial strain gages. The location matrix was designed so that strain gages were placed at approximately the centers and edges of weld nuggets and heat-affected zones. This arrangement gave maximum information at reasonable cost and provided checks on actual symmetry and similarity of response between symmetrical or similar points of individual specimens, and with it, the ability to lump data from different speciments upon establishment of such similarity.

In order to assure that weld quality was not adversely affected by pre-straining, X-ray examination of all weldments was to be conducted, and determination of mechanical properties and metallurgical structures to be made.

BENEFICIAL EFFECT OF THERMAL PRE-STRAINING OF WELDMENTS

Weldments of suitable (closed circular) configuration were to be thermally (shrink-fit) pre-strained at three different levels and evaluated with respect to comparative warpage and residual stress.

MECHANICS ANALYSIS

A mechanics analysis based on a unit cube model was to be developed, checked for validity and accuracy against test results, and refined in accordance with the findings.

TRANSLATION INTO PRODUCTION

If pre-straining was found to have actual merit, conceptual tooling plans were to be made for applicable Saturn S-II parts.

MATERIAL PROPERTIES

Salient mechanical and thermal properties, as required for a mechanics analysis, have been established as functions of temperature on 2014-T651 aluminum alloy and 2319 weld filler material. They are presented in graphical form in Figures 1 through 6 as follows:

Effect of temperature on compressive and tensile yield strength (F_{cy} and F_{ty})

Effect of temperature on the ultimate tensile strength (F_{tu})

Effect of temperature on modulus of elasticity (E)

Effect of temperature on specific heat (C)

Effect of temperature on thermal conductivity (K)

Effect of temperature on total thermal expansion

Material properties at room, cryogenic, and elevated temperatures are presented. In view of the complete lack of direct data on 2319 "as-cast" material for much of the temperature range, the assumption was made that its properties would be similar to those of 2219 in the annealed condition. The accuracy of this assumption is in line with the expected analytical ones. In the accumulation of these data, use was made of NAA's contractual agreement with the Thermophysical Properties Research Center of Purdue University.

The material property curves show design strength properties and related characteristics of wrought 2014-T651 and "as deposited" 2319 aluminum used in this program. The design strength properties (F_{tu} and F_{ty}) are "A" values (99-percent probability, 95-percent confidence level). Elastic modulus and physical property values are average values taken from selected experimental data and are considered design values.

Material properties data were accumulated from the following sources:

1. Material suppliers' data sheets, published and unpublished
2. Government publications and reports (References 2, 3, 4, and 5)

3. NAA reports, data sheets, and structures manuals (References 6, 7, 8, and 9)

4. Private communications (References 10 and 11)

A critical review was made of all available data and values that appeared the most reliable on the basis of sound engineering judgment.

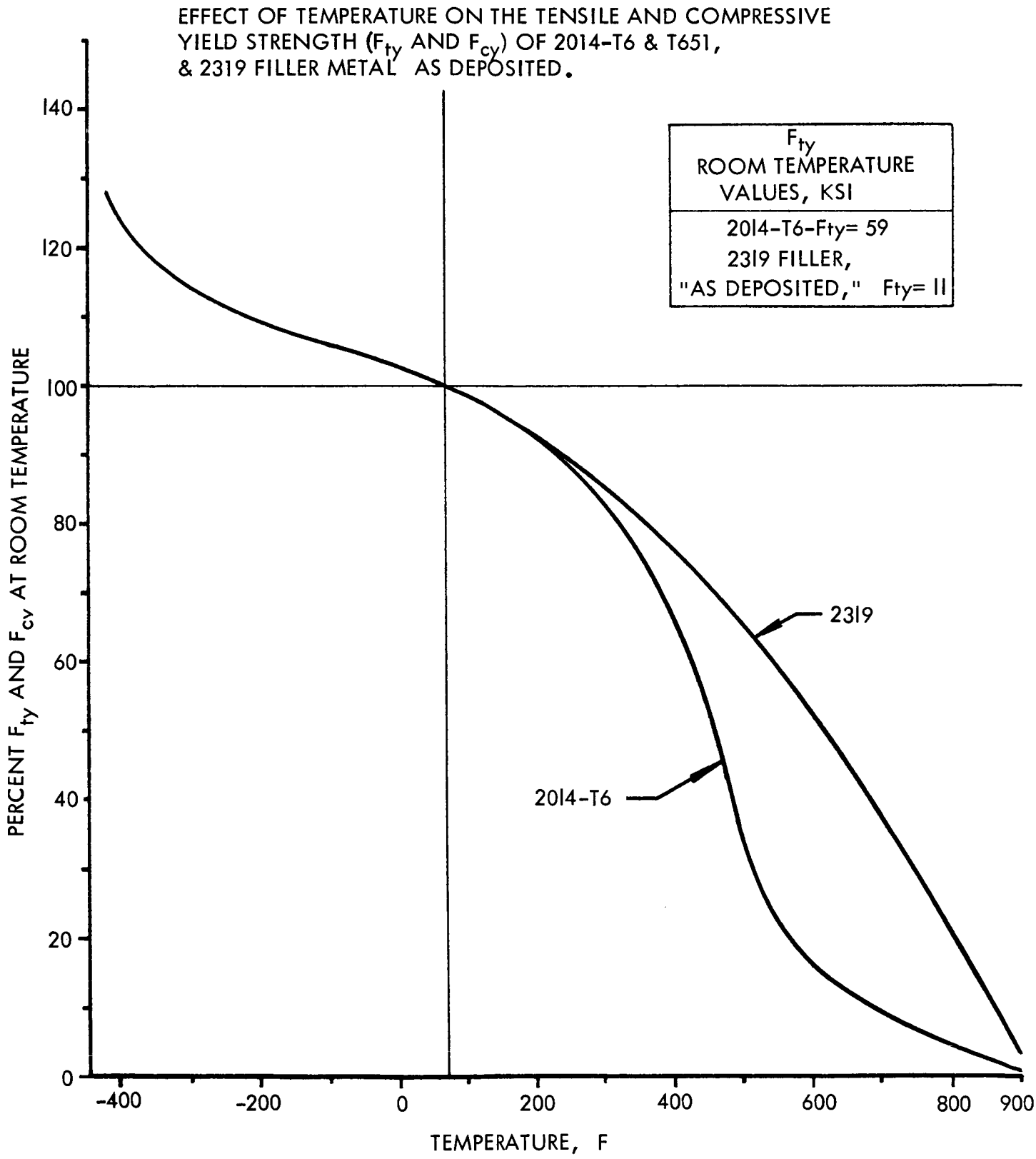

Figure 1. Effect of Temperature on the Tensile Yield Strength (F_{ty})

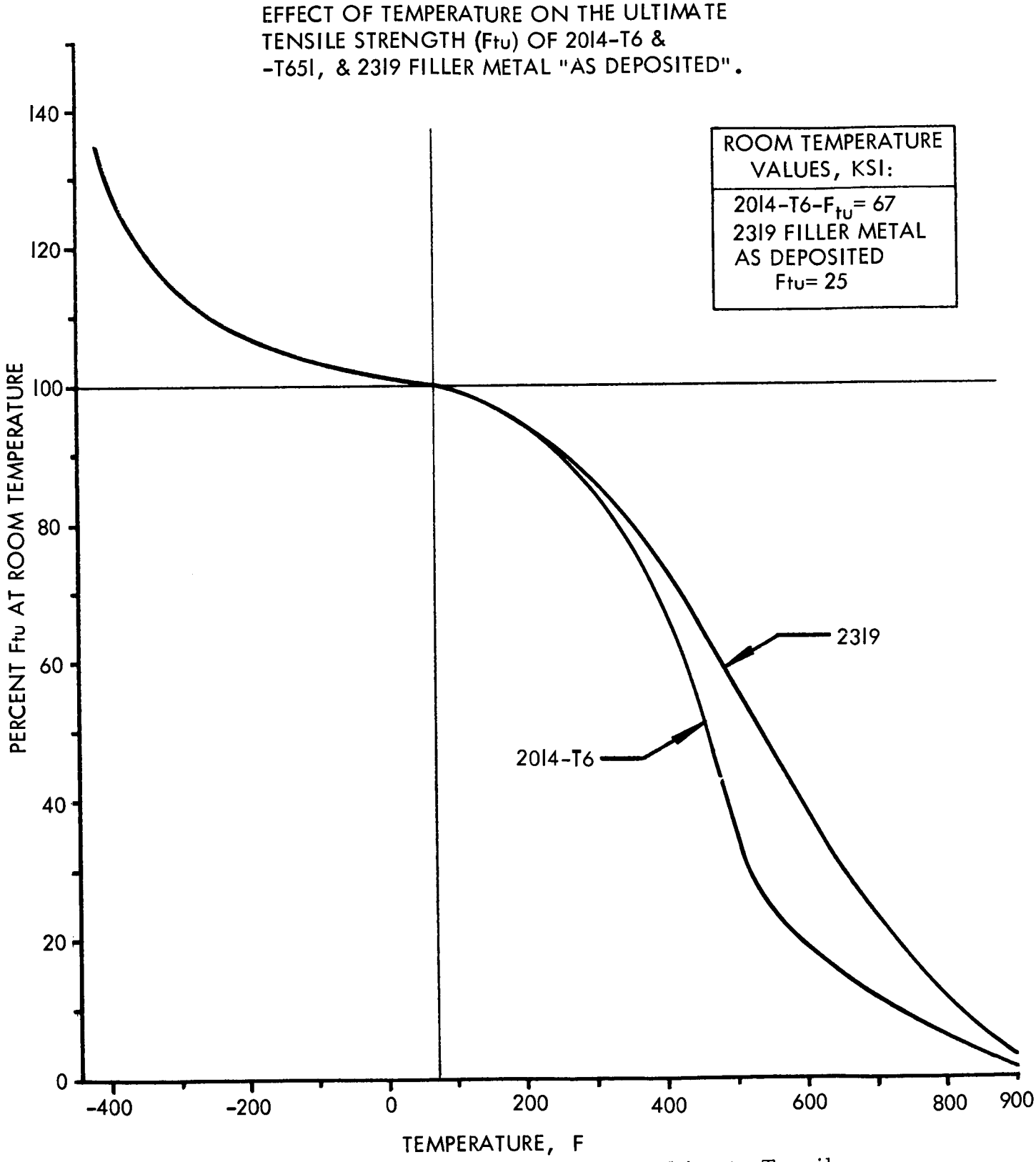

Figure 2. Effect of Temperature on the Ultimate Tensile Strength (F_{tu})

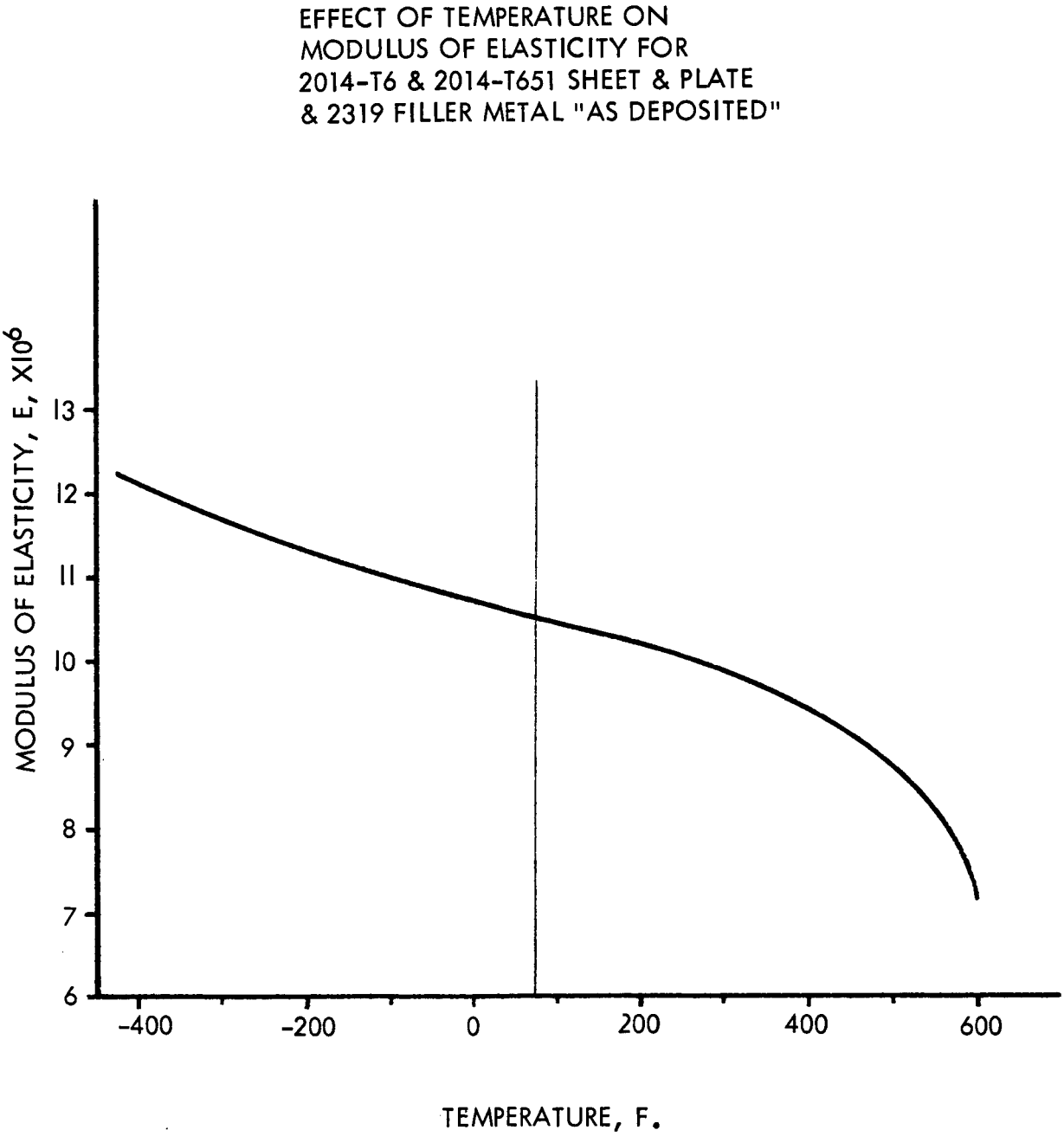

Figure 3. Modulus of Elasticity

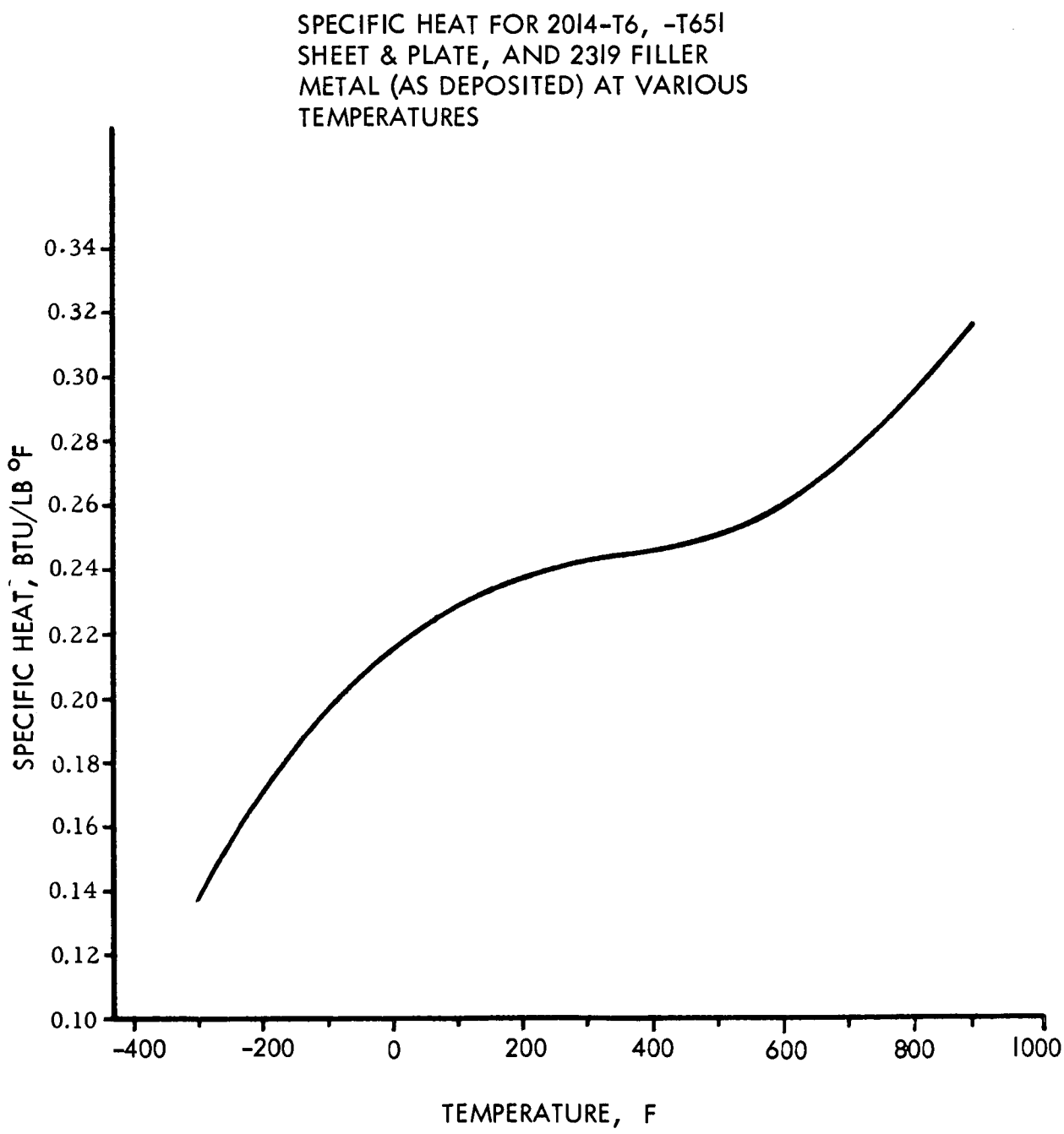

Figure 4 . Specific Heat

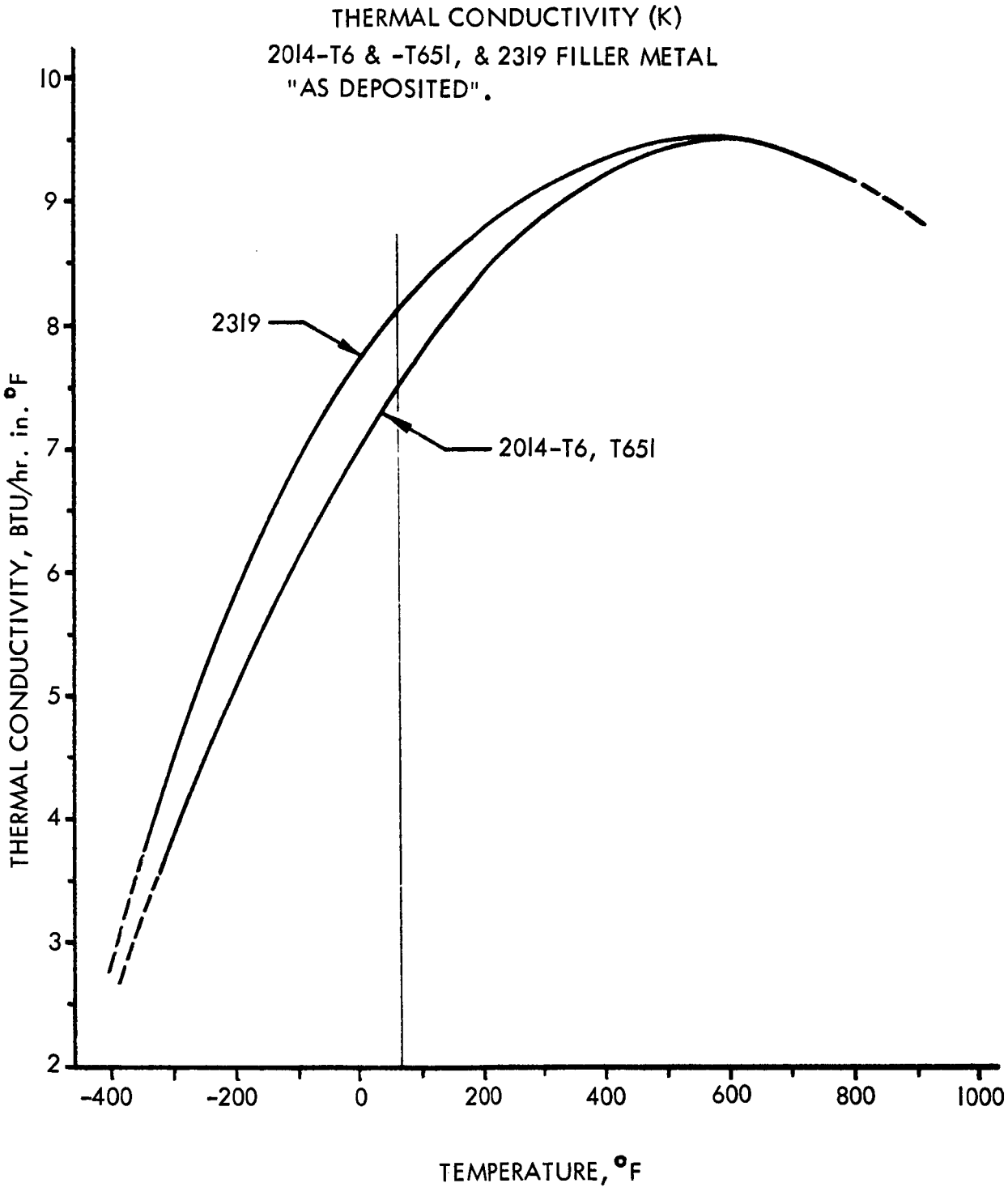

Figure 5. Thermal Conductivity (K)

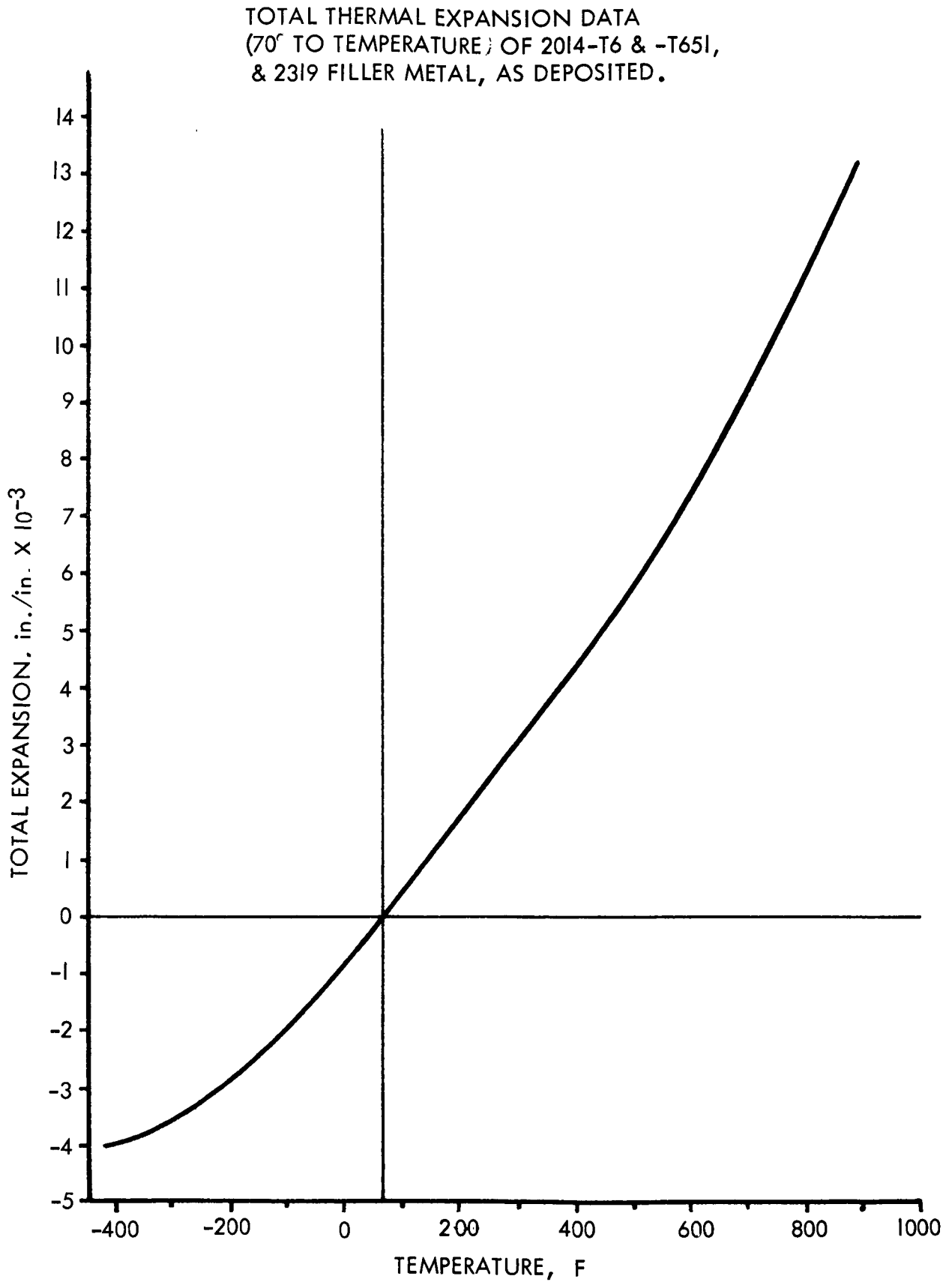

Figure 6. Total Thermal Expansion Data (70 Degrees to Temperature)

PRELIMINARY WORK

ESTABLISHMENT OF WELD SETTINGS

Because variations in welding procedures influence distortion and residual stress, weld certifications were established before welding of test panels to ensure consistency of weld parameters for each panel thickness.

All preliminary verification and test weldments were chemically cleaned to Specification MA 0110-110, and the edges and welding area were prepared in accordance with all Saturn S-II manufacturing requirements. Machine fusion welding was accomplished in accordance with Specification MA0107-016E, utilizing the gas tungsten-arc (TIG) welding process. All weldments were visually and radiographically inspected to ensure that quality requirements were maintained.

Two panels, each 16 by 72 inches, were mated to form a square-edge butt joint and welded in the flat position using the TIG process (direct current-straight polarity) with 2319 filler material in a single pass.

The alignment tooling materials used, representative of Saturn manufacturing practices, consisted of stainless steel for the backup bar and aluminum for the hold-down segments. The hold-down gap was 3/4-inch (tooling being 3/8 inch from weld centerline).

The welding parameters established and used for panel weldments of 0.250-inch weld-land thickness are listed in the following welding schedules:

Welding specification:	MA 0107-016
Welding process:	TIG, dc-straight polarity
Materials employed:	Base metal - 2014-T651
	Filler alloy - 2319 (1/16-inch)
	Electrode - 1/8-inch tungsten (2-percent thoriated)
	Shielding gas - helium

Welding parameters:	Potential - 11 volts
	Current - 230 amps
	Filler metal rate - 22 ipm
	Welding rate - 8.75 ipm
	Shielding gas rate - 130 cfh
Hold-down pressure during welding:	90 psig

The welding parameters for the 0.165-inch and 0.190-inch material are identical to those used for 0.250-inch material except as follows:

0.165-inch Material	0.190-inch Material
Current - 160 amps	Current - 180 amps
Filler rate - 20 ipm	Filler rate - 21 ipm

Specimens having 2:1 weld land to panel thickness ratio were used; thickness noted is the thickness of the 1 1/4-inch wide weld land.

Joints were of square-edge butt design.

STRAIN GAGE REMOVAL METHOD FOR RESIDUAL STRESS DETERMINATIONS

Since residual stress determinations were to be one of the primary criteria in evaluating the possible beneficial effects of pre-straining, it was necessary to determine the magnitude of stress introduced by strain gage removal and the most efficient and convenient removal method. Sample cutting of strain gages by mechanical (saber saw) and electrical-discharge (Eleroda machine) methods according to the test plan of Figures 7 and 8 was accomplished satisfactorily. The results show that stresses introduced by either method are of a low order of magnitude (less than 750 psi) and would not interfere with the accuracy of the residual weld stress determinations. Strain gages may be placed close together without undue effects during the removal procedure. The electrical-discharge method appeared to be less difficult and time-consuming and, therefore, was used in the test program.

DETERMINATION OF CUTTING METHOD FOR REMOVAL OF STRAIN-GAGED PLUGS

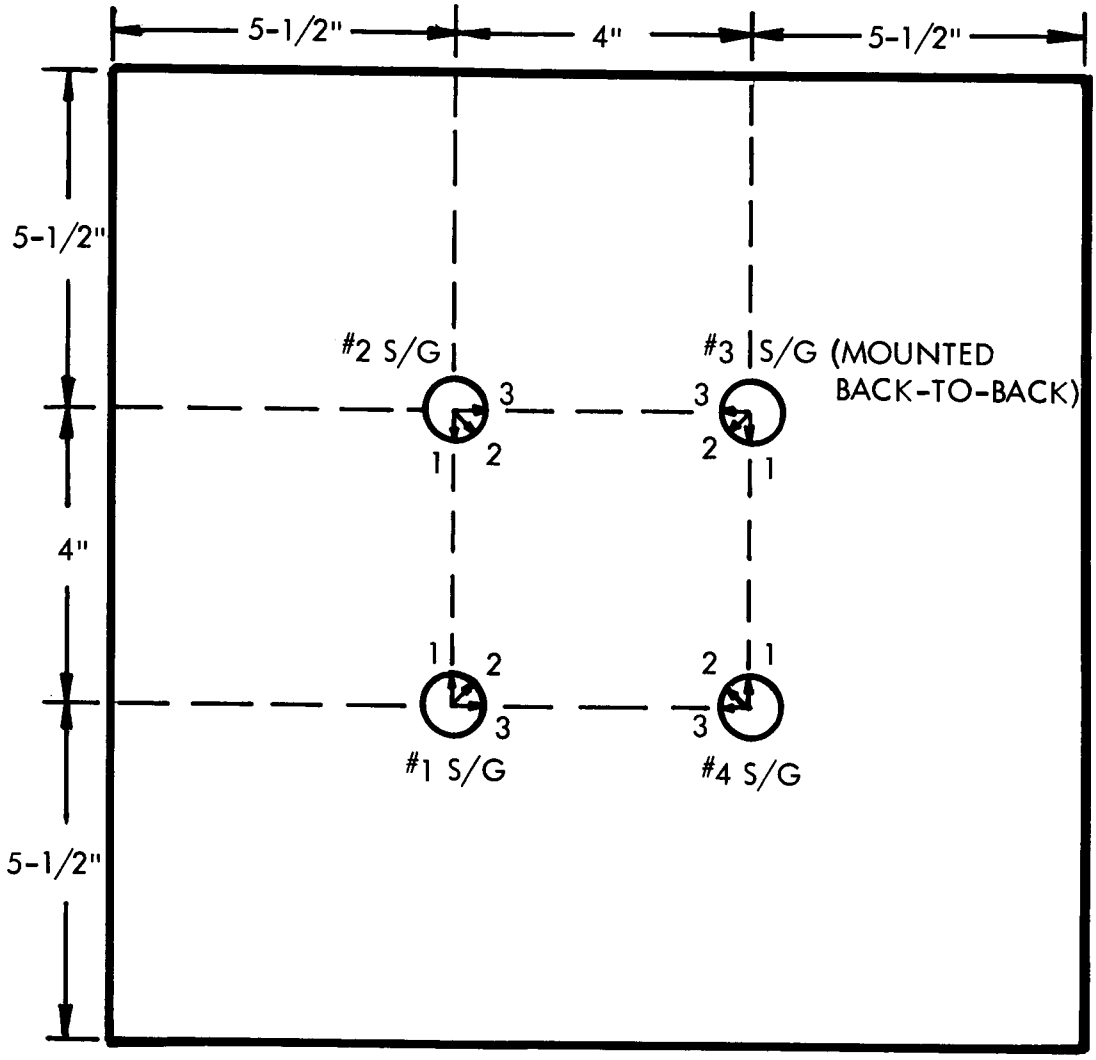

GAGE NO.	PROTECTIVE COATING
1	RT ✓ 102
2	GAGEKOTE #2 OVER GAGEKOTE #5
3	GAGEKOTE #2 OVER GAGEKOTE #5
4	RTV 102

SCHEMATIC, S/G INSTALLATION PANEL #3

Figure 7. Determination of Cutting Method for Removal of Strain-Gaged Plugs

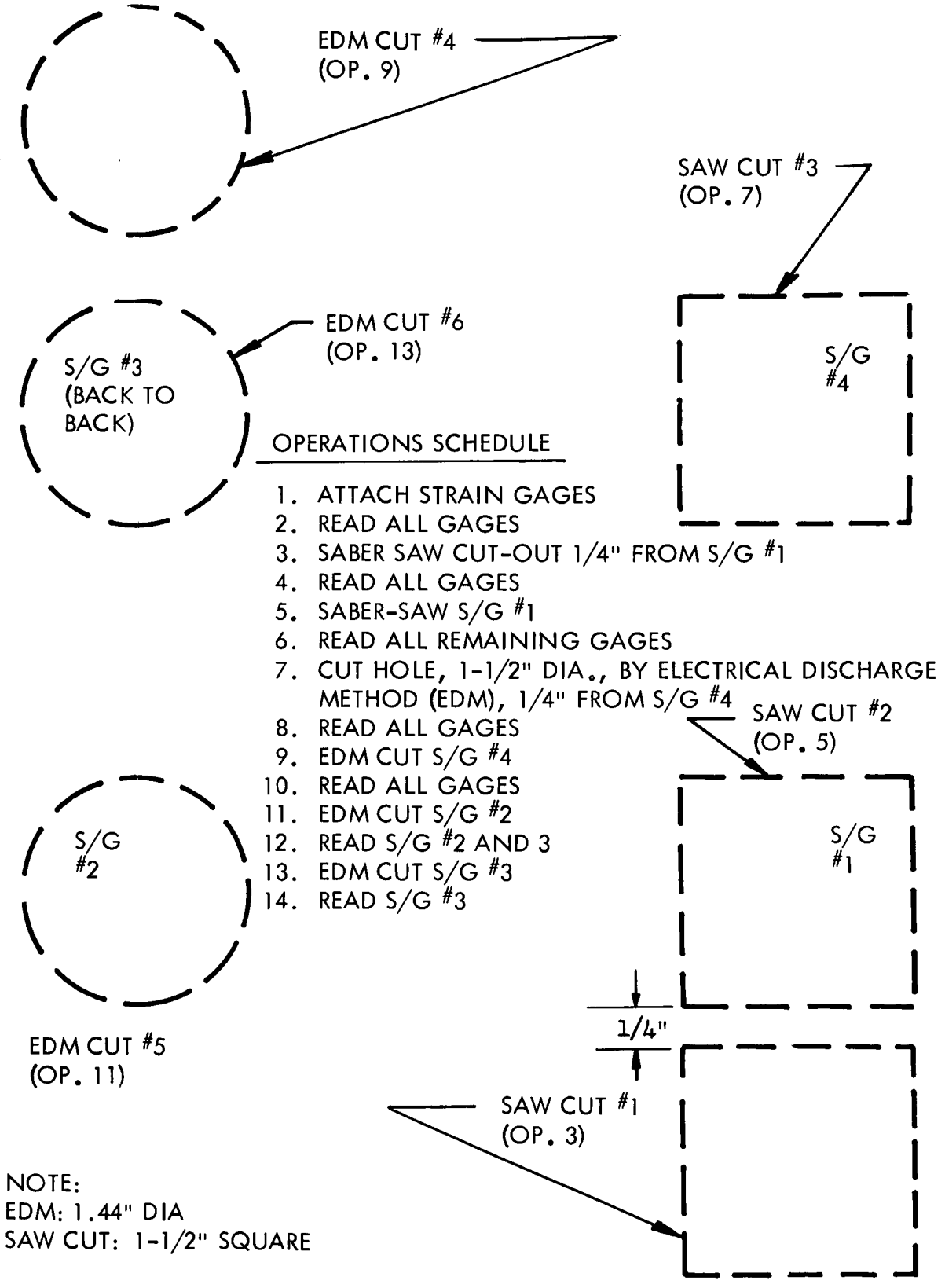

Figure 8. Detail Sketch S/G Removal (Panel No. 3)

MECHANICALLY APPLIED PRE-LOAD SETTINGS

Preliminary pre-strain experiments were conducted to measure and evaluate the level and uniformity of pre-strain applied to the test parts through use of a hydraulically operated attach fixture.

Panel sets were instrumented with strain gages so that the amount of pre-strain was measured and compared with strain calculated by using pressure readings of the hydraulic loading fixture.

Uniaxial strain gages were located at Stations 12, 24, 36, 48, and 60 on the edge of the weld land on both left and right panels to check symmetry of induced strains with various pre-loads. Figure 9 shows the location of the strain gages and the strain measured at various pressure gage settings of the pre-loading accessory. Readings were found to be repeatable when loads were reapplied, and good agreement also existed with respect to symmetry at a given point, both longitudinally and transversely. Output of the strain gage at Station 12 (or 60) was used as the reference in establishing pressure settings. Hold-down pressure effect was found to be negligible (Table 1).

Results of this preliminary phase showed pressure gage settings to be a reliable criterion for measuring the level of pre-strains imposed by the hydraulic load attaching system.

Typical stresses (as percentages of nominal tensile yield strength) developed in the weld land area due to mechanical pre-loading are shown in Figure 10 for each 12-inch station location for Weldments 6, 7, 8, and 9. Weldment 6 panels (3L and 6R) failed when held for 12 minutes at 6600 psi pre-load (40-percent F_{ty}) pressure for total applied load of 47,600 pounds. Weldments 7, 8, and 9 exhibited a stress-distance relationship, as shown, at a pressure gage setting of 5200 psig.

The formula used in this stress computation is the simple uniaxial equation neglecting transverse effects:

$$\text{Percent Pre-Load} = \frac{\sigma_a}{F_{ty}} \times 100 = \frac{E\epsilon}{F_{ty}} \times 100$$

Since actual control of unidirectional strain application in practice would be accomplished by simple uniaxial load or deflection criteria. It is recognized that the actual stress in the pre-strained part would differ from the reported one by Poisson's effect.

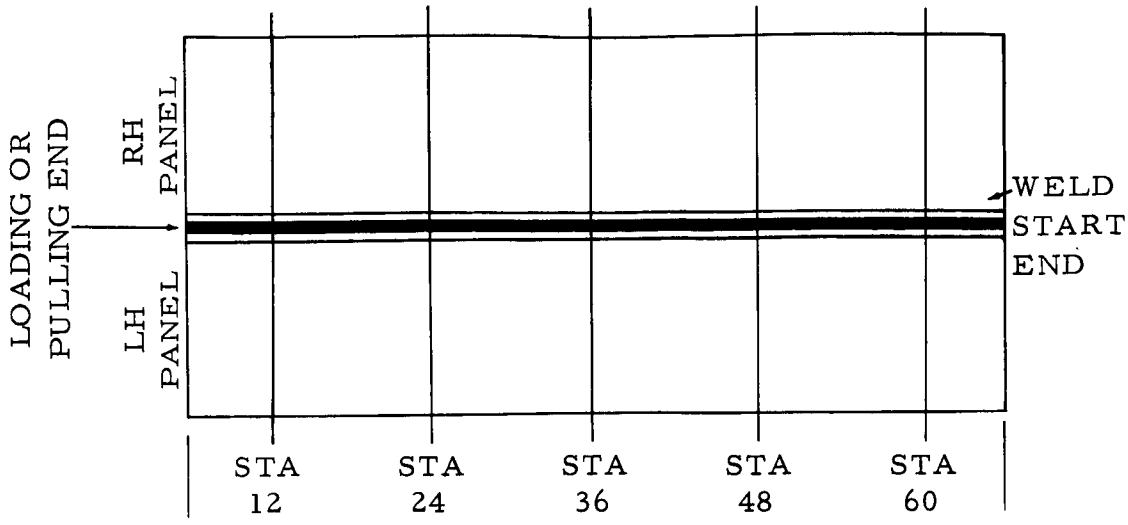

Distance in inches from loading end

NOTE: Hydraulic Loading Device, ram area factor = 7.216

Figure 9. Strain Measurement at Various Pressure Gage Settings of the Pre-Loading Accessory

Table 1. Pre-Weld Strains (μ In./In.) Due to Mechanical Pre-Loading

Intended Weldment	Panel No.	Pre-load Gage Pressure (psig)	Line Hold Down Pressure (psig)	Station (inches from loading end)				
				12	24	36	48	60
No. 7	15 L	5200	None	1705	1145	980	1150	1760
	9 R			1710	1110	975	1200	1710
	15 L	5100	90	1640	1100	845	1080	1855
	9 R			1505	1050	1005	1120	1515
No. 6	3 L	5200	20	1615	1020	925	1140	1720
	6 R			1685	1035	925	1170	1695
	3 L	6600*	90	2200	1360	1320	1500	2280
	6 R			2175	1375	1250	1550	2285

*Intended weldment No. 6 failed after holding for 12 minutes at 6600 psig pre-load pressure, for total load applied to weldment of 47,600 pounds.

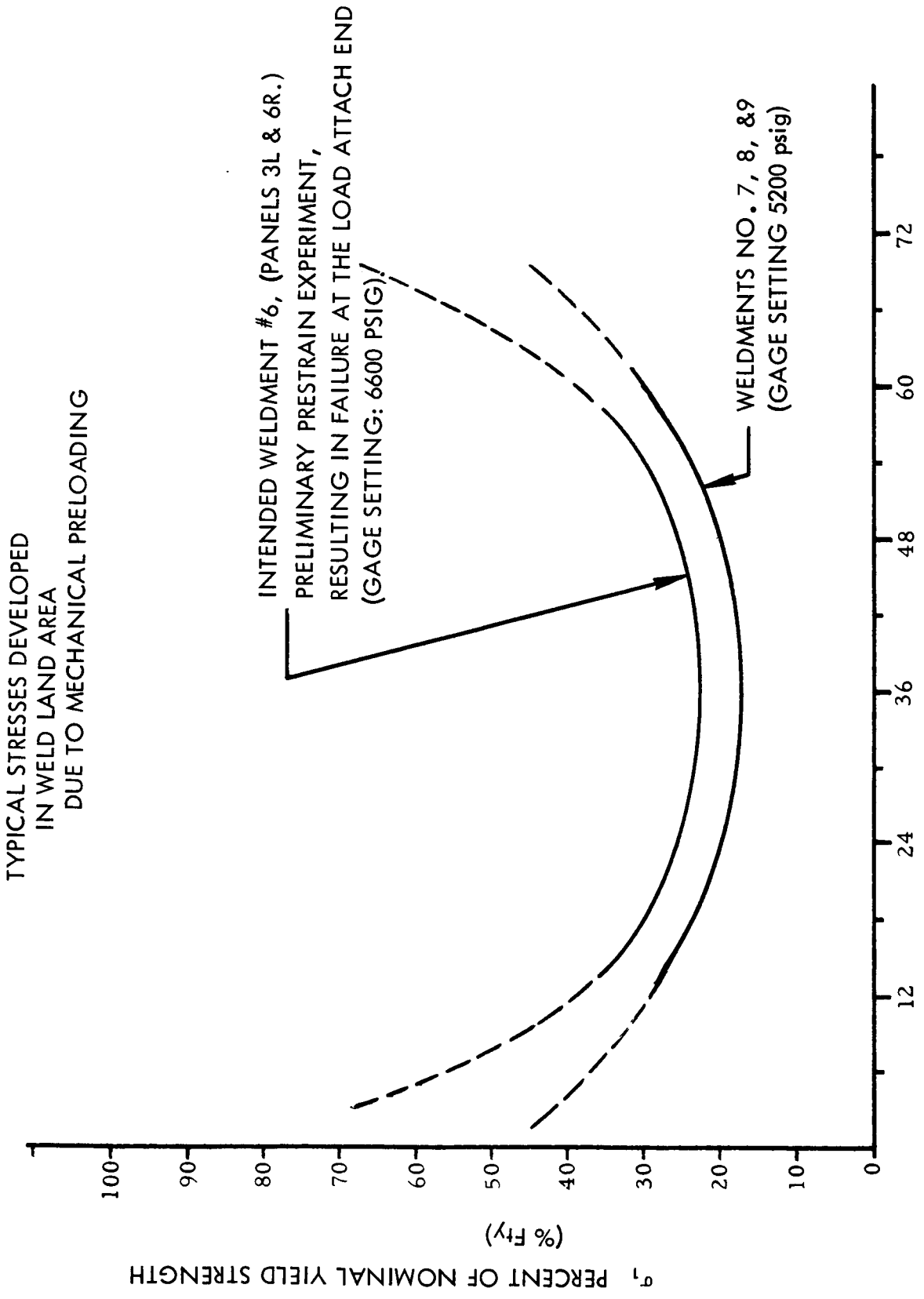

Figure 10. Percent Pre-Load Versus Distance

Strains corresponding to various percentages of yield stress were then used in establishing reliability of pressure gage settings as a criterion of pre-straining. The intended relation between strain gage settings and percent of nominal yield strength used in this program were as follows:

$\% F_{ty}$	Strain, μ in/in
40	2290
30	1715
20	1145
10	570

HEAT FLOW PATTERN DUE TO WELDING

Heat flow patterns, as a function of weld head locations, were established on two sheet gages (measuring 0.125 and 0.080 inch, with 1-1/4 inch-wide raised weld lands 0.250- and 0.160-inch thick, respectively) by installation and monitoring of micro-temperature probes and thermocouples (Figure 11). Layout for Weldment 1 (250 inches) is shown in Figure 12. A similar layout was used for Weldment 2. Actual thermocouple and micro-probe coordinates were established from X-ray readings, depicted typically in Figure 13 and used in plotting corrected temperature profiles. Typical graphs of thermocouple readings, as a function of time for specific station lines, are shown in Figures 14, 15, and 16. Sufficiently close agreement was found that a quasi-steady state of temperature distribution around the weld head can be stipulated soon after initiation of welding. An isotherm plot for the 0.250-inch weld land thickness panel was prepared, as shown in Figure 17, and used in the mechanics analysis. It agrees well with the configuration of such weld isotherms reported in related literature (Reference 12). Since the micro-probes inserted in the weld center of Panel 1 (0.250-inch weld-land thickness) had not produced smooth readings in the vicinity of maximum temperature rise, an attempt was made to obtain greater smoothness by inserting capacitors into the corresponding circuitry of Panel 2 (0.160-inch weld-land thickness). This attempt, however, was not successful; no readings were obtained from these probes. It is reasonable to assume that they reached the same temperature as corresponding ones of thicker weldment.

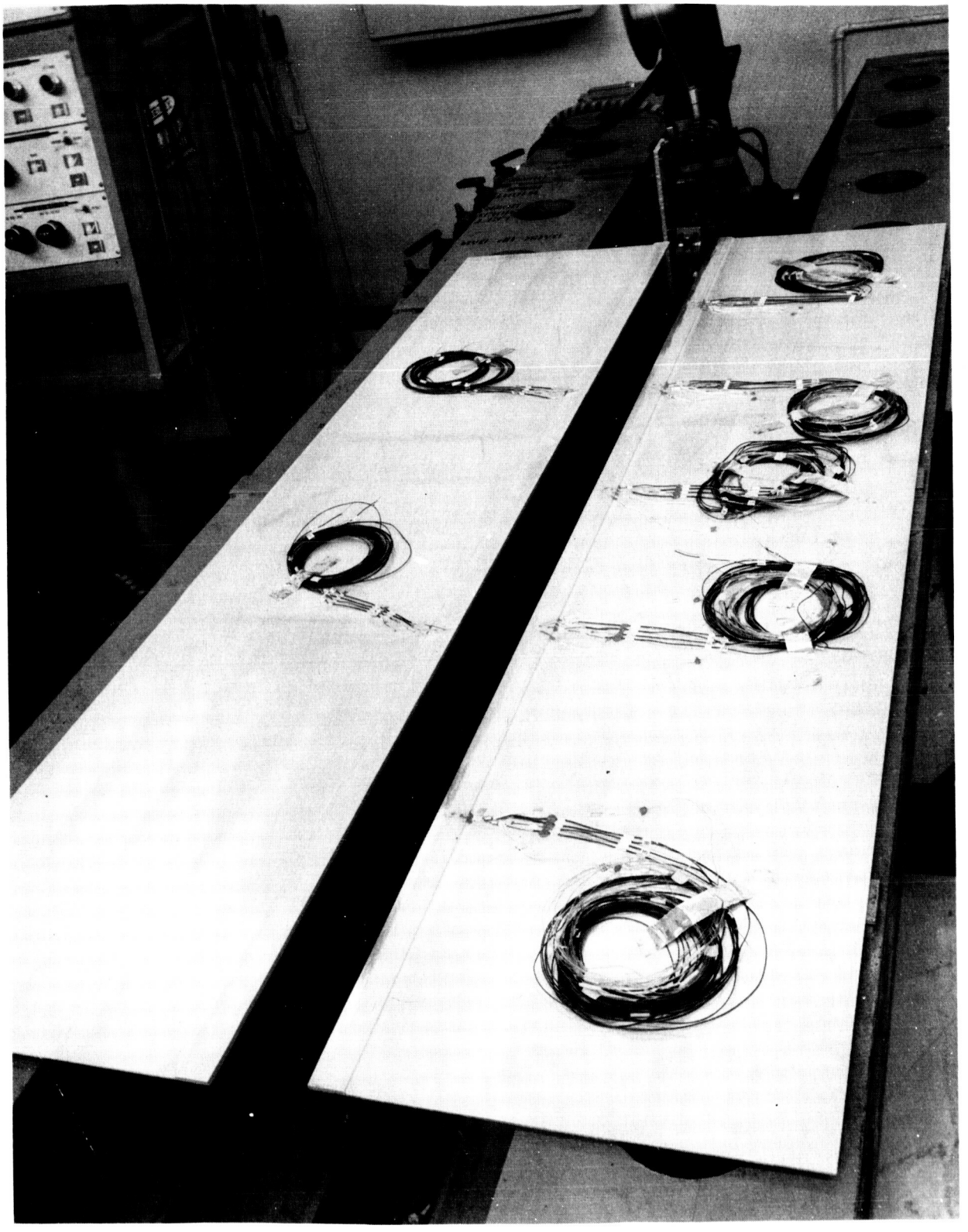

Figure 11. Test Panels Showing Thermocouple Installation

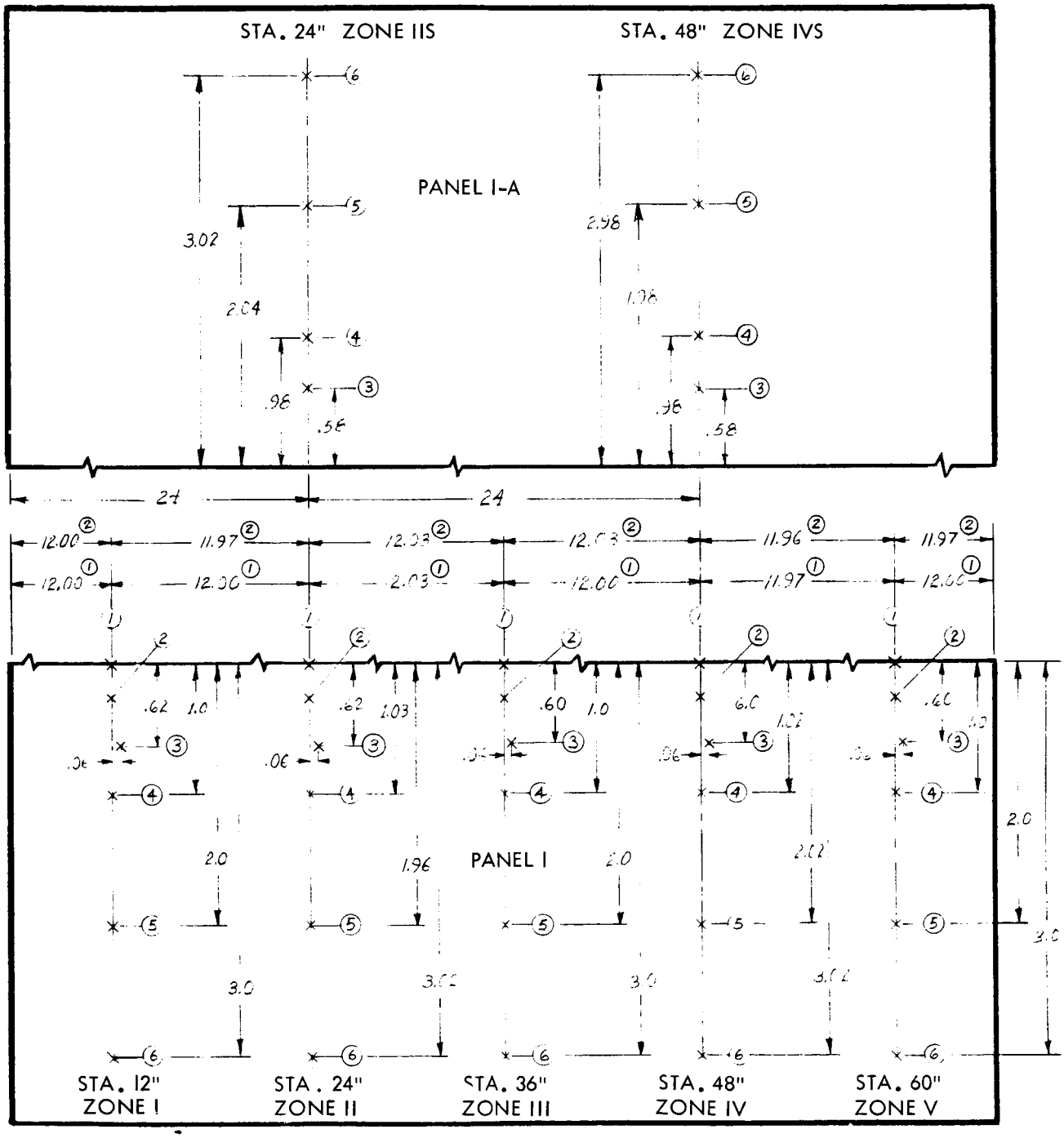

PRESTRAIN WELD DEVELOP. PANELS (.250 in.)
PANEL I AND I-A (NO SCALE)

Figure 12. Thermocouple Layout Weldment 1

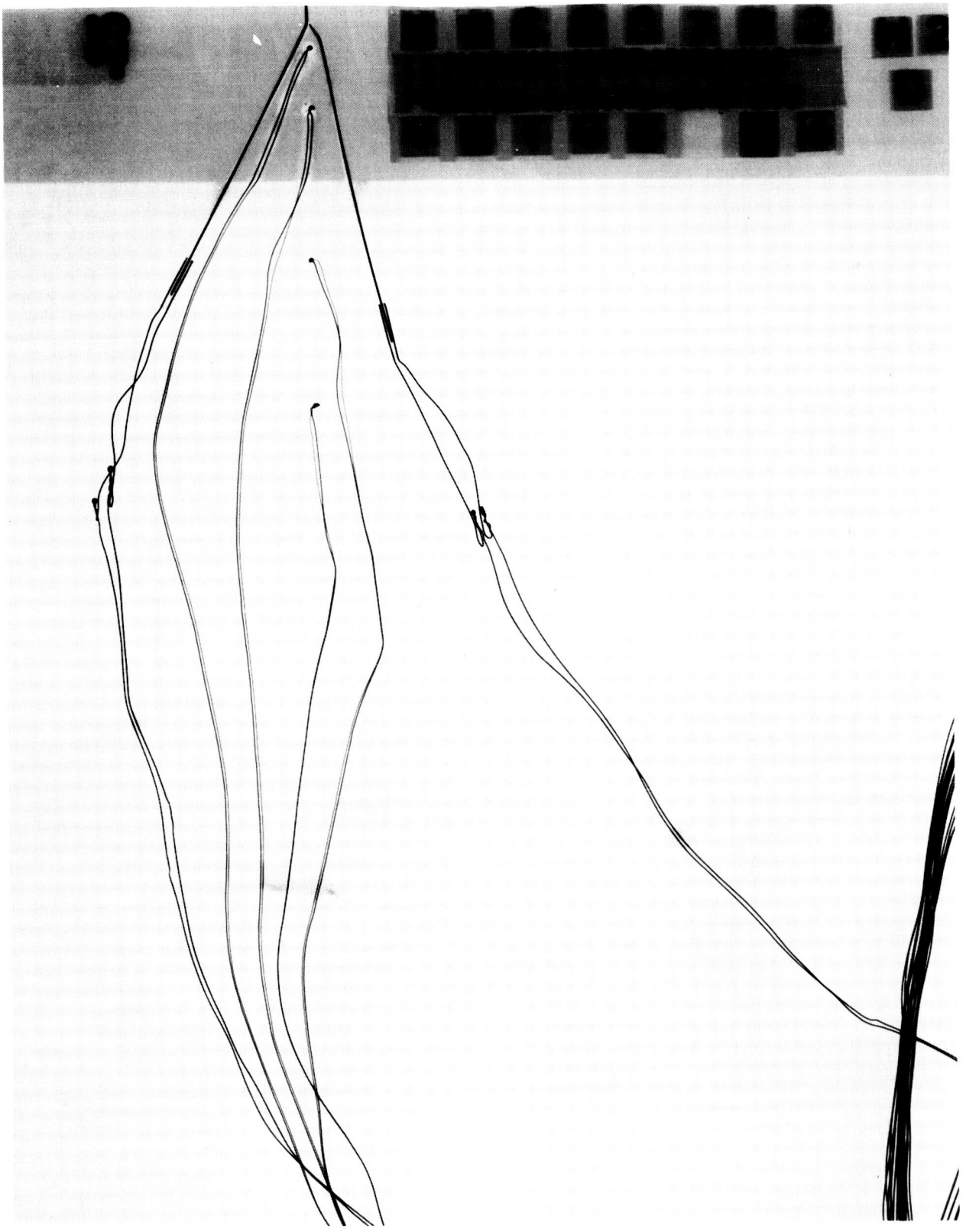

Figure 13. Temperature Probe and Thermocouple Location, X-Ray Typical of Weldment No. 2, X-Ray No. TWC287P2

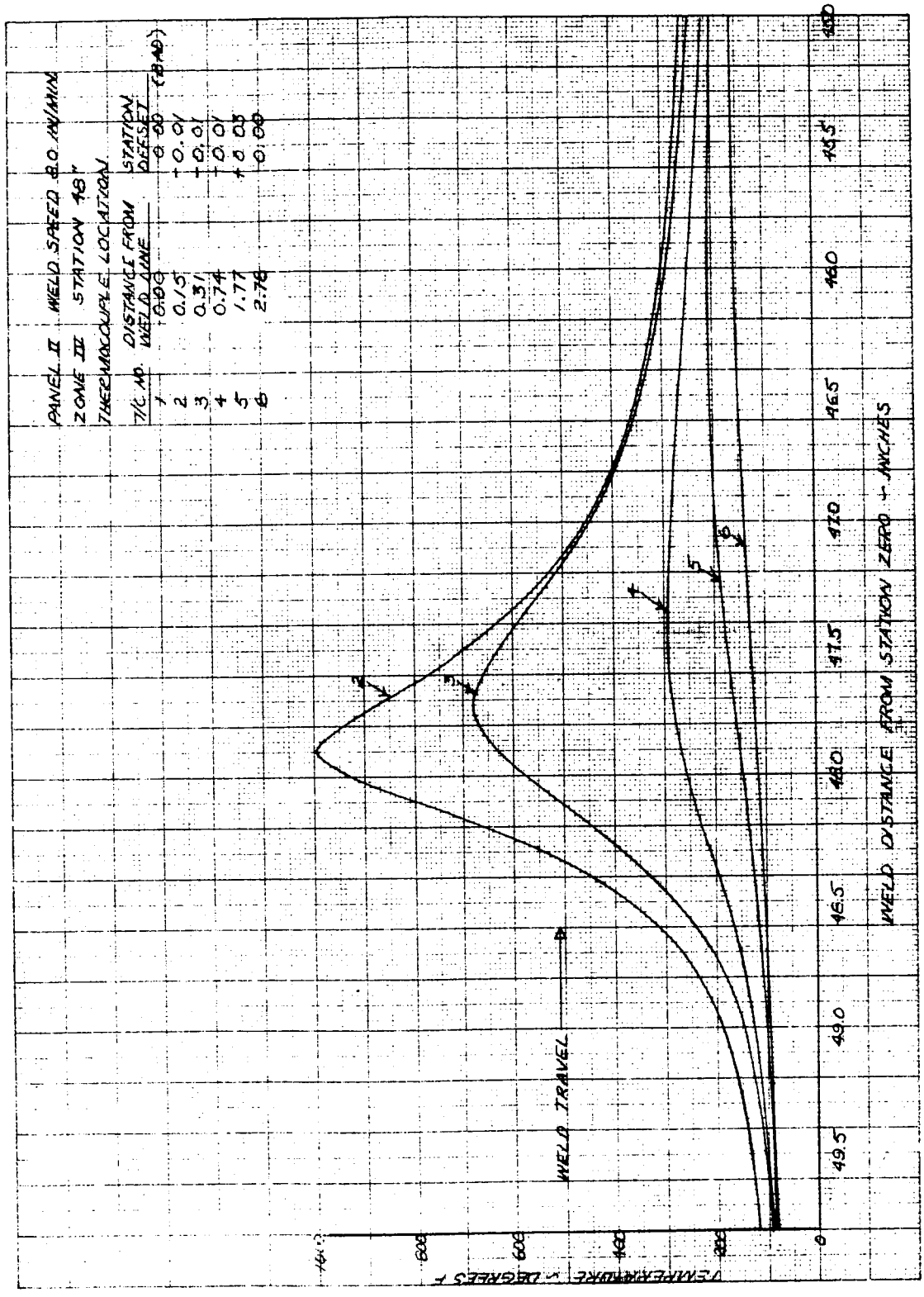

Figure 14. Thermal Profiles at Station 48, Weldment 2

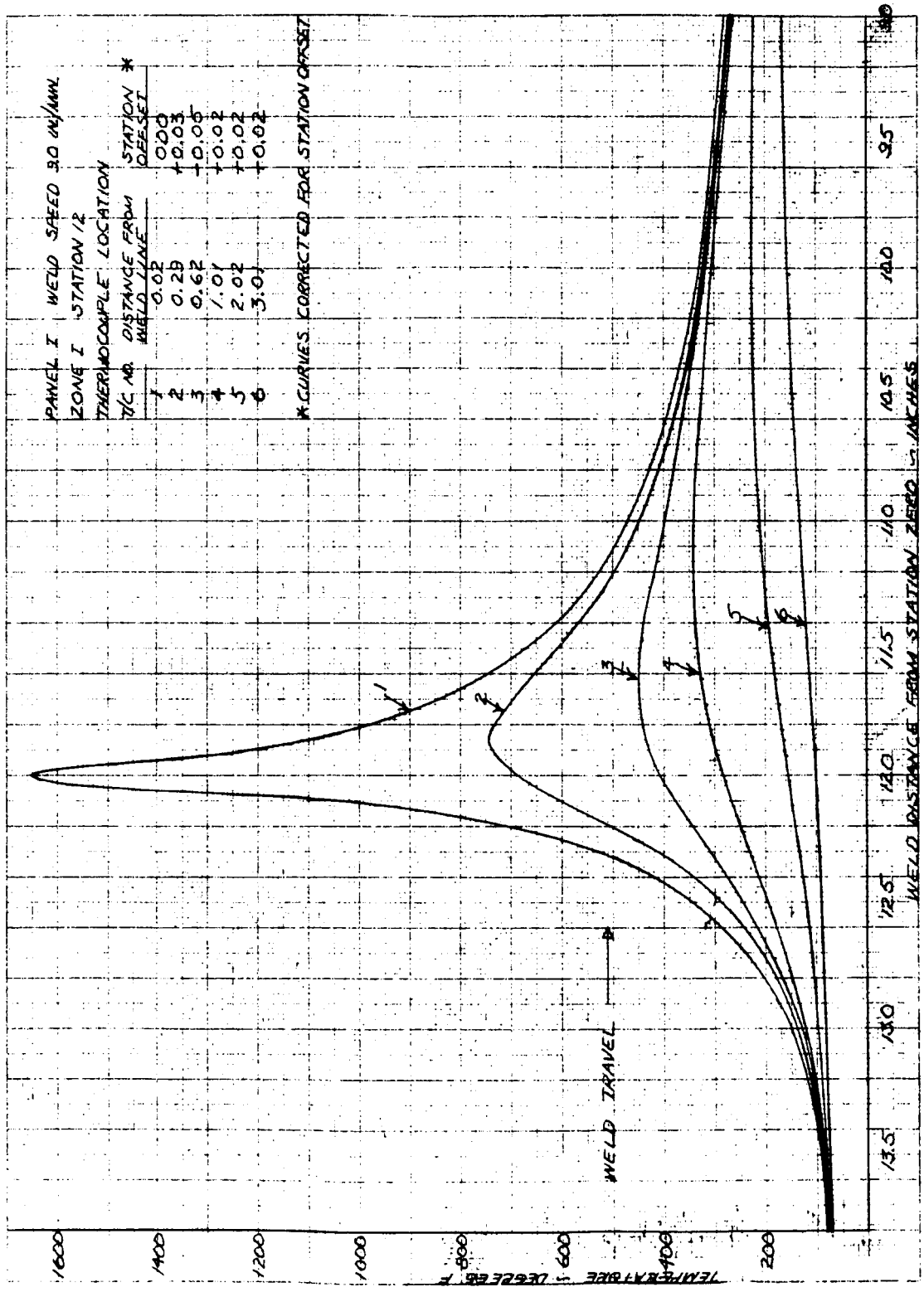

Figure 15. Thermal Profiles at Station 12, Weldments 4, 7, 8, and 9

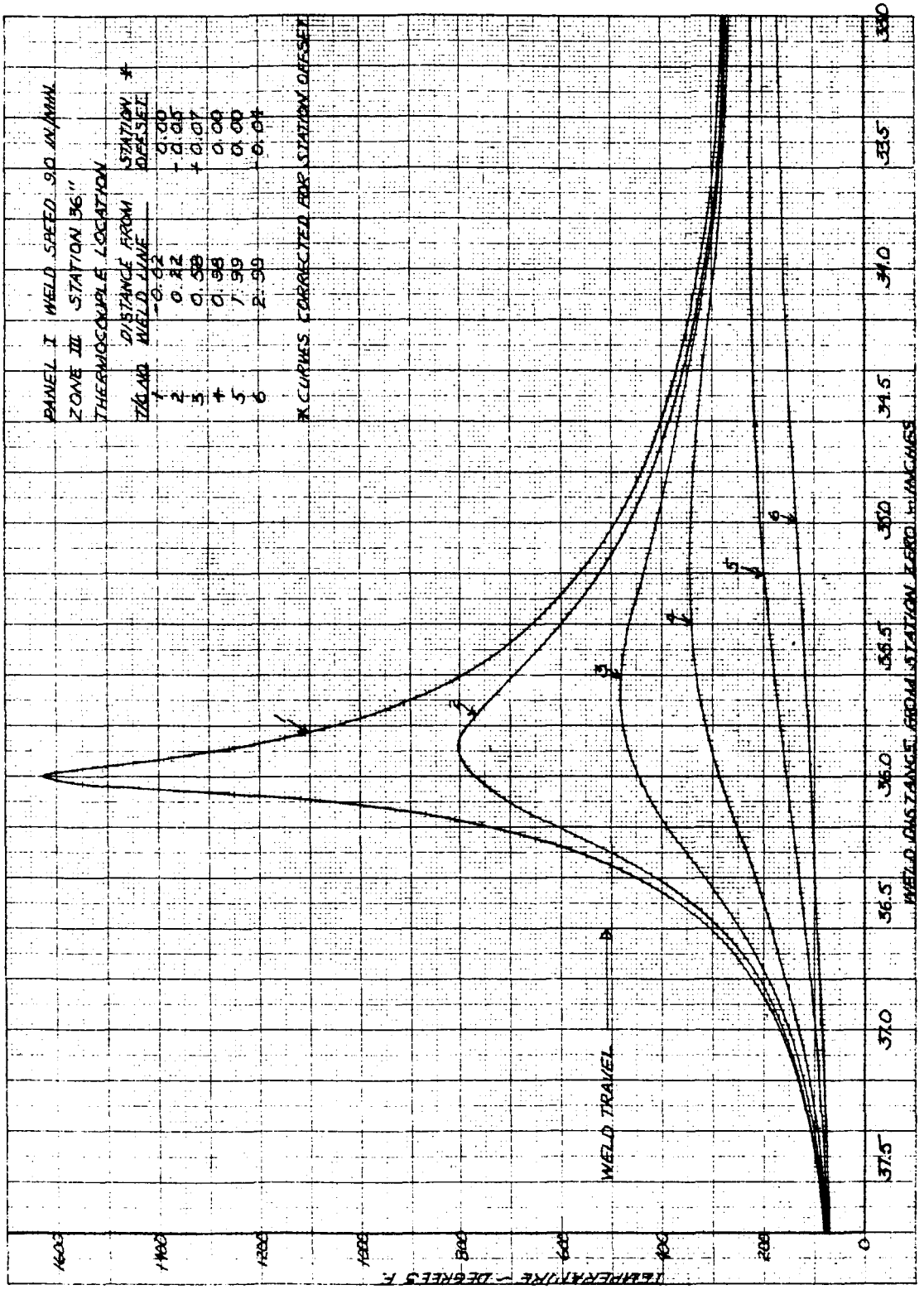

Figure 16. Thermal Profiles at Station 36, Weldments 4, 7, 8, and 9

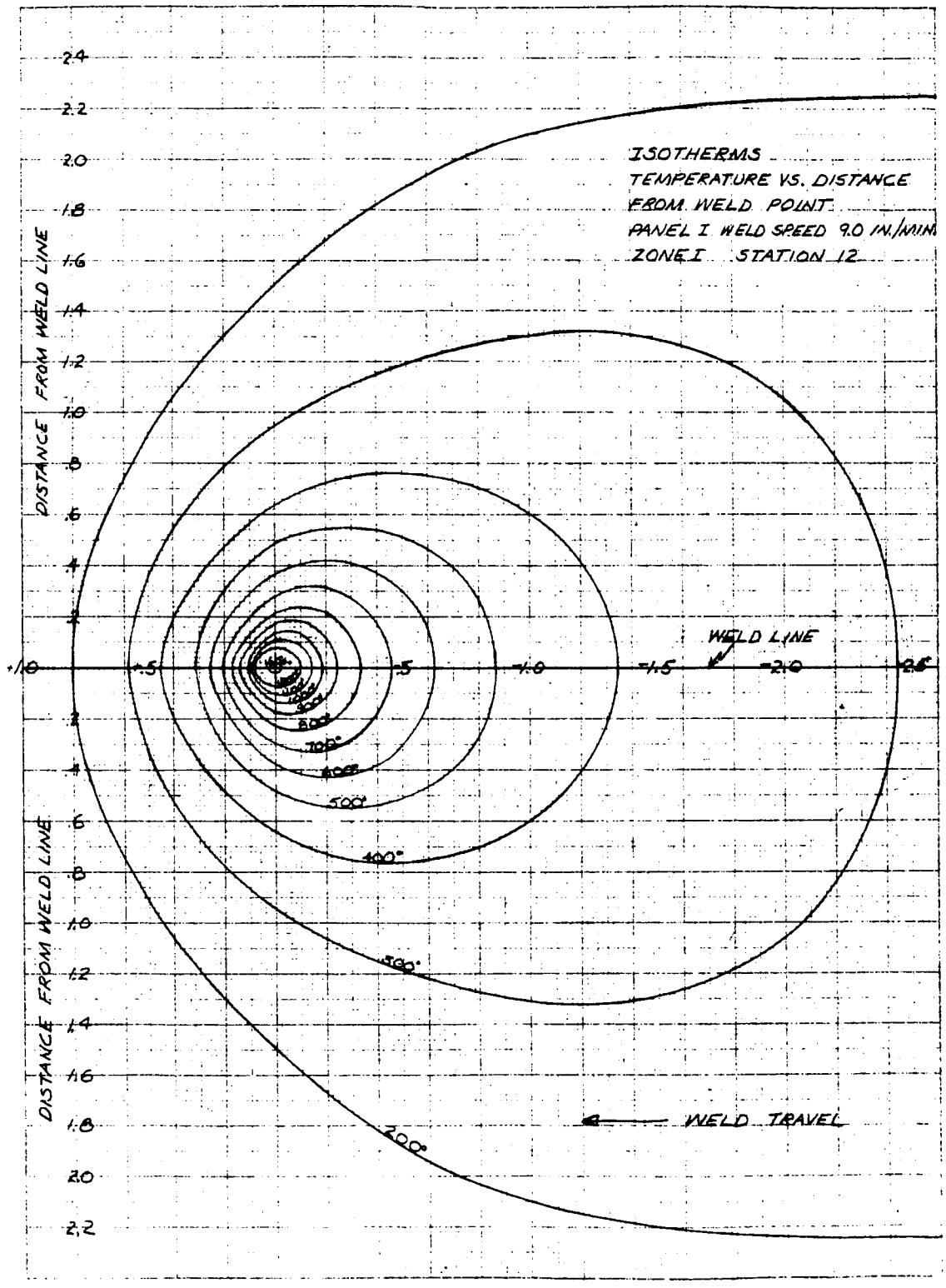

Figure 17. Thermal Distribution of Weldments 4, 7, 8, and 9

DEFINITION OF PRE-STRAIN

The possible methods of pre-straining weldments fall into three main categories: (I) load pre-strain, (II) thermal pre-strain, and (III) position pre-strain. This study involves only the first category, which is subdivided as follows:

I. Load Pre-Strain

a. Mechanically applied load pre-strain such as uniaxially or biaxially applied tension, compression, or moment forces.

b. Thermally applied load pre-strain produced by thermal shrink-fitting of one part inside another and allowing the combination to return to room temperature before welding. (The term "thermal pre-load" used in the RFP and Contract refers to the thermally applied load pre-strain, which more properly is classified in Category I as "load pre-strain." The thermal shrink-fit readily produces beneficial biaxial stresses for closed circular weldments.)

The other categories, not investigated in this study, are—

II. Thermal Pre-Strain

(Thermal pre-strain involves the use of temperature differentials from ambient and thermal gradient profiles applied during welding to oppose the action of the weld temperature profile.)

a. Thermal Differential Pre-strain

b. Thermal Gradient Pre-strain

III. Position Pre-Strain

(Position pre-strain involves the compensation of weld distortion by locating the parts to be joined so that weld shrinkage will warp the parts into the desired final shape. Transverse weld shrinkage usually produces low residual axial and moment stresses if allowed to deflect. It is desirable to allow deflection to occur toward the final part configuration rather than away from such a location. Weld peaking is readily avoided by position pre-strain.

It is obvious that no single subcategory of weld pre-strain will reduce or cancel all residual stresses or avoid all distortion. For each type of weld, however, there exists a pre-strain combination that will produce the desired results. The unit cube model described in the Mechanics Analysis section is capable of predicting the type of weld method (i.e. single arc, twin arc, electron beam, etc.) that will produce the lowest residual stresses and distortions.

MECHANICAL PRE-STRAINING OF WELDMENTS

Mechanical pre-straining of weldments was accomplished by the hydraulically operated mechanical clevis arrangements shown in Figure 18. A sizable delay in the program occurred because the tool originally designated for this purpose was found to be inadequate, and could not sustain the applied force commensurate with the prestrain intensity levels to be investigated in the program. Construction and preparation of another welding tool of adequate strength resulted in a delay of several weeks. Preliminary investigations conducted on panels intended for Weldments 6 and 7 indicated excellent agreement and reproducibility between pressure gage and strain gage readings, and produced a relatively small effect of hold-down pressure. This result confirmed the expected fact that only the middle third of the weldments would be of relatively uniform strain intensity. When the applied pressure was raised, Weldment 6 failed after a 12-minute hold, which simulated the maximum weld period anticipated in the bolted down section. The applied stress profile, as computed, is shown in Figure 10. Therefore, it was decided to conduct the mechanical pre-strain portion of the program at applied pre-loads of 5200 psig pressure, corresponding to the lower curve stress profile in Figure 10.

It is realized that investigation at higher pre-strain levels in the relatively uniformly stressed center portion of the panels would be more desirable; however, this would require a different attach arrangement, similar to that shown schematically in Figure 19. The limitation of the simple load application arrangement used was known; since ready future translation into S-II production was a major consideration in this program, the simple arrangement was finally chosen.

EXPERIMENTAL PROCEDURE

Panels of 2014-T651 aluminum alloy measuring 16 inches by 72 inches of 0.250-inch and 0.190-inch weld-land and 0.125 and 0.095 weld thickness were prepared by Chem Milling. The weld land was 1-1/4 inches wide, simulating Saturn S-II welding conditions. These panels were joined by welding both with or without applied pre-strain (Table 2). The welding tool used (T7200300) was previously employed to develop Saturn S-II weld parameters. The tool uses a grooved stainless steel back-up bar and segmented aluminum hold-down fingers (Figure 20). The tool was modified by adding pre-load applying hardware, and hydraulic load cylinder and pump (Figure 18). Pre-strain readings, as a function of distance, were run on Weldment 7 by installing and reading five uniaxial strain gages

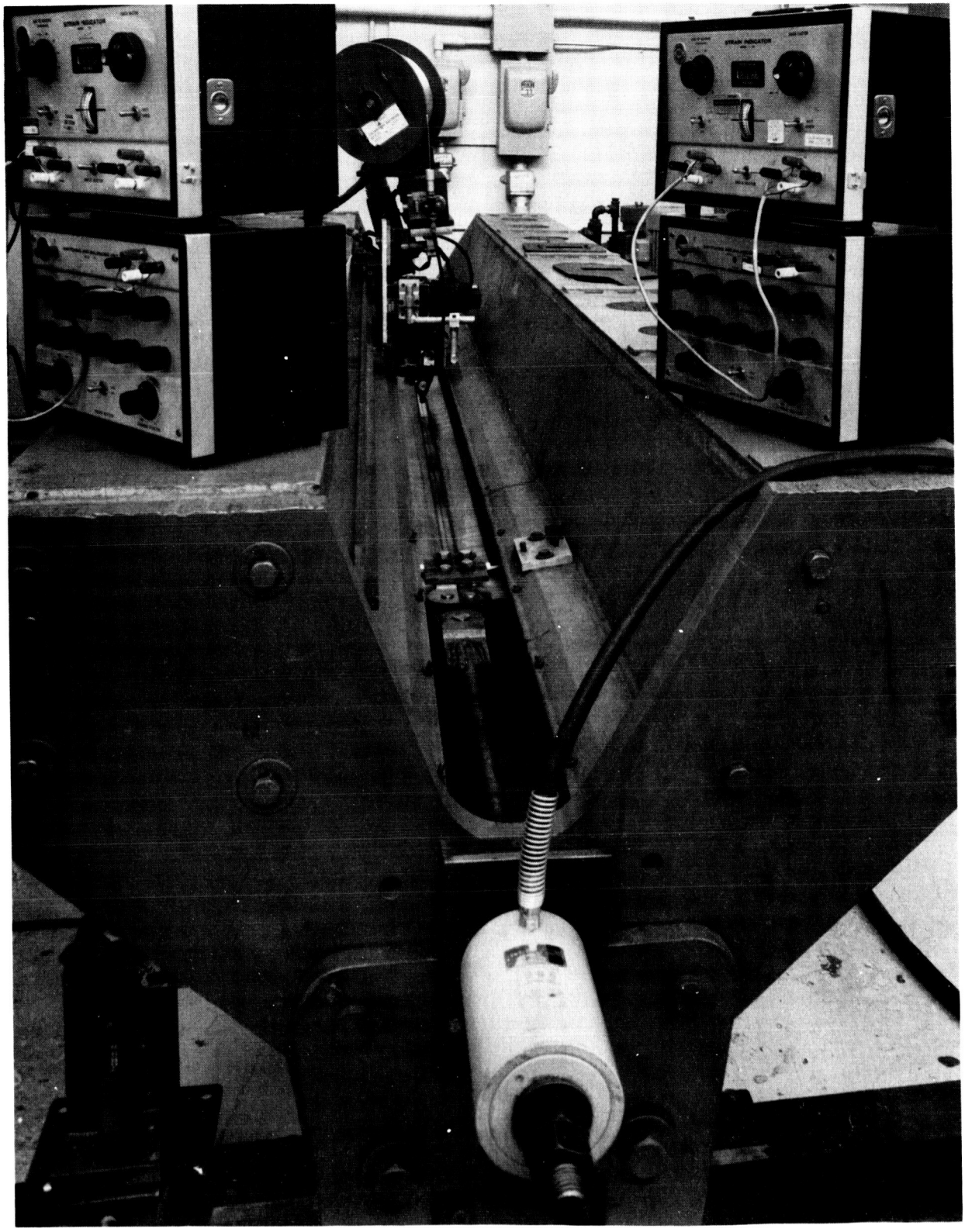

Figure 18. Welding Tool with Pre-Load Accessories and Pre-Load Indicators

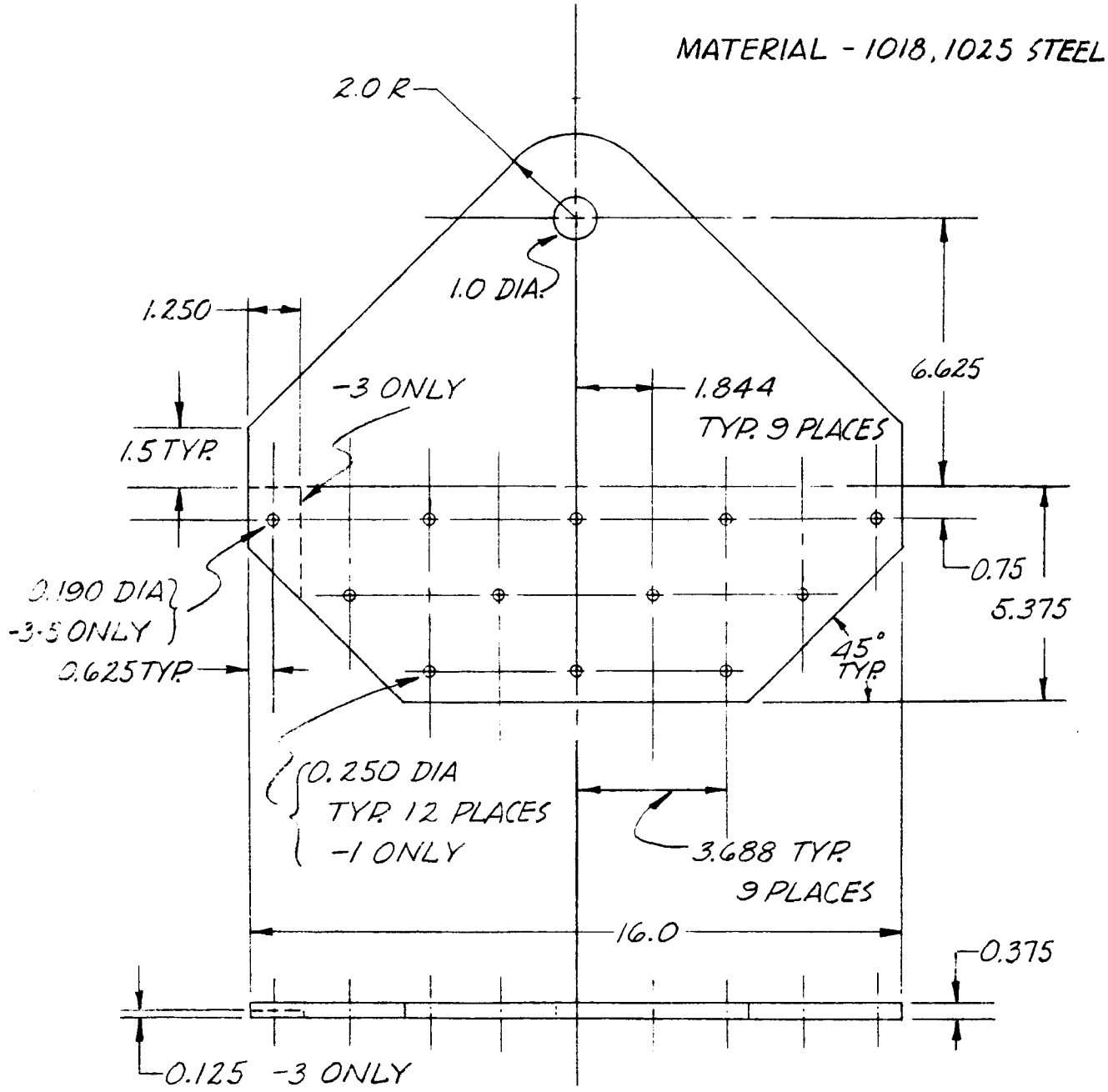

NOTE:

-1 BASIC PLATE AS SHOWN
-3 LEFT HAND AS SHOWN
-5 RIGHT HAND (OPPOSITE -3)

Figure 19. Loading Attachment, Pre-Strain Welding

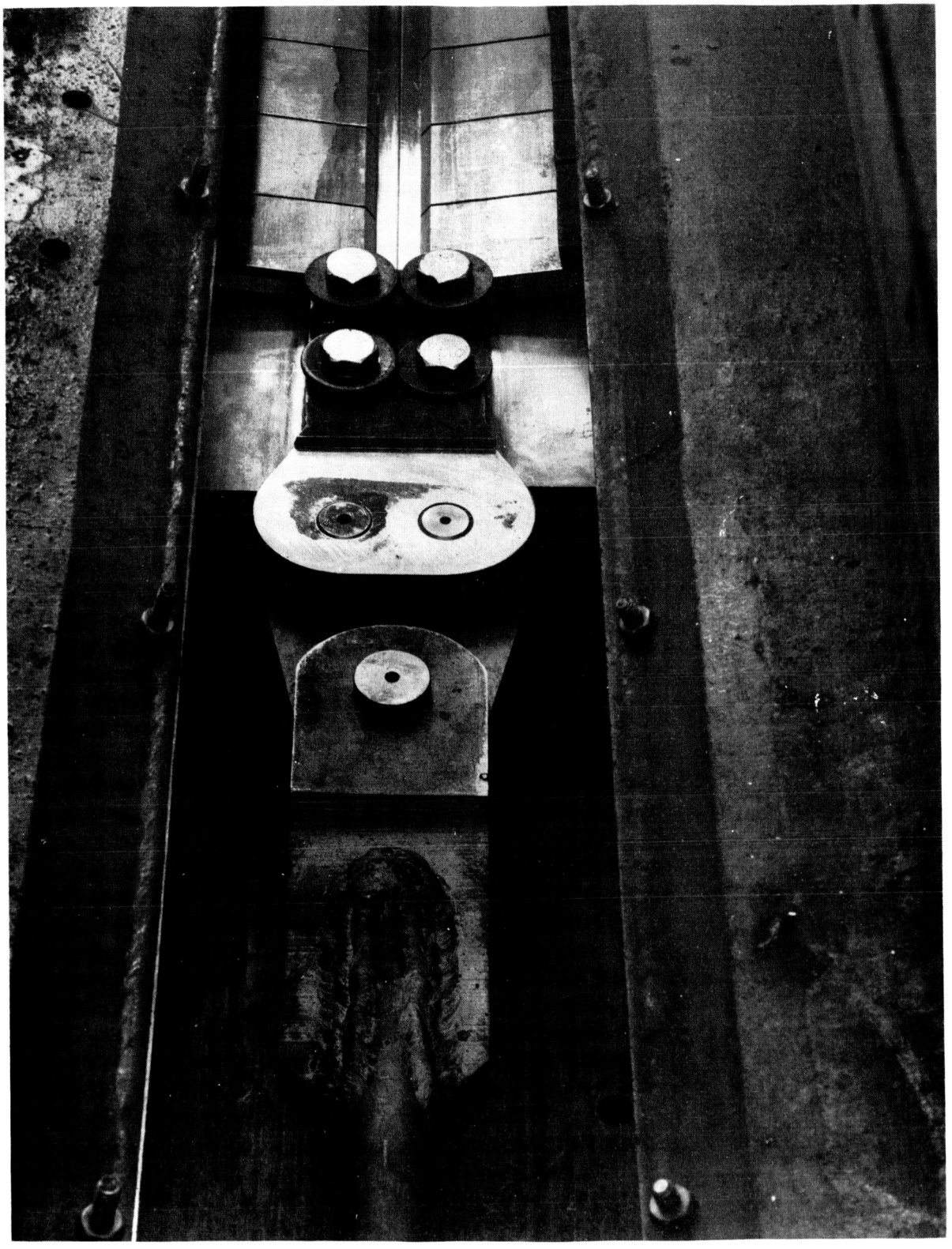

Figure 20. Attachment of Pre-Load Accessories to Test Panels

along the weld land at intervals (Figure 20a), the distance from the centerline being approximately 1/8-inch. Rough estimates proved this to be sufficiently accurate for these tests. For the remainder of the weldments, the corresponding pressure-gage reading was used to monitor the desired strain intensity level. The next step was attachment of pre-load applying clevises to the ends of the panels. The panels were clamped down with the hold-down fingers. Attach holes were then drilled, and reamed, and attachment bolts inserted and tightened. SR4 indicators were hooked up to the gages, and reference readings were taken with hold-down fingers resting lightly on those panels on which pre-strain gages were used.

Table 2. Mechanical Pre-Strain Weld Experimental Schedule

Weldment	Panel		Weld-Land Thickness-(Inches)	Approximate Pre-Strain Percent of Nominal Yield Strength		
				Station		
	Left	Right		12	24	36
4	4L	5R	0.250	0	0	0
5	7L	16R	0.190	0	0	0
7	15L	9R	0.250	30	20.5	17
8	12L	10R	0.250	30	20.5	17
9	2L	11R	0.250	30	20.5	17

Using hydraulic pressure, the panels were stretched until the desired percentage of nominal tensile yield strength was reached — indicated by the strain gages and/or pressure gage. Hold-down finger pressure was applied at this point and on the hydraulic cylinder locked to prevent movement. The parts were welded by the approved machine TIG method used in Saturn S-II production. Detail weld techniques and parameters are described in the Preliminary Work section of this report

The detail experimental procedures used in determining residual strains and distortions, which were used as criteria for evaluating the

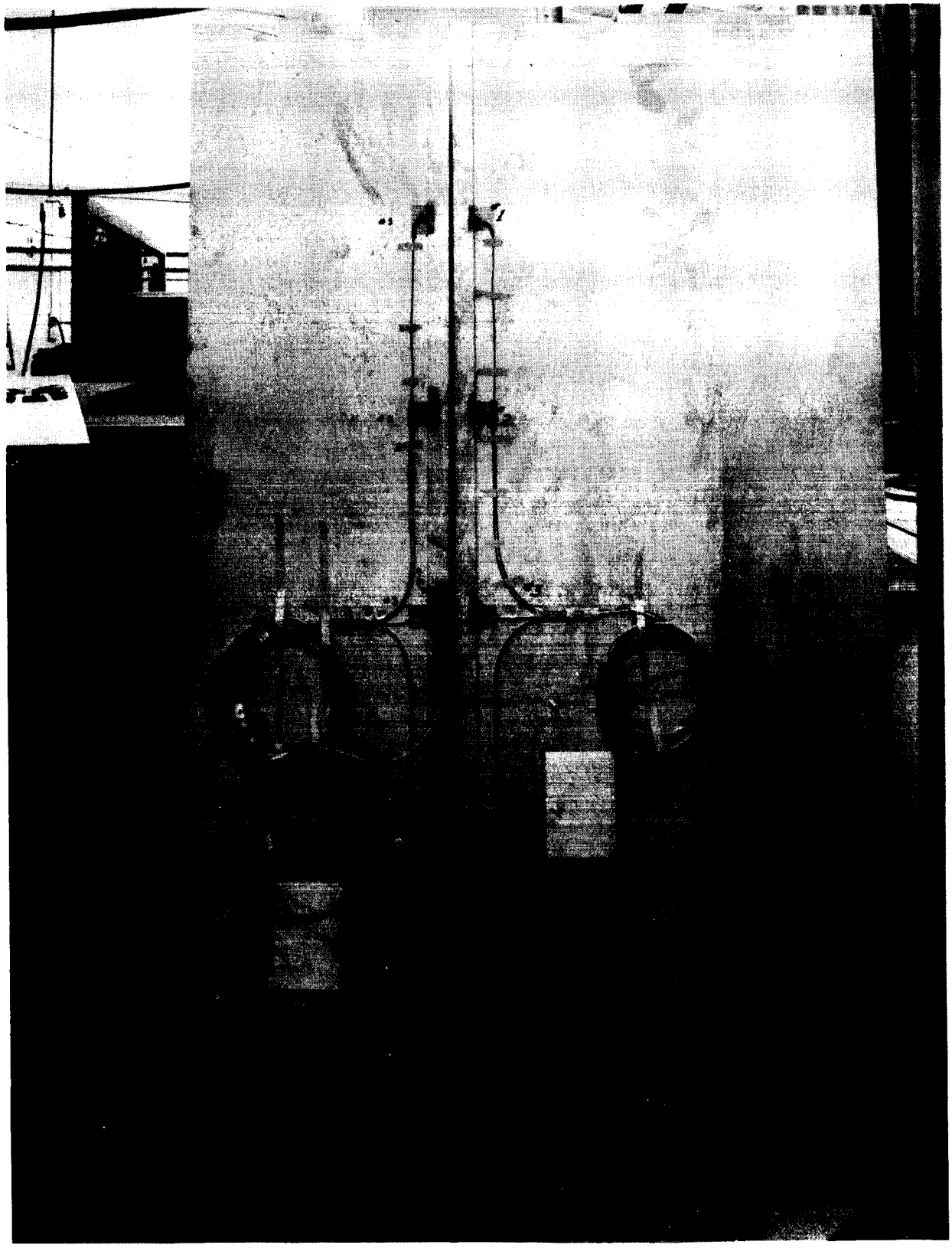

Figure 20a. Pre-Load Strain-Gage Placement

efficacy of mechanical pre-strain applications, are described in Residual Stress Determinations Section and the Distortion Section together with the results of these investigations. Tests establishing soundness of weld quality are described in the following paragraphs.

Weld Quality

X-ray Inspection

All weldments made during the program were inspected by X-ray and found to conform to Saturn S-II standards (NAA Specification MA0107-016E with the exception of the 0.165 weld-land thickness thermocoupled panels (Weldment 2) which showed some defects at the center weld line micro-probe locations. It had been expected that probes projecting into the weld puddle would interfere locally with weld quality; therefore, panels intended for determination of heat-flow patterns were not used for any simultaneous mechanical studies.

Metallurgical Evaluation

To assure further that pre-straining produces no detrimental effects on weld quality, tensile tests and metallographic examinations were conducted as follows.

Tensile Tests - Parent metal tensile specimens were machined from Weldment 4 in the locations shown in Figure 21. Since the weld area was being evaluated in this investigation, it was necessary to design a special weld tensile specimen to assure failure in the weld zone. The locations of the weld tensile specimens for Weldments 4 and 8 are shown in Figures 21 and 22. The properties determined for parent metal and weld specimens were as follows:

Parent Metal (Panel 4 Only)	Weld Specimens (All Weldments)
1. F_{tu}	1. F_{tu}
2. F_{ty} at 0.2-percent offset	2. Percent elongation in 1-1/2
3. Percent elongation in 2 inches	3. Percent elongation in 1-1/2 inches

The parent metal test values obtained from Control Weldment 4 (not strained prior to welding) met all the strength requirements for 0.250-inch 2014-T651 plate specified in NAA Specification MB0170-021. The tensile test data are shown in Table 3.

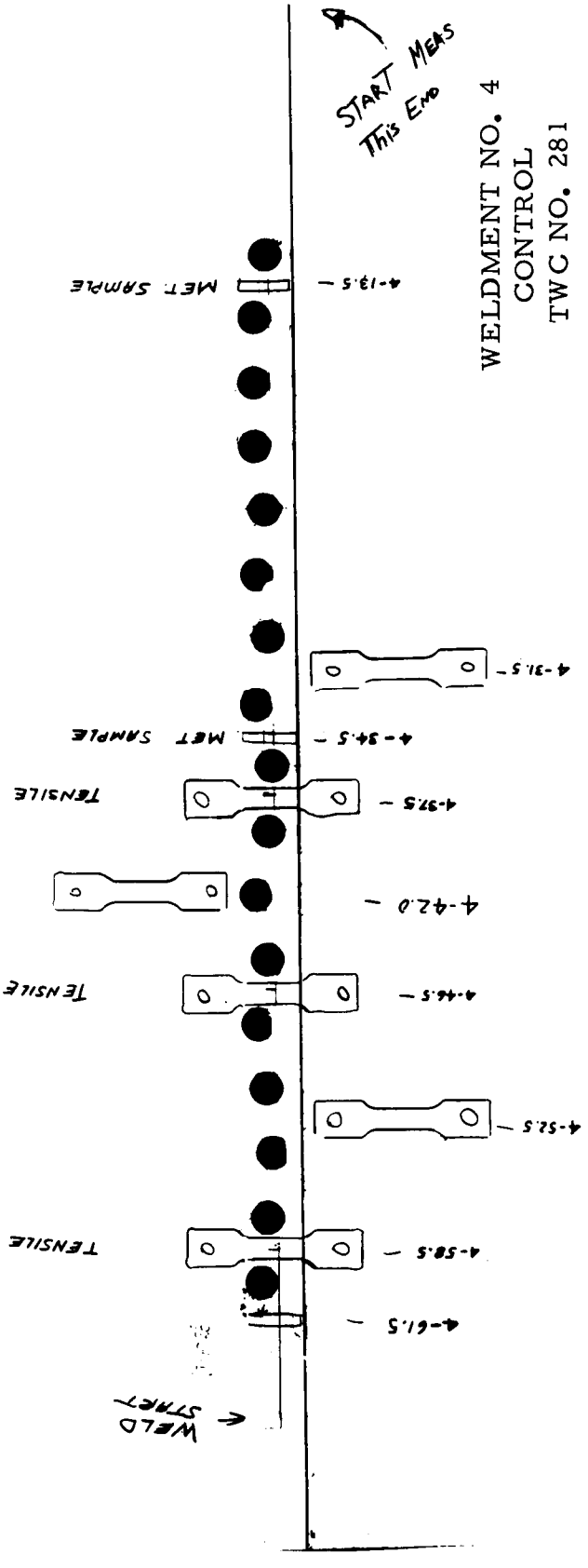

Figure 21. Location of Tensile and Metallographic Samples for Control Weldment No. 4 (Not Strained Before Welding)

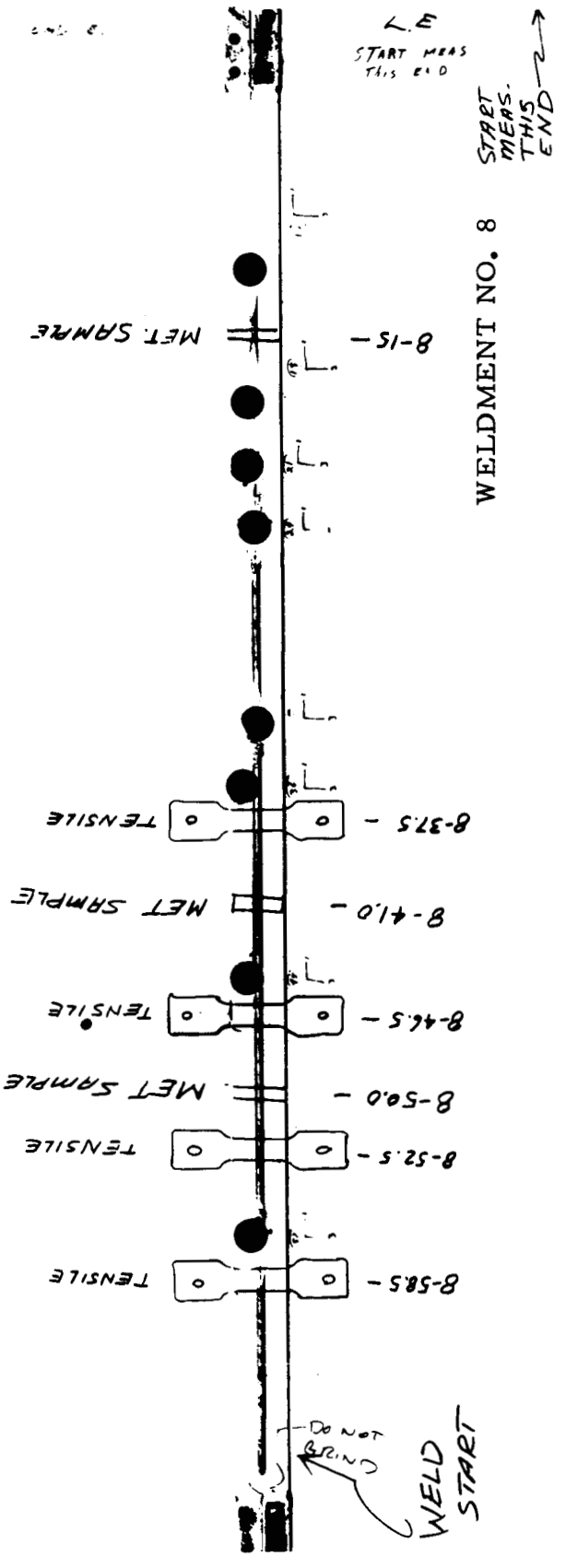

Figure 22. Location of Tensile and Metallographic Samples for Weldment No. 8 (Strained Before Welding)

Table 3. Parent Metal Tensile Test Data

Weldment	Weldment Location Station No.	F_{tu} ksi	F_{ty} at 0.2-Percent Offset, ksi	Percent Elongation in 2 Inches
4	31.5	69.0	61.0	10.5
4	42.0	68.8	61.7	9.0
4	52.5	68.6	61.4	10.5
MB0170-021 Minimum Require-ments		67.0	59.0	7.0

No appreciable difference was noted in the strength properties of the specimens from the pre-strained Weldment 8 and 9 and the Control Weldment 4 which was not strained prior to welding. The data met the minimum strength requirements for 0.250-inch weldments in Specification MA0107-016, and appeared to be typical as compared to other unpublished data obtained for 0.250-inch single pass weldments fabricated with 2319 filler wire. The weld tensile data are shown in Table 4.

Metallographic Examination - Representative samples were taken from each weldment for evaluation of macrostructure and microstructure of the weld and heat affected zone. The samples were examined at a magnification of 100X and 500X with the exact location of each specimen noted in Figures 21 and 22.

Selected typical macrostructures and microstructures of the weld-cross-sections are presented in Figures 23 through 27. There was no appreciable difference in structure between the samples taken from the pre-strained Weldments 8 and 9, and the Control Weldment 4. The macrostructure and microstructure of the samples examined appeared to be typical of 2014-T651 weldments now in actual production in Saturn S-II fabrication.

RESIDUAL STRESS DETERMINATIONS

Back-to-back biaxial strain gages were installed on Weldments 4, 5, 7, 8, and 9 in accordance with location layouts shown in Table 4. The locations perpendicular to the weld axis conform roughly to the center of the weld nugget, edge of the weld nugget, center of heat affected zone, and edge

Table 4. Weld Tensile Test Data

Weldment (1)	Weldment Location Station No.	F_{tu} ksi	Percent Elongation 1/2 In.	1-1/2 In.
4	37.5	43.9	8.0	2.7
4	48.5	46.0	11.0	3.7
4	55.5	51.2	16.0	5.3
Average		46.7	11.6	3.9
8	37.5	47.6	13.0	4.3
8	46.5	47.9	12.0	4.0
8	52.5	50.2	12.0	4.0
8	58.5	51.4	12.0	4.0
Average		49.2	12.2	4.0
9	17.0	48.9	12.0	4.0
9	37.5	47.6	11.0	4.0
9	46.5	49.0	12.0	4.0
9	52.5	46.7	9.0	3.0
9	58.5	47.7	11.0	4.0
Average		47.9	11.0	3.8

Notes: The status of the weldments listed are as follows:

Weldment 4 - Not strained prior to welding
Welement 8 - Pre-strained prior to welding
Weldment 9 - Pre-strained prior to welding

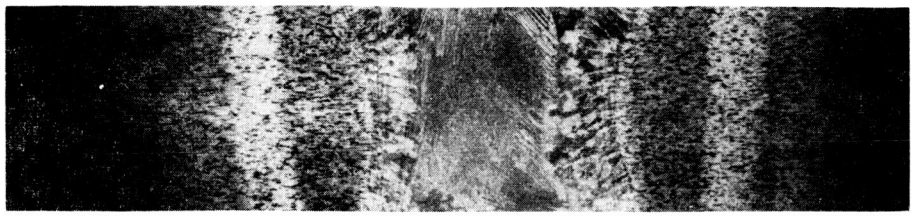

A. Metallographic Sample No. 4-13.5 (Magnification 5X)

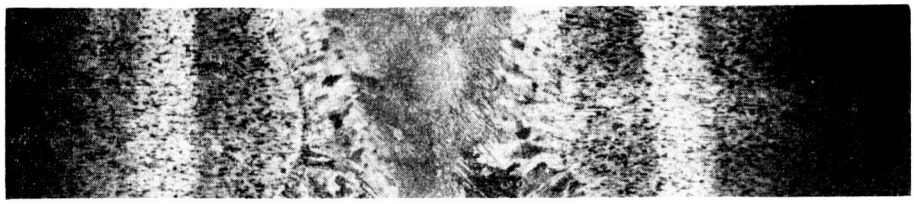

B. Metallographic Sample No. 4-34.5 (Magnification 5X)

Figure 23. Photomacrographs of Weld Cross-Sections Taken from Control Weldment No. 4 (Samples Etched with Keller's Reagent)

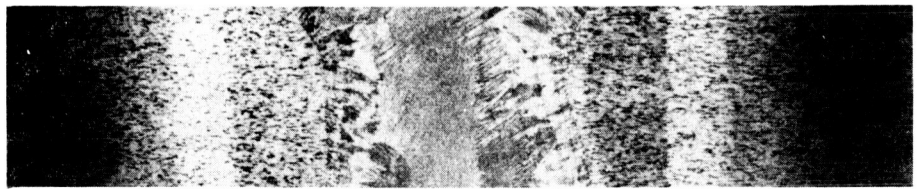

A. Metallographic Sample No. 8-15 (Magnification 5X)

B. Metallographic Sample No. 8-41.0 (Magnification 5X)

Figure 24. Photomacrographs of Weld Cross-Sections Taken from Pre-Strain Weldment No. 8 (Samples Etched with Keller's Reagent)

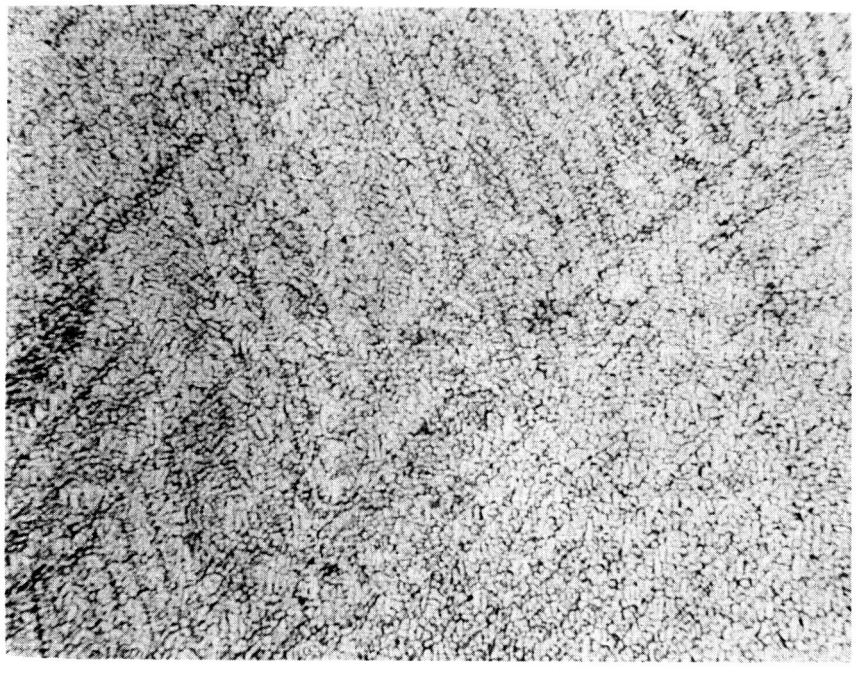

A. Center of the Weld of Sample 4-13.5 (Magnification 100X)

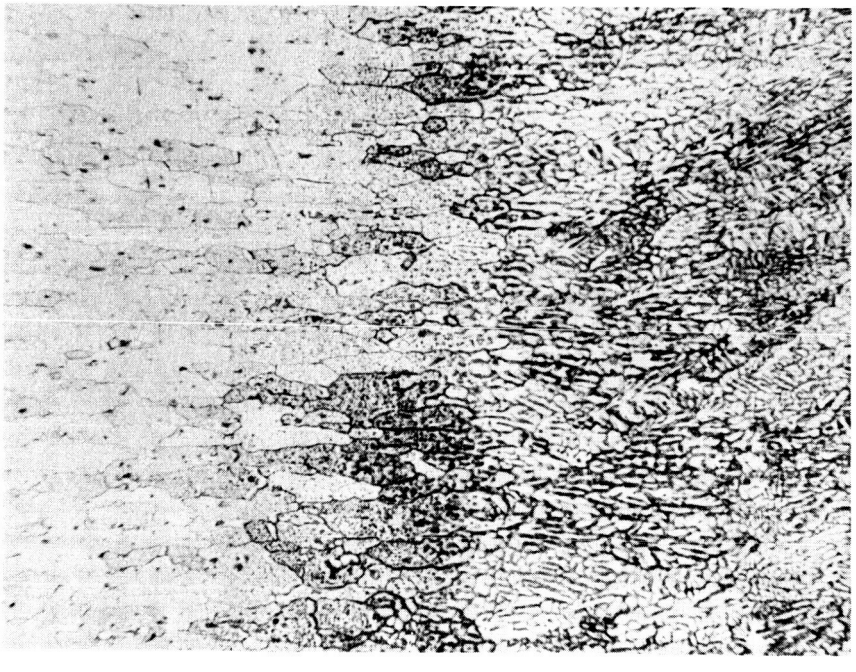

B. Weld Fusion Line of Sample 4-13.5 (Magnification 100X)

Figure 25. Photomicrographs of the Weld Cross-Section of Control Weldment No. 4, Metallographic Sample 4-13.5 (Sample Etched with Keller's Reagent)

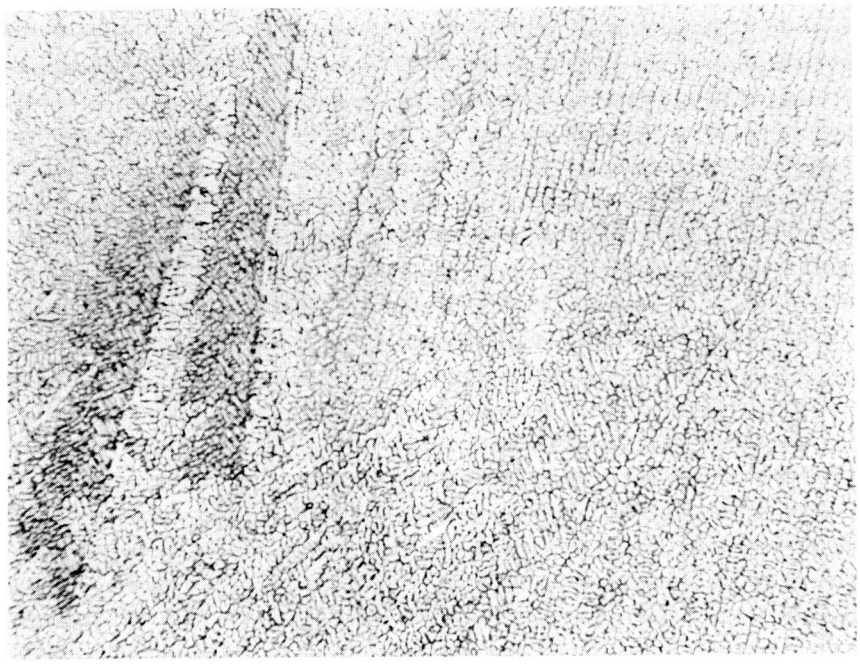

A. Center of the Weld of Sample 4-34.5 (Magnification 100X)

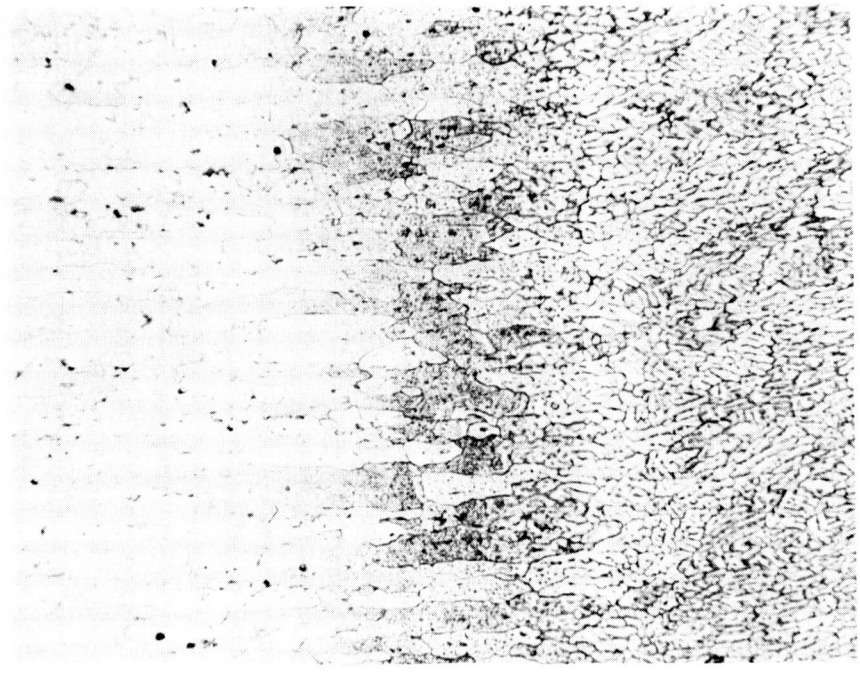

B. Weld Fusion Line of Sample 4-34.5 (Magnification 100X)

Figure 26. Photomicrographs of the Weld Cross-Section of Control Weldment No. 4, Metallographic Sample 4-34.5 (Sample Etched with Keller's Reagent)

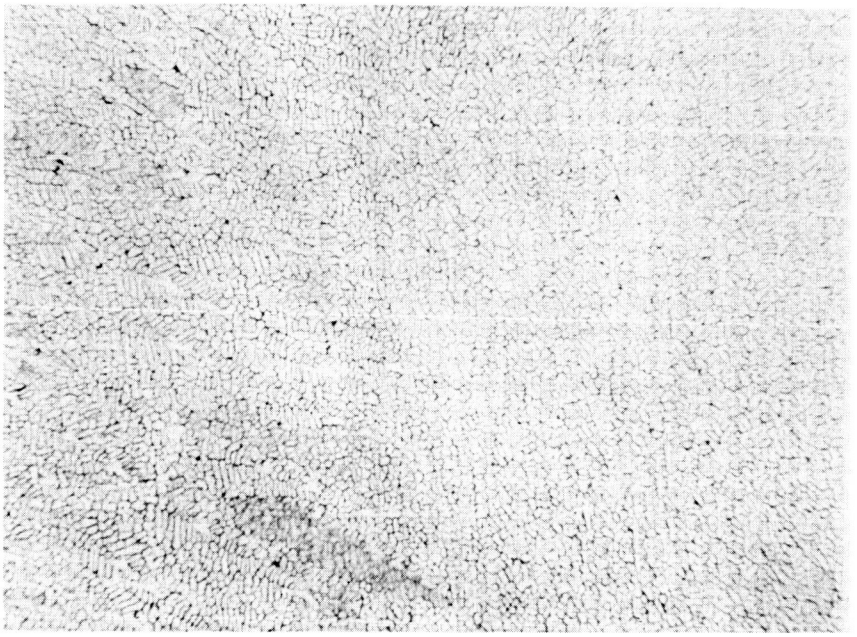

A. Center of the weld of Sample 8-15.0 (Magnification 100X)

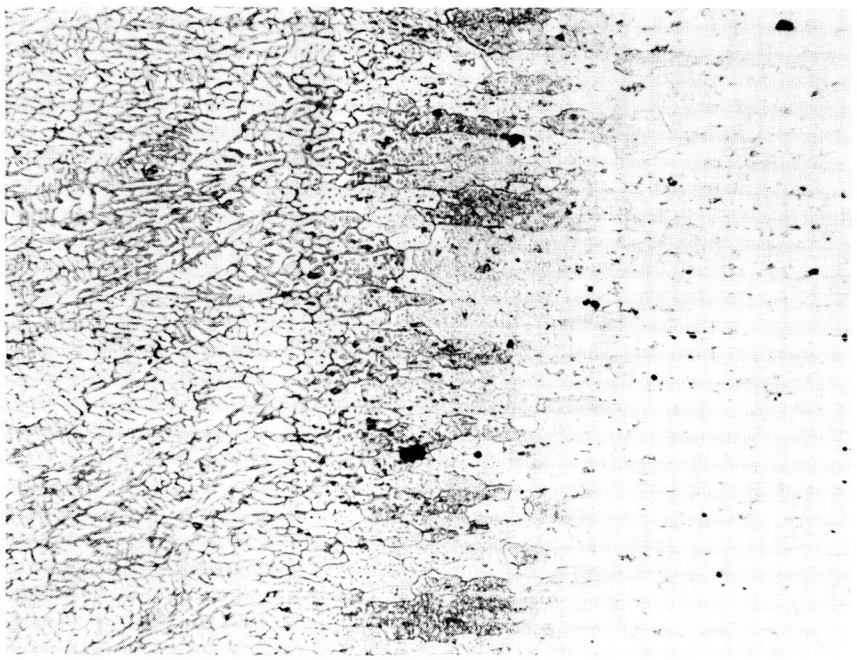

B. Weld Fusion Line of Sample 8-15.0 (Magnification 100X)

Figure 27. Photomicrographs of the Weld Cross-Section of Pre-Strain Weldment No. 8, Metallographic Sample 8-15.0 (Sample Etched with Keller's Reagent)

of heat-affected zone as determined from typical micrograph readings. The strain gages are identified by station location with dash numbers 1 through 4, as follows: -1 (parallel to the longitudinal axis); -3 (parallel to the transverse axis on the upper or weld head side of the weldments); and -2 and -4 (on the lower or backing bar side of the weldment). Locations -2 and -4 are on the opposite side of the weldment from -1 and -3, respectively. Final differential strain readings, obtained after cutting 1.4-inch-diameter circles by electric discharge machining (EDM) (Figures 28 and 29) about the instrumented areas, were recorded. Conversion of strain gage readings to residual stresses are shown in Tables 5 and 6, which also identify their location matrix. They were computed from the following equations, applying a minus sign to the read relaxed strains:

$$1. \quad \sigma_x = \frac{E}{1-\nu^2}(e_x + \nu e_y)$$

$$2. \quad \sigma_y = \frac{E}{1-\nu^2}(e_y + \nu e_x)$$

Graphical representations are shown in Figures 30 and 31. Analysis of the data indicates a very definite and substantial reduction of residual stresses due to applied pre-loads — even in the non-optimized center section of the weldments.

Taking longitudinal residual stress in the most highly affected weld nugget area (coordinates zero and 0.175 inches from weld centerline) from Station 21 through Station 51 gave the most meaningful criteria. It is found that the composite average of such residual stress in Weldments 7, 8, and 9 (8.4 ksi) is reduced by about 27 percent as compared with Control Weldment No. 4 (11.4 ksi) and that it exhibits less scatter (range, 4.5 to 10.7 ksi) than the control weldment (6.1 to 16.0 ksi).

Extrapolation of data trends indicates that the optimum pre-load will occur at a weld-land stress level in the neighborhood of 35 to 40 percent of nominal yield strength, corresponding to a station location of about 6 inches from the ends of the weldments.

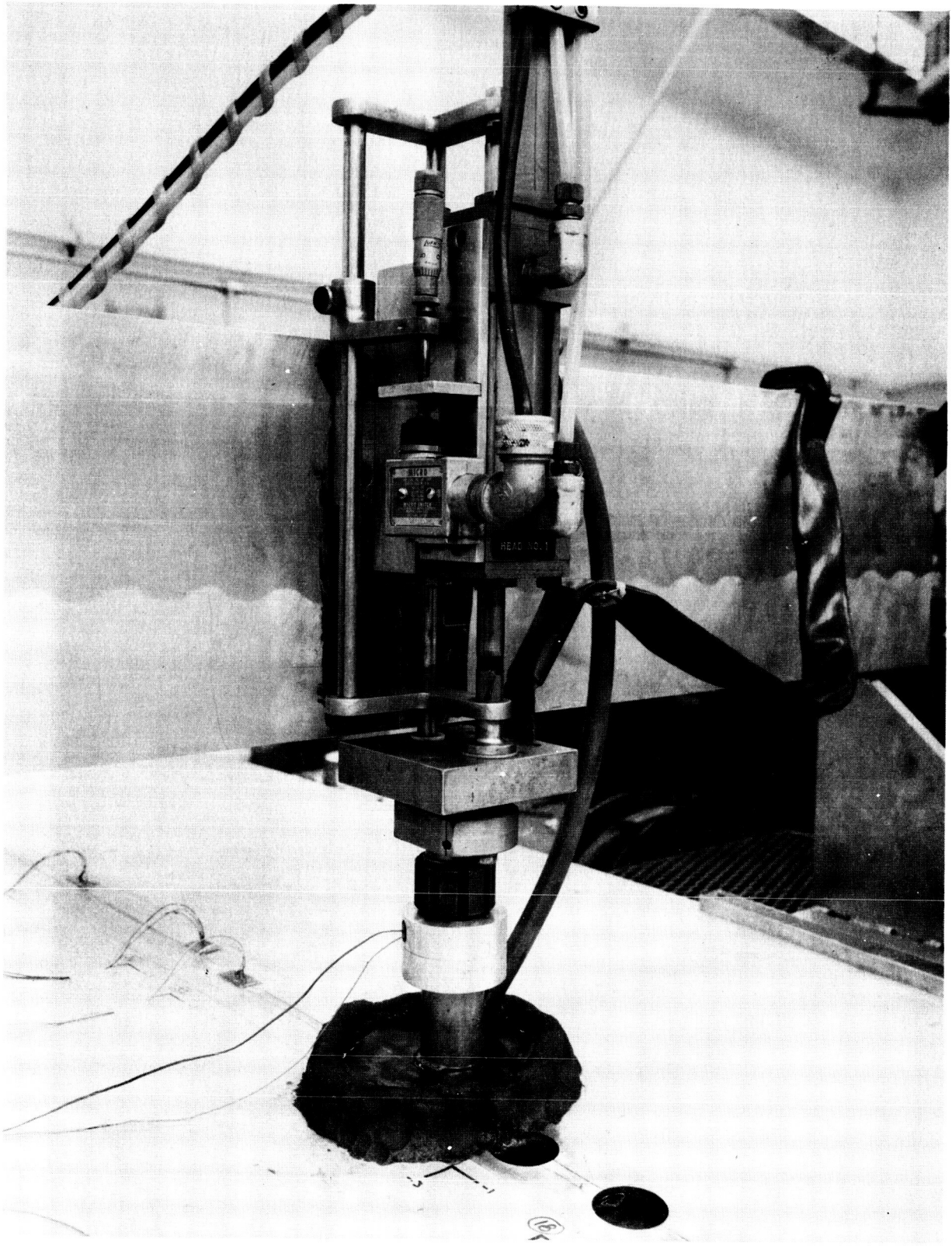

Figure 28. Removing Strain-Gage Specimens by EDM Operation

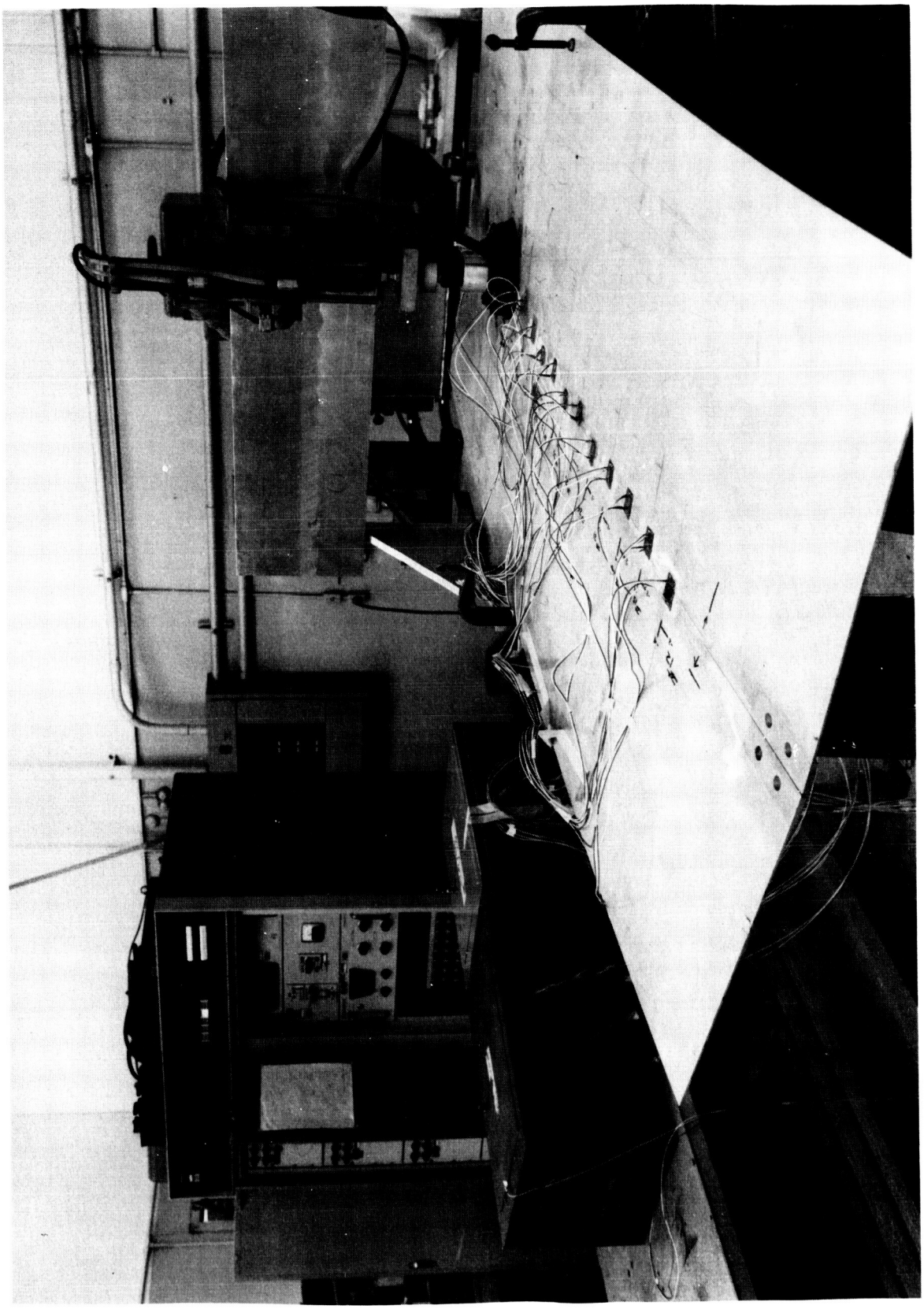

Figure 29. Residual Strain-Gage Recording During EDM Operation

Table 5. Transverse Residual Stresses (ksi)

Station (Inches from pull end)	Weldment Number				
	4	5	7	8	9
12	* -1.4	** -1.8	* 1.5	** 1.2	†† -0.7
15	† -0.2		† -1.5		
18	†† -0.7	** -2.4	†† 0.6	** 0.1	
21	† -0.4	* -0.7	† -0.5	† -1.5	** -4.2
24	* 0	† N.R.	* 3.7	* 1.3	† -2.4
27	†† -0.7		†† -0.3		
30	* -2.0		* -1.4		† -0.3
33	† 0	* -1.2	† -1.1	* -1.8	†† 0.6
36	* -2.4	†† -0.7	* 10.1	†† -0.6	** 0.5
39	** -2.4		** -1.1		
42	†† 0.7		†† N.R.		
45	** -0.3	†† -0.4	** -1.7	†† -0.6	* -1.4
48	†† 0.5		†† -1.5		
51	** 0.2		** N.R.		
54	* 4.1		* -3.2		
57	** 0	† 4.8	** -3.8	† 4.2	* N.R.
60	†† -0.5		†† -2.6		

Legend: (distance in inches from weld center)		Weldment Nos. 4, 7, 8, 9	Weldment Nos. 5
	*	0	0
	**	0.175	0.160
	†	0.400	0.355
	††	0.625	0.550

Table 6. Longitudinal Residual Stresses (ksi)

Station (Inches from pull end)	Weldment Number				
	4	5	7	8	9
12	* -0.6	** 4.8	* 3.4	** 3.4	†† 1.9
15	† 8.4		† 3.0		
18	†† 2.1	** 5.1	†† 2.6	** 3.8	
21	† 9.2	* 8.5	† 4.9	† 4.0	** 8.6
24	* 10.4	† N.R.	* 10.7	* 4.5	† 3.4
27	†† 4.2		†† 2.8		
30	* 9.2		* 9.6		† 5.1
33	† 1.9	* 5.7	† 6.0	* 8.1	†† 1.8
36	* 16.0	†† 0.2	* 10.7	†† 3.2	** 7.4
39	** 6.1		** 7.5		
42	†† 5.1		†† N.R.		
45	** 11.[illegible]	†† 0.5	** 9.7	†† 2.0	* 7.2
48	†† [illegible].6		†† 2.1		
51	** 15.1		** N.R.		
54	* 9.9		* 6.8		
57	** 13.8	† 1.6	** 4.8	† 3.6	* N.R.
60	†† 4.3		†† 5.1		

Legend: (distance in inches from weld center)		Weldment Nos. 4, 7, 8, 9	Weldment Nos. 5
	*	0	0
	**	0.175	0.160
	†	0.400	0.355
	††	0.625	0.550

Strain gage test data were processed by the same method used to reduce the Saturn S-II common bulkhead measurement data. Basically, the method involves a systematic check of data by:

1. Comparing the absolute positive value order set of gage strains versus x and y position

2. Comparing the algebraic value order set of gage strains versus x and y position

3. Comparing the upper and lower surface back-to-back gage difference set versus x and y position

4. Comparing the longitudinal versus lateral set ratios versus x and y position

5. Comparing items 1 through 4 against the measured distortion of the test panels as to magnitude and rates of change of magnitude versus x and y position

6. Perspective cross plotting of the residual average longitudinal stresses. (the average transverse stresses proved to be low in value and random sign, as expected, and was not plotted)

It was impossible to provide the usual data check of summation of forces and moments to equal zero because the strain gage pattern was concentraded near the weld since there were no gages located on a full section line, either longitudinally or transversely to the test panel. In addition, maximum use of the principles of symmetry was made. This analytical step seemed justified since the thermal patterns were completely uniform along the weld path (except for the weld start and termination).

Corrections applied as indicated from data trend plotting are clearly marked as such in Figures 30 and 31.

The test data indicate that the temperature-time functions of strain occurrence by-passed by the strip model described in the Mechanics Analysis section should be taken into account, not only in plane of the material, but with thickness as well. The perspective plots indicate that proper application of pre-strain stress welding can significantly reduce, or eliminate, residual stresses. The slope of the longitudinal stress profile shows that the stress surface would have penetrated the zero-stress reference plane near Station 6 corresponding to an expected optimum pre-load level of 35 to 40 percent of nominal yield strength of the parent material.

DISTORTION

Distortion resulting from welding was determined by measuring displacement of grid points on the surface of the test panels before and after welding.

A grid (Figure 32) was marked on the surface of the panels before welding, and, using a flat surface and height gage, the displacement from a flat plane was recorded.

The panels, after being joined by welding, were re-positioned on the surface table and vertical displacement of the grid points was again recorded.

The dimensions given in Tables 7 through 11, represent amount of movement of panels at the grid points. The tables are arranged representing the grid points as they would appear in a plan view of the weldment. The horizontal line across the center of the tables represents the weld bead between the two panels. Minus readings indicate that the point was moved in a negative or downward direction.

Amount of movement was developed by taking the difference between the before and after vertical displacement readings of each grid point.

The dimensions after welding were compensated to provide a common base index point on each panel, that is, before and after welding. In the charts, this base reference point is indicated by zero recorded displacement.

The results, comparing non-pre-strained Weldment No. 4 with analogous pre-strained Weldments Nos. 7, 8, and 9, show a substantial reduction of weld-induced distortion by mechanical pre-load application.

Reversal of warpage direction from the control weldment in both dihederal and camber was observed when pre-straining was employed.

This condition is indicative of sensitivity of the weld shrinkage strain phenomenon to the thermal profile normal to the plane of material. For a non-pre-strained weld, the chill bar side of the weld solidifies (for 1/4-inch material) approximately 1 to 1-1/2 times the material thickness sooner than the torch side. The parent metal radius of curvature (thermally) is away from the torch. Since the bottom surface attains a material allowable sooner than the torch side, the shape is set. The compressive upset of the lower surface occurring during heating is not relieved as much on cooling as the top surface. Pre-straining the weld, however, more nearly equalizes the stress relief by tensile yielding, permitting the higher temperature differential of the torch side to shrink the material further than the cooler

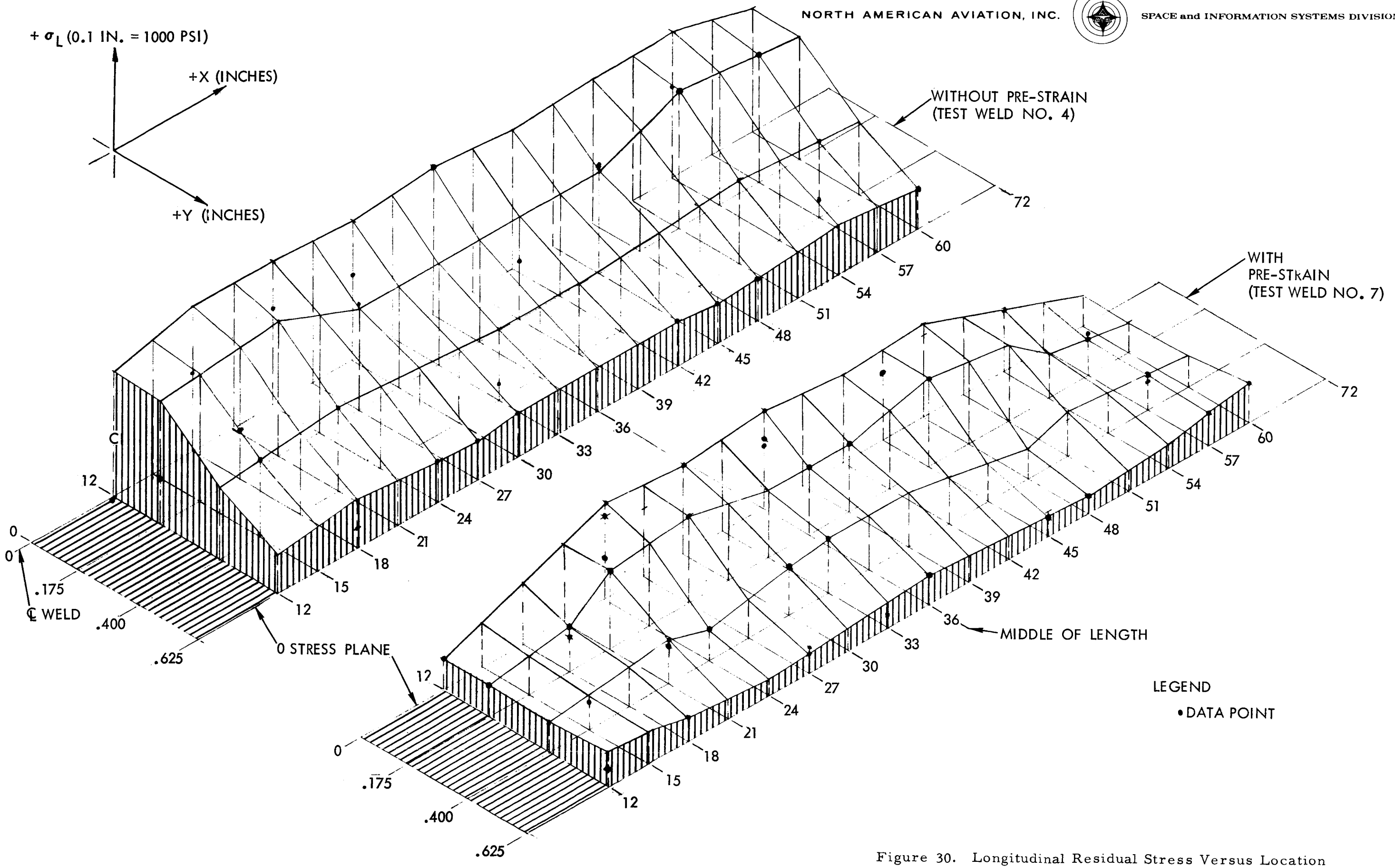

Figure 30. Longitudinal Residual Stress Versus Location

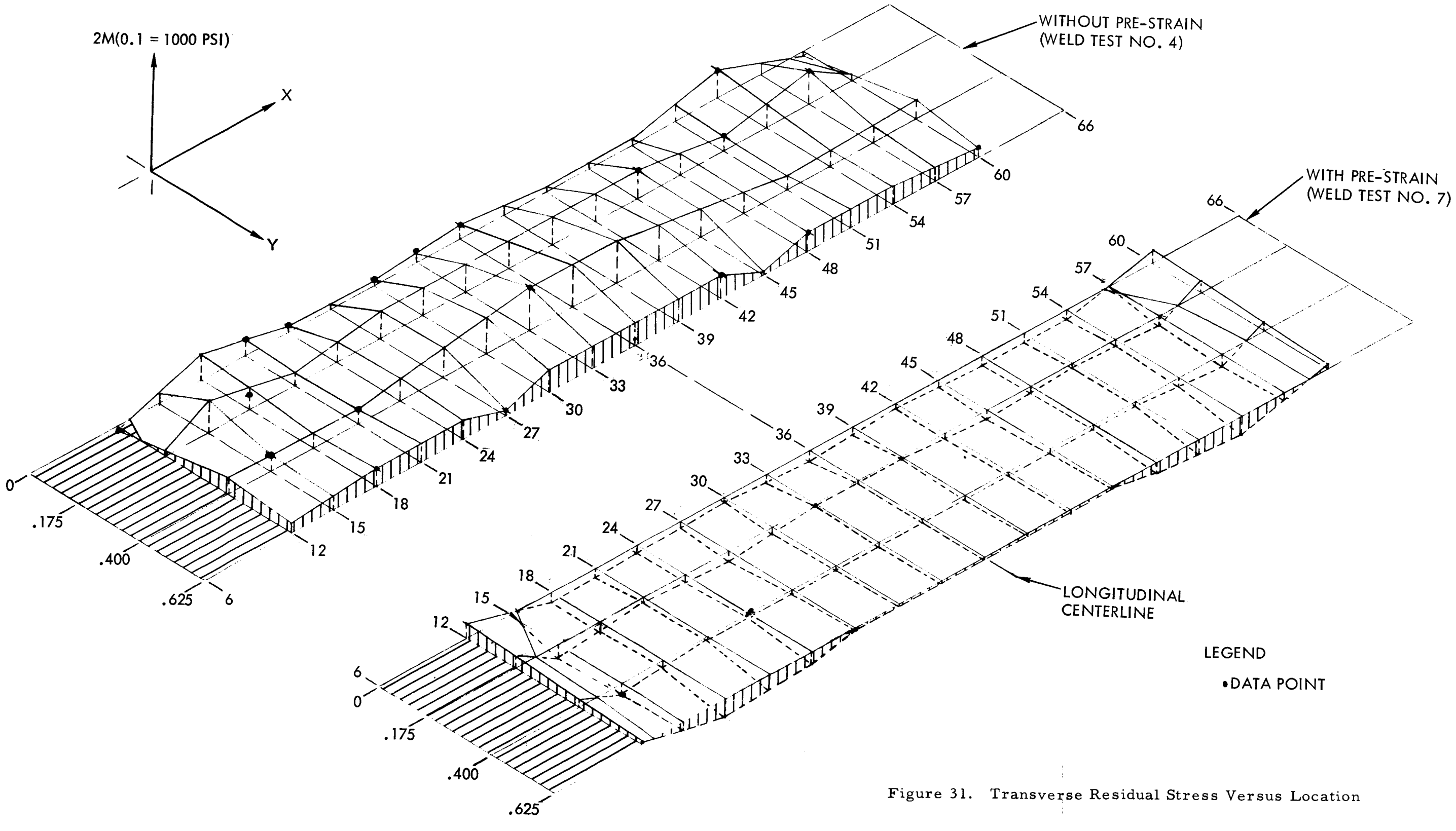

Figure 31. Transverse Residual Stress Versus Location

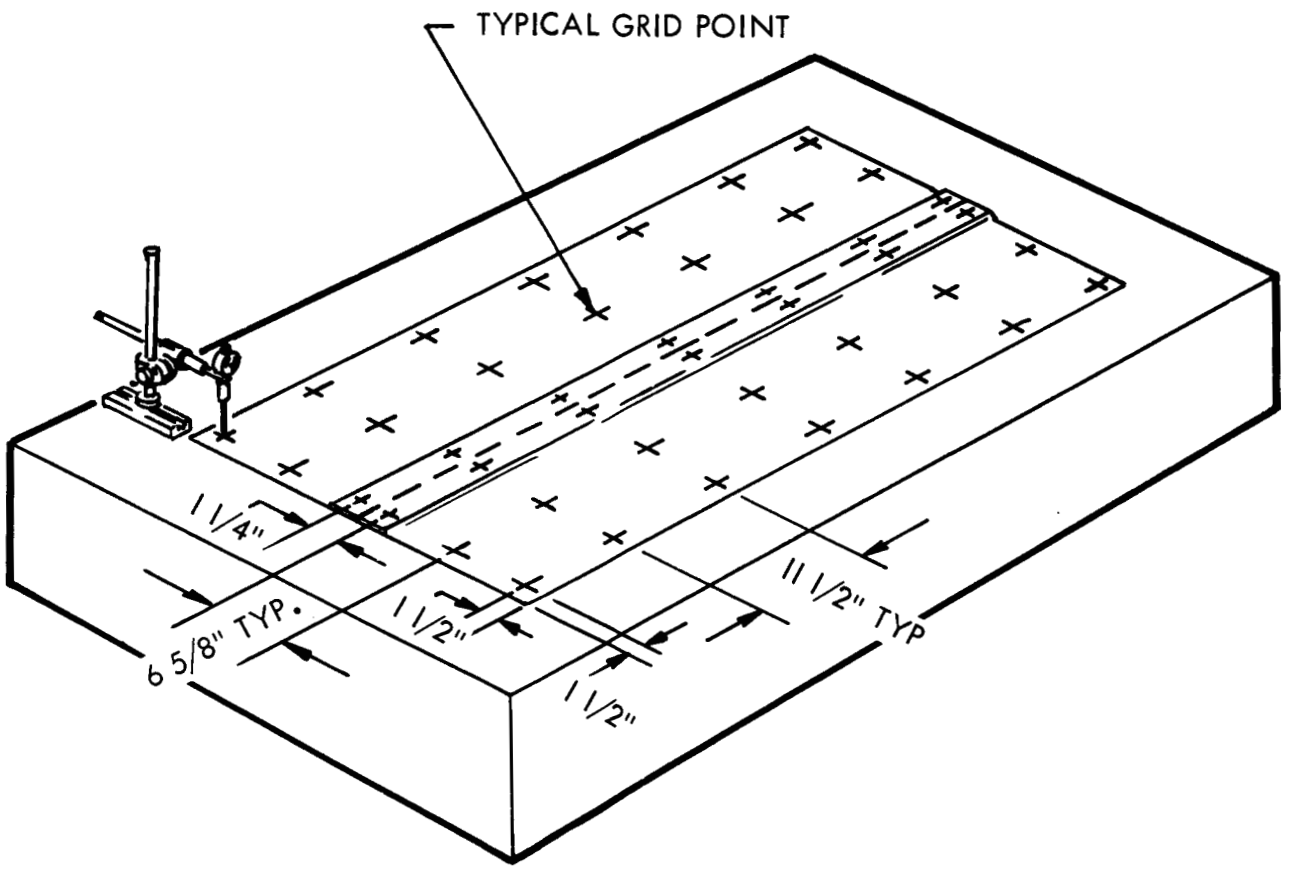

Figure 32. Measuring Distortion of 32 - X 72 -Inch Test Weldment

Table 7. Weldment No. 4

Panel No. 5	-1.379	-0.531	-0.068	0.004	-0.053	-0.453	-1.322
	-1.500	-0.614	-0.125	0	-0.093	-0.573	-1.550
	-1.588	-0.657	-0.189	-0.047	-0.187	-0.694	-1.756
Panel No. 4	-1.553	-0.649	-0.182	-0.044	-0.185	-0.694	-1.743
	-1.405	-0.577	-0.116	0	-0.110	-0.603	-1.589
	-1.214	-0.455	-0.040	0.019	-0.049	-0.480	-1.412

Table 8. Weldment No. 5

Panel No. 16	-0.800	-0.022	0.039	0.048	0.040	-0.118	-0.687
	-1.105	-0.272	-0.044	0	-0.033	-0.278	-1.009
	-1.407	-0.523	-0.225	-0.136	-0.215	-0.517	-1.320
Panel No. 7	-1.413	-0.535	-0.240	-0.151	-0.230	-0.528	-1.347
	-1.085	-0.291	-0.047	0	-0.043	-0.261	-1.686
	-0.766	-0.126	0.015	0.013	0.006	-0.126	-0.738

Table 9. Weldment No. 7

Panel No. 9	0.527	0.047	-0.049	-0.057	-0.256	-0.008	0.309
	0.852	0.265	0.052	0	0.030	0.189	0.678
	1.142	0.403	0.126	0.036	0.095	0.300	0.952
Panel No. 15	1.165	0.425	0.147	0.052	0.115	0.303	0.953
	0.875	0.271	0.056	0	0.035	0.194	0.729
	0.532	0.073	-0.012	-0.019	-0.019	0.032	0.404

Note: All dimensions are in inches.

Table 10. Weldment No. 18

Panel No. 10	0.774	0.089	0.038	-0.053	-0.043	0.037	0.477
	1.137	0.328	0.073	0	0.047	0.254	0.857
	1.600	0.470	0.161	0.040	0.102	0.381	1.401
Panel No. 12	1.620	0.460	0.142	0.037	0.105	0.374	1.359
	1.157	0.326	0.078	0	0.043	0.289	1.111
	0.770	0.060	-0.058	-0.071	-0.061	0.067	0.788

Table 11. Weldment No. 9

Panel No. 11	0.550	0.020	-0.050	-0.076	-0.070	0.055	0.653
	0.892	0.250	0.065	0	0.040	0.250	0.934
	1.396	0.409	0.160	0.083	0.160	0.388	1.332
Panel No. 2	1.396	0.390	0.140	0.071	0.146	0.377	1.270
	0.895	0.252	0.050	0	0.049	0.229	0.802
	0.572	0.019	-0.075	-0.088	0.083	-0.023	0.435

Note: All dimensions are in inches.

(estimated 100 F to 300 F) lower surface. An analytical model considering only the temperature differentials involved would predict that all flat butt welds should distort toward the torch in camber and dihedral. The unit cube model described in the Mechanics Analysis section fully predicts the test distortion qualitatively, and closely agrees quantitatively.

THERMALLY APPLIED PRE-LOAD PRE-STRAIN

EXPERIMENTAL PROCEDURE

Test specimens of 2014-T651 aluminum alloy were machined and contoured to simulate Saturn S-II LH_2 cylinder sections and fuel line fitting inserts. From test specimens available, three were chosen. The shrink factors, or planned interference fit for the nominal 17-inch weld circle diameter, are as follows:

Specimen No. 1 - 0.019 - 021 inches
Specimen No. 2 - 0.042 - 054 inches
Specimen No. 3 - 0.053 - 058 inches (recommend in present S-II practice)

Test inserts were chilled by immersion in LN_2 at -320 F for 15 minutes, placed into LH_2 cylinder sections immediately, and heated by lamps to expand into a tight fit and remove any trace of moisture. The parts were welded by the approved TIG method used in Saturn S-II production. Figure 33 illustrates the Weldment Geometry. The detail experimental precedures used in determining residual strains and distortions are described in the Residual Stress Determinations and Distortions section together with the results of these investigations.

Weld Quality

Analysis of welded specimens by X-ray and attendant physical property tensile coupon tests showed they met requirements of Specification MA0107-016E.

RESIDUAL STRESS DETERMINATIONS

Biaxial strain gages were centered, back to back, on the weld nugget at two locations (9:00 and 12:00) of Weldments 1 and 2, and 9:00 and 6:00 on Weldment 3 when fire caused loss of its 12:00 gages. Gage legs 2 and 4 were located radially and 1 and 3 circumferentially, the 1-2 rosette being on the weld crown (concave) side of the specimens (Figure 33).

Initial strain gage readings were taken prior to clamping specimens into position for cutting.

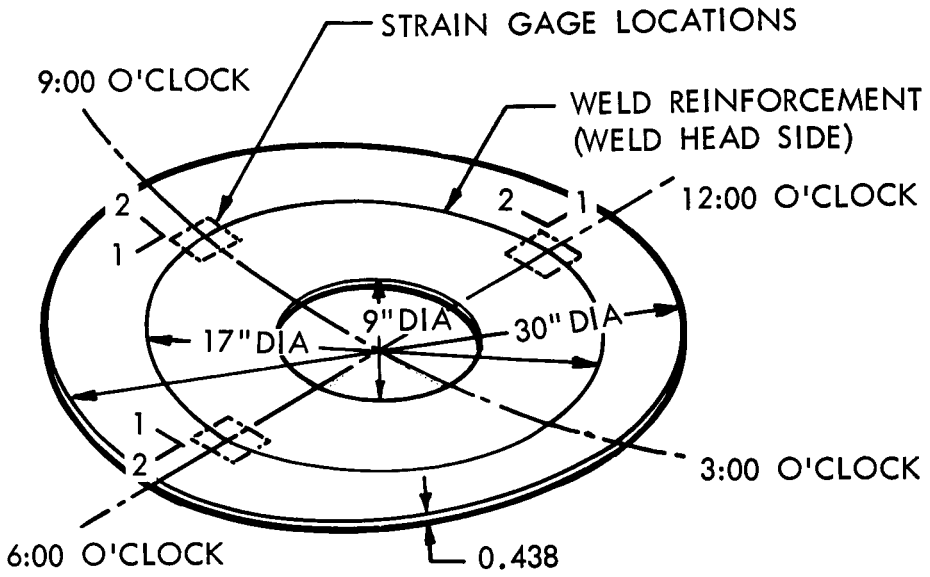

Figure 33. Circular Weldment Geometry

The specimens were first placed on a flat surface with Gages 3 and 4 facing up and the strain indicator was "zeroed." The specimen was then turned over and with Gages 3 and 4 facing down, the readings were checked. No change from the previous reading was discernible.

Water immersion of weldments resulted in no discernible "zero" shift. The specimens were placed on edge and strain readings were observed. There was no change from the previous readings.

An electric discharge erosion cutting tool was used to make 1.4-inch-diameter circular cutouts about the instrumented areas.

Residual stresses were computed from the following equations, applying a minus sign to the read relaxed strains:

$$\sigma_\theta = \frac{E}{1 - \nu^2} (\epsilon_\theta + \nu \epsilon_r)$$

$$\sigma_r = \frac{E}{1 - \nu^2} (\epsilon_r + \nu \epsilon_\theta)$$

The results are:

Circular Weldment No.	Position	$\sigma_{\theta_{rs}}$ ksi	$\sigma_{r_{rs}}$ ksi
1	9:00	+ 2.27	+15.3
	12:00	+14.7	+ 8.4
2	9:00	+11.4	+ 0.32
	12:00	+13.8	+ 1.67
3	9:00	+13.7	+ 8.7
	6:00	+13.8	+ 2.8

Inspection of results indicates that the measured circumferential residual stresses do not follow the expected pattern of increasing quality from Weldment 1 to Weldment 3. It is surmised that an unfortunate location was chosen for the circumferential strain gages. Placement on an intended weld nugget center for these specimens is extremely sensitive because of the differential circumferential stress levels existing between inner and outer annulus. A slight mislocation may therefore have a great effect on the strain result obtained.

In contrast, the radial residual stress readings conform largely to the expected pattern. Although the readings of Weldment 2 at the two comparison locations chosen are somewhat lower than those of Weldment 3, in view of the overlap in shrink-fit factors, they are sufficiently close to be considered reasonable and to allow the conclusion that an appreciable reduction in residual stress is attainable by thermal pre-load pre-straining of closed weldments.

DISTORTION

The amount of weld-induced distortion was measured by checking radius in the circumferential direction and flatness in the axial direction against the nominal configuration, fitting a cylinder of 198-inch radius. These distortions were checked before and after welding. It was noted that welding caused the single contoured disks to become saddle-shaped.

Measurements after welding indicated the following changes:

Test Part	Radius (inches)	Transverse Distortion (inches)
1	80	7/32
2	95	7/32
3	125	7/32

Figure 34 illustrates the method of measuring distortion.

Although distortion still exists, even for the recommended interference, it can be concluded that application of thermally induced (shrink fit) pre-loads are beneficial, and that this controlled experiment indicates that presently established S-II practices are probably not too far from attainable optimum.

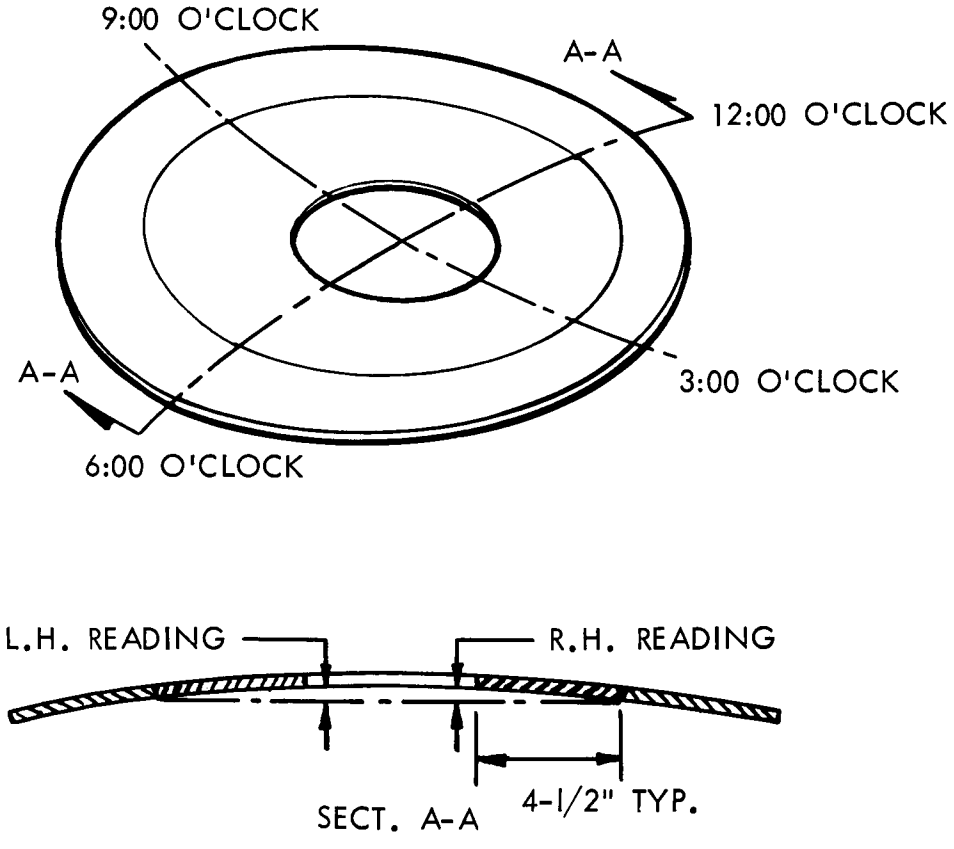

Figure 34. Circular Weldment Distortion

MECHANICS ANALYSIS

MECHANICS OF PRE-STRAIN WELDING

Normally an analysis in mechanics involves the study of forces and motion without regard or need to know the agent that produces the forces and motions. A study of thermodynamics related to the behavior of solids and liquids when subjected to temperature variations and heat flow also is performed independent of mechanics considerations. Properties of material and relations of stress and strain can be studied in a similar independent fashion. The industrial process of fusion welding with regard to distortion and residual stresses is better understood when the discipline studies are combined with emphasis placed on cause and effect of interdiscipline considerations. The mechanics of pre-strain welding therefore brings these various study disciplines to bear as required to obtain a better understanding of the process of welding.

When a small element of material (i.e., a unit cube), is exposed to a cycle of heating and cooling and the cycle is investigated in detail, the pertinent observations described in the following paragraphs can be made.

If the element is allowed to expand and contract as required by material properties, the cycle is reversible. With the exception of metallurgical factors such as recrystallization or irreversible phase changes, the sequence of events that occurs during heating occurs in reverse order during cooling, with recovery of the initial condition. The temperature-time heating cycle in general may degrade the strength properties of materials so exposed. There may be some residual stress on a microscopic scale associated with the crystal structure but none significant to the structural analysis discipline.

If a unit cube is exposed to a similar thermal cycle and it is prevented from expanding as required by material properties (i.e., some of the six faces of the unit cube are constrained to zero deflection) the cycle reversibility may be destroyed and initial condition recovery may be prevented.

Detailed study of the second cycle reveals:

1. There is a thermal cycle involving the temperature rise of the unit cube from ambient temperature to critical temperature and return to ambient temperature, where cycle sequence reversibility is retained. There is an analytical solution for critical temperature associated with each combination of axis constraint of the unit cube. The more axes of the unit cube constrained, the lower the critical temperature relative to ambient temperature for which cycle reversibility exists.

2. When the temperature of the thermal cycle exceeds critical temperature but does not involve melting, the material can store thermal strain elastically only to the proportional limit of the material at temperature, and the excess thermal strain can produce material flow from the axis or axes constrained to the free or unconstrained axis. The amount of material cross-flow (plastic or inelastic deformation) is completely dependent upon the interrelated parameters of (1) material coefficient of expansion (α); (2) stress (σ); (3) strain (ϵ); proportional limit or yield stress (F_y) as a function of temperature (T) as qualitatively related by:

$$\text{Inelastic deformation} = f(\alpha, \sigma, \epsilon, F_y, T)$$

If we conserve the volume of the unit cube, the quantitative amount of inelastic deformation can be calculated. The material property of elastically storing thermal strain energy quantitatively is related inversely to temperature. When the temperature cycle is reversed, the elastic strain is recovered but the inelastic strain is not. As cooling proceeds toward ambient, the initial elastic strain (a compressive strain quantity) decays to zero and is replaced by a second elastic strain process involving the tension properties of the material. It is possible for a new critical temperature associated with tensile yielding to occur. The amount of residual strain retained on the constrained axes by the unit cube upon return to ambient can be large because material properties increase as temperatures decrease. Fortunately, the temperature-time cycle usually permits greater material elongation, and some of the compressive material cross-flow occurring on the thermal rise cycle is recovered during the cooling cycle.

3. For the thermal cycle involving the melting of the unit cube, cycle reversibility is lost. The residual stresses occurring during cooling may be quite high if the unit cube is restrained during freezing and cooling.

When all thermal cycles and constraint combinations are compared for the fusion welding process, approximately one-third of the residual forces retained in the weldment are produced by the cast-metal zone and two-thirds of the residual forces are produced by the integral action of the critical temperature cycles occurring in the parent metal adjacent to or in the heat-affected zone of the weldment.

The physical width of the heat-affected zone, as shown by photomicrographs of weldment cross-sections, is closely related to the physical width of material that can be shown to have had a temperature cycle above critical temperatures.

It is the main premise of the pre-strain welding theory that residual stress fields can be reduced significantly by the superposition of desirable

pre-strain fields during the welding process that will either retain the free unit cube cycle reversitiliby or greatly extend the elastic range associated with the critical temperature available for elastic expansion characteristics.

It is also contended in the theory that the quantitative values of residual stress can be computed accurately and documented by controlled experimentation. The use of the modern computer permits the solution of the several constraint cases available and the creation of production control tables related to the process.

The pre-strain theory is sufficiently general to permit solution of elevated temperature structural loads and inelastic deformation of flight structures.

ANALYTICAL MODEL CONCEPTS

A unit cube model in combination with a strip model has been developed at S&ID to represent simply the thermophysical behavior of material during fusion welding described in the previous section. This combination model permits accurate analysis of residual stresses and strains resulting from fusion welding. It also permits the identification of pre-strain conditions that should exist during welding and which will minimize, and in some cases eliminate, the undesirable residual stresses normally associated with fusion welding. Pre-strain may involve the use of uniaxial or biaxial pre-load strains, pre-position of weldment strain and temperature differential and thermal gradient strains. These may occur singularly or in combinations as required to oppose the thermally applied strains of welding.

The unit cube model involves the study of triaxial strains occurring in material subjected to a field of simultaneously occurring triaxial thermal profiles resulting from a single heat source as a function of time. To restrict the number of variables involved, a condition of quasi-steady-state is assumed for single traveling thermal discontinuity in the material being welded. In other words, if the thermal profiles are viewed relative to the welding electrode, a steady thermal pattern will exist for each type of weldment under study. In addition, the unit cube model incorporates the concept of the "conditions of constraint" that might permit or prevent the movement of the six faces of the cube when its material undergoes temperature changes as a function of time. Finally, the presumption that input thermal energy equals internal elastic plus inelastic strain energy on a minimum energy basis is sufficiently satisfied by the conservation of volume and distortion of the unit cube.

The scope of the program did not permit full investigation of the mechanics of weld shrinkage in all possible detail respects. Since establishment of technical feasibility is the principal objective of the program, the unit cube model has been greatly simplified and the strip model is used to replace the temperature-time functions involved. The assumption of quasi-steady-state thermal profile is proved by the thermocouple data acquired in laboratory tests. Development of the simplified models is described in this section of the report, as well as comparison with test results.

DEVELOPMENT OF EQUATIONS

A typical test panel is shown in Figure 35. The two half panels become effectively a single panel after welding. Therefore, the following analysis treats the composite panel.

A theory capable of predicting the elastic stress σ_x as a function of P, x, y, and material properties for the case shown in Figure 35 would be extremely difficult to generate. A theory for the simpler case of a uniform member subjected to a parabolic end load has been reported by Timoshenko and Goodier (Reference 13). An Airy stress function and the principle of least work were used in this approach.

While a completely rigorous theory is not attempted in this investigation, several observations can be made. Since the aspect ratio is quite high, the member in question is intermediate between a plate and a tension member. Near the center of the plate (i.e., in the neighborhood of $x = L/2$), St. Venant's principle would indicate that elementary theory might apply. Thus, consider the half panel shown in Figure 36. Since the force P/2 is applied eccentrically, it is advantageous to represent this force system as a concentrically applied force P/2 and a bending moment M as shown in Figure 35. It can be seen by consulting Figure 35 that the centroid of the left half panel is located at $\bar{y} = \frac{\frac{b}{2}^2 - a^2}{2(b-a)}$ from the left edge. Thus the bending moment M is given by $M = \frac{P}{2}\bar{y} = \frac{P(ab)}{8(b-a)}$. Figure 37 shows the half panel in its deflected position.

Since the point of application of the tensile load P/2 does not move laterally (i.e., in the y direction), but is capable of moving longitudinally, the half panel can be rather accurately treated as a pin-ended beam tension member. A line diagram of the member is shown in Figure 37. Employing the standard elementary beam theory equation relating bending moment and curvature (viz., $M = -EI\, d^2y/dx^2$), the lateral deflection y is obtained (by a simple integration) as

$$y = \frac{ab}{8(b-a)} \left[\frac{(\cosh (kL - 1)) \sinh kx}{\sinh kL} - \cosh kx + 1 \right] \qquad (1)$$

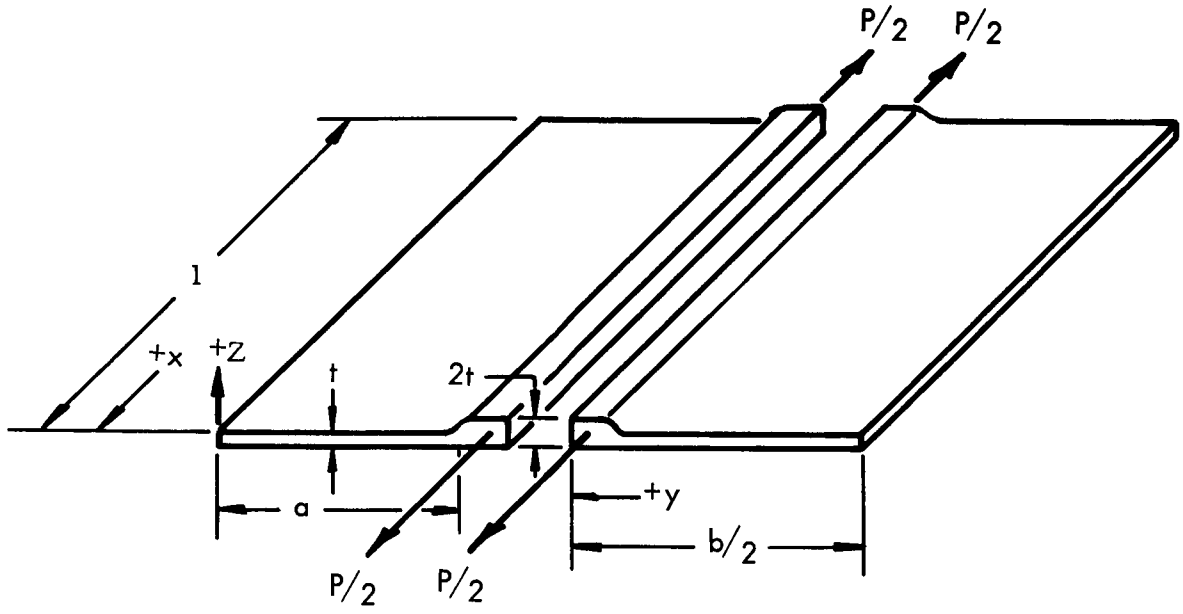

Figure 35. Test Panel

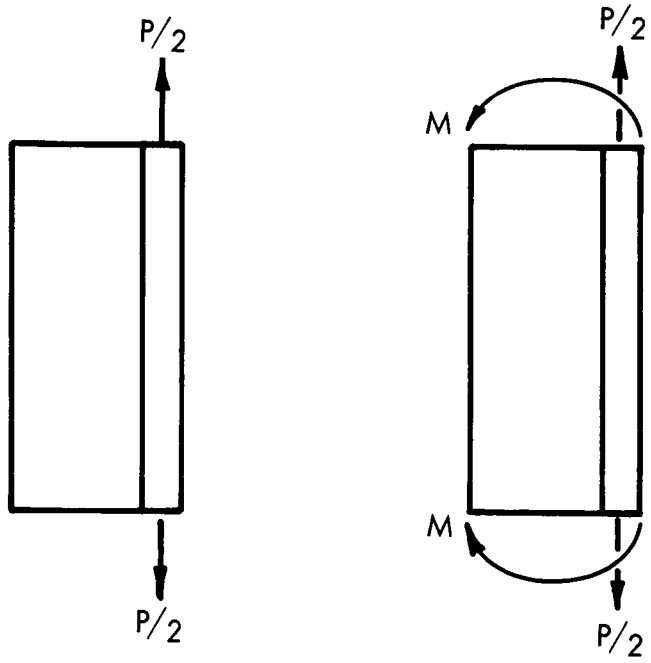

Figure 36. Undeformed Half Panel

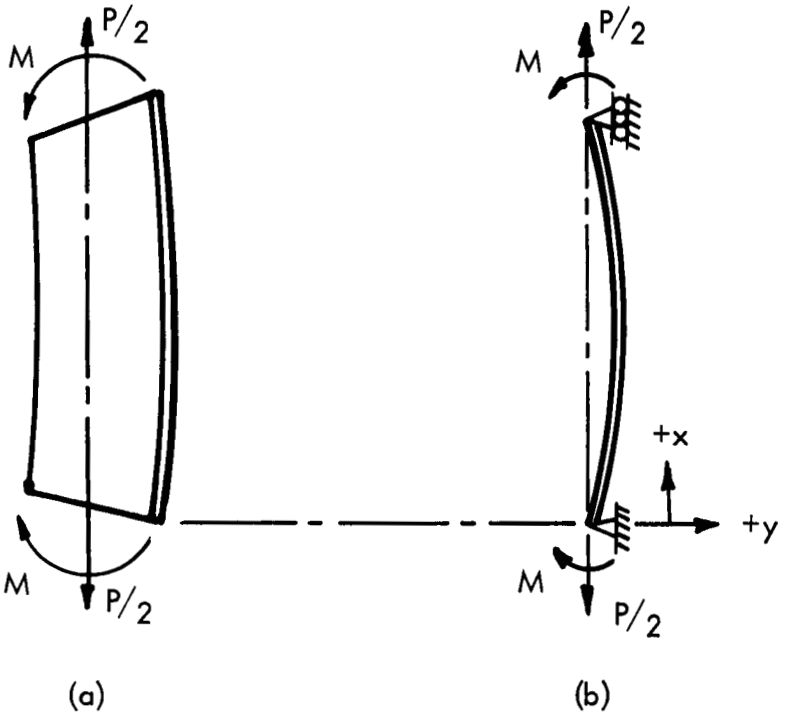

Figure 37. Deformed Half Panel

In this equation, the variables a, b, and L are the same as those given in Figure 35 and the parameter k is defined as $k = \sqrt{\frac{P}{2EI}}$. E is the modulus of elasticity of the material and I is the moment of inertia of the cross-section. In terms of the symbols of Figure , at

$$I = \frac{ta^3}{12} + \frac{2t\left(\frac{b}{2} - a\right)^3}{12} + \left[\frac{a}{2} - \frac{\frac{b^2}{2} - a^2}{2(b-a)}\right]^2$$

$$+ \left(\frac{b}{2} - a\right)(2t)\left[\left(\frac{a}{2} + \frac{b}{4}\right) - \frac{\frac{b^2}{2} - a^2}{2(b-a)}\right]^2 \qquad (2)$$

So far the effects of the right half panel exerting a pressure on the left half panel have been disregarded. That is to say, the deflections given by Equation 1 cannot occur, because the presence of the right half panel inhibits the deflections of a "free" left half panel. It is very difficult to quantify the effect of the right half panel, but an approximation of uniform pressure appears to be not unreasonable. The actual pressure exerted by the right

half panel may be nonuniform, but for the present purpose, p(x) in Figure 38 is assumed to be uniform. The assumption is made that the magnitude of p(x) is such that $y_{x=L/2}$ vanishes. From Equation 1

$$y_{x=\frac{L}{2}} = \frac{ab}{8(b-a)} \left[\frac{\cosh (kL-1) \sinh \frac{kL}{2}}{2 \sinh \frac{kL}{2} \cosh \frac{kL}{2}} - \cosh \frac{kL}{2} + 1 \right]$$

Using trigonometric identities, $y_{x=L/2}$, for the case in which the pressure exerted by the right half panel is disregarded, is

$$y_{x=\frac{L}{2}} = \frac{ab}{8(b-a)} \left[0.54308 \cosh \frac{kL}{2} - 0.77154 \operatorname{sech} \frac{kL}{2} - 1.17520 \sinh \frac{kL}{2} + 1 \right] \quad (3)$$

where a, b, L, and k are the same as in Equation 1.

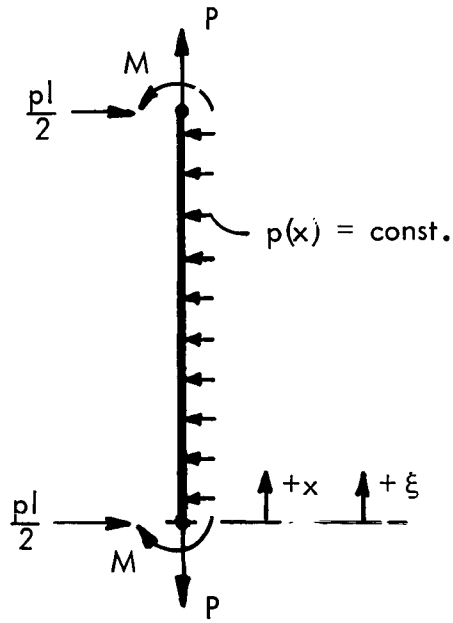

Figure 38. Right Half Panel Resistance

The deflection due to a uniform load p acting along with an axial tension P is

$$y = \frac{p}{EIk^4}\left[\frac{\cosh\left(\frac{kL}{2} - kx\right)}{\cosh\frac{kL}{2}} - 1\right] - \frac{p}{2EIk^2}x(L - x)$$

For the point $x = \frac{L}{2}$, it follows from

$$y = \frac{p}{EIk^4}\left[\operatorname{sech}\frac{kL}{2} - 1\right] - \frac{pL^2}{8EIk^2}$$

that

$$y_{x=\frac{L}{2}} = \frac{p}{EIk^2}\left[-\frac{L^2}{8} + \frac{\operatorname{sech}\frac{kL}{2} - 1}{k^2}\right] \tag{4}$$

Since the superposition of the applied moment and the pressure are presumed to yield zero deflections at $x = L/2$, we equate Equations 3 and 4 to yield

$$p = \frac{EIk^2 ab}{8(b-a)} \frac{0.54308\cosh\frac{kL}{2} - 0.77154\operatorname{sech}\frac{kL}{2} - 1.1752\sinh\frac{kL}{2} + 1}{\left(\frac{\operatorname{sech}\frac{kL}{2} - 1}{k^2} - \frac{L^2}{8}\right)} \tag{5}$$

or

$$p = \frac{EIk^2 ab}{8(b-a)} G(kL) \tag{6}$$

Hence the bending moment $M_{L/2}$ at $x = L/2$ is

$$M_{\frac{L}{2}} = M + \frac{pL^2}{8} - \frac{pL^2}{4} = M - \frac{pL^2}{8}$$

so

$$\sigma_{x=\frac{L}{2}} = \frac{P}{A} \pm \frac{M_{\frac{L}{2}}\, y}{I}$$

$$= \frac{P}{A} \pm \frac{y}{I}\left[M - \frac{pL^2}{8}\right]$$

Using previous results,

$$\sigma_{x=\frac{L}{2}} = \frac{P}{A} \pm \frac{y}{I}\left[\frac{P}{8}\frac{ab}{b-a} - \frac{EIk^2abL^2}{64(b-a)}G(kL)\right]$$

$$= \frac{P}{A} \pm \frac{y}{I}\left[\frac{P}{8}\frac{ab}{b-a} - \frac{Pab\,L^2}{128(b-a)}G(kL)\right]$$

$$= \frac{P}{A}\left[1 \pm \frac{yabA}{8I(b-a)}\left(1 - \frac{L^2}{16}G(kL)\right)\right] \qquad (7)$$

Although Equation 7 could now be used to evaluate the stress existing anywhere in the panel, it must be recognized that several of the results utilized in arriving at the equation depended for their validity on the assumption that plane sections remain plane after bending. Therefore, use of Equation 7 should be restricted to areas in which the plane sections do remain plane. In the interests of simplicity, the assumption is made that the contributions of the load eccentricity and the right half panel resistance compensates exactly near the center of the panel (i. e., the bracketed term in Equation 7 is nearly unity). While this may appear at first glance to be a rash assumption it will be seen later that comparison of theory and test substantiates it. Alternatively, values of a, b, k, L, I, A, and P corresponding to test values can be substituted in Equation 7 and the results will be seen to be $\approx P/A$ for the middle third of the panel.

Use of the above assumption implies that $\sigma_x = P/A$ might be reasonably accurate near the center of the panel. Thus, near the center of the panel, σ_x might be nearly independent of x. As the ends of the panel are approached, however, elementary theory becomes increasingly less accurate and a definite dependence of σ_x on x is noted. Even if the stress concentration effect of the concentrated load is completely neglected, the elementary approach is badly in error because one of the basic tenets of elementary

theory — that plane sections remain plane — is violated in the present problem.

Despite the absence of a completely general external load/internal stress relationship, a significant analysis of the beneficial effects of pre-straining can be performed if the analysis is restricted to the middle third of the plate. The following section contains results that are valid only near the middle third of the plate.

ELASTIC PRE-STRAIN

Treating the composite half panels after welding, it can be seen that although the loads are not applied at the centroid (i. e. , along the weld bead) the symmetrical loading arrangement is such that flexural effects are reduced. Hence, ϵ_x due to the mechanical pre-strain can be computed from

$$\epsilon_x = \frac{P}{AE} \tag{8}$$

In the notation of Figure ,

$$\epsilon_x = \frac{P}{[2at + (b-2a)\ 2t]\ E} \tag{9}$$

Equation 9 is the analytical expression for mechanically induced pre-strain.

Sample Calculation

For one of the panels tested, the following data apply:

$E = 10.5 \times 10^6$ psi

$t = 0.125$ in.

$\frac{b}{2} = 16.0$ in.

$a = 14.75$ in.

$P = 37,400$ lb.

$L = 72$ in.

In this case, Equation 9 yields

$$\epsilon_x = \frac{37,400}{(29.50)(0.125) + (2.50)(0.250)} \times \frac{1}{10.5 \times 10^6} \qquad (10)$$

$$\epsilon_x = 825 \ \frac{\mu \text{ in.}}{\text{in.}}$$

The strains actually measured by SR-4 gages at various values of $\frac{x}{L}$ are as follows:

$\frac{x}{L}$	$\epsilon_{MEAS.}$ $\frac{\mu \text{ in.}}{\text{in.}}$	$\epsilon_{CALC.}$ $\frac{\mu \text{ in.}}{\text{in.}}$
$\frac{1}{6}$	1615	825
$\frac{1}{3}$	1020	825
$\frac{1}{2}$	925	825
$\frac{2}{3}$	1140	825
$\frac{5}{6}$	1720	825

It can be seen that the solution given by Equation 10 is approximately correct for the center gage. The dimensions of the panel are such that even in the middle third, elementary theory does not quite apply. If the $\frac{b}{L}$ ratio were about half as large, the middle third strains would more nearly be given by Equation 10.

UNIT CUBE MODEL

The effect of welding heat on the panel can be explained simply by postulating a model for detailed study. Previous work at NAA/S&ID has indicated that many of the phenomena exhibited during welding can be represented by using a unit cube model.

Consider the cube shown in Figure 39. While the material of the cube is in the elastic range, the following strain-temperature relations apply:

$$\epsilon_1 = \alpha_1 (\Delta T)_1$$

$$\epsilon_2 = \alpha_2 (\Delta T)_2$$

$$\epsilon_3 = \alpha_3 (\Delta T)_3$$

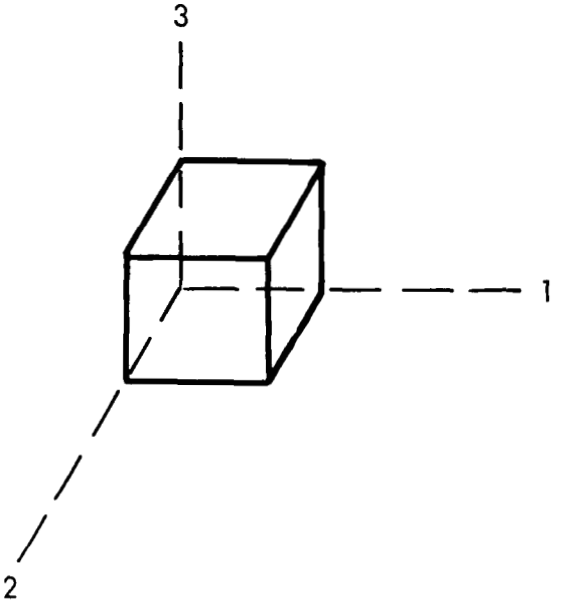

Figure 39. Unit Cube Model

If the cube is taken small enough, the temperature changes in the three orthogonal directions in a given period of time are nearly equal. Hence, for a cube of material that is completely free to expand, the three normal strains are all nominally equal. That is,

$$\epsilon_1 = \epsilon_2 = \epsilon_3 = \alpha \Delta T \tag{11}$$

the coefficient of linear expansion α is a function of temperature.

In the present application, the cubes of material in the panel are not free to expand in the three orthogonal directions. As a matter of fact, in the middle third of the panel, where the elastic analysis of the previous section is most nearly valid, the expansion in tangential directions is almost completely inhibited by the presence of surrounding material and the application of tooling pressures. Hence the strains ϵ_1 and ϵ_2 can be set equal to zero as a valid approximation. Since the surrounding material in the tangential directions inhibits expansion, it exerts a stress on the material in the postulated unit cube.

Thus, as long as elastic action alone takes place, the generalized Hooke's law can be used, as follows

$$\epsilon_1 = \alpha \Delta T + \frac{1}{E}\left[\sigma_1 - \nu (\sigma_2 + \sigma_3)\right]$$

$$\epsilon_2 = \alpha \Delta T + \frac{1}{E}\left[\sigma_2 - \nu (\sigma_1 + \sigma_3)\right]$$

$$\epsilon_3 = \alpha \Delta T + \frac{1}{E}\left[\sigma_3 - \nu (\sigma_1 + \sigma_2)\right]$$

The previous discussion leads to $\epsilon_1 = \epsilon_2 = 0$. Also, since there is a minimum amount of constraint in the normal direction, σ_3 can be taken as equalling 0.

The generalized Hooke's law then reduces to

$$\epsilon_1 = 0 = \alpha \Delta T + \frac{1}{E}\left[\sigma_1 - \nu \sigma_2\right]$$

$$\epsilon_2 = 0 = \alpha \Delta T + \frac{1}{E}\left[\sigma_2 - \nu \sigma_1\right]$$

$$\epsilon_3 = \alpha \Delta T - \frac{\nu}{E}(\sigma_1 + \sigma_2)$$

In the middle third of the panel, the constraint imposed on the unit cube by the material in the transverse and longitudinal directions is nearly the same, hence the valid approximation can be made that $\sigma_1 = \sigma_2$. The preceding equations then become

$$\sigma_1^{EH} = -\frac{E\alpha\Delta T}{1-\nu}$$
$$\epsilon_3 = \alpha\Delta T - \frac{2\nu\sigma_1}{E} \qquad (12)$$

It is recognized that Equations 12 are elastic; if the temperatures encountered were such that σ_1 never exceeded F_{cy}, the thermal behavior described would be completely reversible, and no residual stresses would develop. By using the first portion of Equations 12, it can be seen that the critical temperature change ΔT at which plastic action first begins upon heating is

$$(\Delta T)_{cr}^{H} = -\frac{\sigma_1}{E\alpha}(1-\nu) = \frac{F_{cy}(1-\nu)}{E\alpha} \qquad (13)$$

In Equation 13, F_{cy} is taken as a positive quantity, although it is realized that σ_1 is compressive. Although F_{cy}, ν, E, and α are variables, they can be expressed as functions of T for a given initial temperature (ordinarily, room temperature). Then $(\Delta T)_{cr}^{H}$ can be obtained using Equation 13.

For those values of $\Delta T > (\Delta T)_{cr}^{H}$, plastic strains occur. In this case, the equations for the normal strains of the unit cube become

$$\epsilon_1 = \epsilon_1^e + \epsilon_1^P = \alpha\Delta T - \frac{F_{cy}}{E}(1-\nu) + \epsilon_1^P = 0$$
$$\epsilon_2 = \epsilon_1^e + \epsilon_2^P = \alpha\Delta T - \frac{F_{cy}}{E}(1-\nu) + \epsilon_2^P = 0 \qquad (14)$$
$$\epsilon_3 = \epsilon_3^e + \epsilon_3^P = \alpha\Delta T + \frac{2\nu F_{cy}}{E} + \epsilon_3^P$$

By virtue of the homogeneity of the material, $\epsilon_1^P = \epsilon_2^P$. Then the first two parts of Equation 14 yield

$$\epsilon_1^P = \frac{F_{cy}}{E}(1-\nu) - \alpha\Delta T \qquad (15a)$$

and the third part is

$$\epsilon_3 = \alpha \Delta T + \frac{2\nu F_{cy}}{E} + \epsilon_3^P \qquad (15b)$$

It should be noted that, if desired, the plastic (irreversible) strain in the normal direction also can be calculated. This can be done by imposing the principle of constancy of volume in the plastic range.

Hence

$$\epsilon_1^P + \epsilon_2^P + \epsilon_3^P = 0$$

and

$$\epsilon_3^P = -2\epsilon_1^P$$

$$= -\frac{2F_{cy}}{E}(1-\nu) + 2\alpha\Delta T \qquad (16)$$

Figure 40 illustrates the results obtained so far. Suppose the room temperature is 70 degrees; as the cube is heated, the stress σ_1 in the

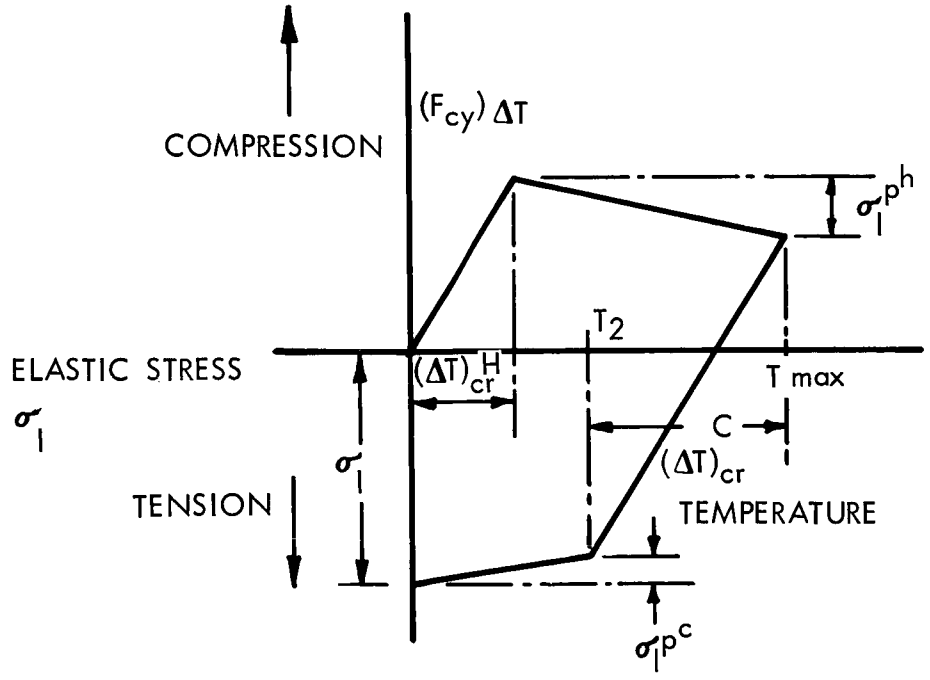

Figure 40. Stress-Temperature Diagram

compressive sense is increased nearly linearly in accordance with Equation 12. When the temperature corresponding to $(\Delta T)^H_{cr}$ given by Equation 13 is reached, a break occurs in the curve. At this value of T, $\sigma = (F_{cy})_{\Delta T}$.

If the temperature T is increased to T_{max}, plastic strains $\epsilon_1{}^P$, given by Equations 15a, will occur. As the thermal strain $\alpha\Delta T$ continues to increase with increasing temperature, F_{cy} and E decrease with increasing temperature and the plastic strain $\epsilon_1{}^P$ is presumed to be the difference between the thermally applied ΔT strain and the storable elastic strain. Had the temperature T been increased to melt temperatures, the ability of the material to store energy in the form of elastic strains becomes zero and the total of applied thermal strain $\alpha\Delta T$ would involve only plastic strains $\epsilon_1{}^P$. Then the elastic stress σ_1 would become zero at T_{max}. Thus we see that the elastic stress σ_1 is reduced by the amount $\sigma_1{}^{PH} = E_{avg}\left[\frac{F_{cy}}{E}(1-\nu) - \alpha\Delta T\right]$ when $\Delta T > (\Delta T)^H_{cr}$. Of course, $\sigma_1{}^{PH}$ is bounded by the fact that it must be $\leq \sigma_1{}^{EH}$. Hence

$$\sigma_1{}^{PH} = \begin{cases} E_{avg}\dfrac{F_{cy}}{E}(1-\nu) - \alpha\Delta T & E_{avg}\left[\dfrac{F_{cy}(1-\nu)}{E} - \alpha\Delta T\right] \leq \sigma_1{}^{EH} \\ \sigma_1{}^{EH} & E_{avg}\left[\dfrac{F_{cy}(1-\nu)}{E} - \alpha\Delta T\right] > \sigma_1{}^{EH} \end{cases} \tag{17}$$

Upon cooling, the material unloads elastically until a new critical temperature change $(\Delta T)^C_{cr}$ is reached. This includes the effect of relief of the elastic compressive strain remaining at T_{max} plus the inclusions of new tensile strains occurring as the elastic stress varies from F_{cy} to F_{ty}.

For cooling, Equation 13 becomes

$$(\Delta T)^c_{cr} = -\frac{\sigma_1(-\nu)}{E\alpha} = \frac{\left[(F_{cy})_{TMax} + (F_{ty})_{T2}\right](1-\nu)}{E\alpha} \tag{18}$$

Further cooling again gives rise to inelastic strains, given by

$$\epsilon_1{}^P = \frac{F_{ty}}{E}(1-\nu) + \alpha\Delta T$$

where ΔT is measured from T_{max} (and is a negative value). Thus

$$\sigma_1^{PC} = E_{avg}\left[\frac{F_{ty}}{E}(1-\nu) + \alpha\,\Delta T\right] - \sigma_1^{EH} + \sigma_1^{PH}$$

Hence σ_1 increases until it reaches room temperature. The residual stress obtained in this manner is tensile. Note that this type of behavior has been observed and documented (Reference 14).

In the next section, the results of this section will be applied to the case of the welded panels tested in the laboratory (without pre-straining).

PARALLEL STRIP MODEL - THERMAL STRAINS

In this simplified approach, the actual panel is thought of as a series of parallel strips, each of which initially has a length equal to the panel length L (Figure 41). The width of a typical strip is given by the dimension dimension Δ. The strips do not all have to have the same thickness.

The fact that welding proceeds along the central line of the panel gives rise to a nonuniform temperature distribution transverse to the weld axis. That is, by restricting attention to a given value of x, it is observed (from thermocouple readings, for example) that for all times under consideration, Strip 1 will be at a higher temperature than Strip 2, Strip 2 will be at a higher temperature than Strip 3, etc., until steady-state conditions prevail. Stated mathematically, for any given x,

$$T_1 \geqslant T_2 \geqslant T_3 \geqslant T_4 \cdots$$

Before proceeding with the actual welding analysis, consider a simpler case in which two half panels again are involved, but under the following conditions. Initially, the half panels are the same length and at room temperature. If the temperature all along the line of intersection increases simultaneously (i. e., at any given instant of time), the temperature distribution will be independent of x, but will vary transverse to the line of intersection. As the temperature increases, the critical temperature change $(\Delta T)_{cr}^{H}$ given by Equation 13 eventually is reached. Since this temperature will occur all along the length of the panel, the strip in which this $(\Delta T)_{cr}^{H}$ occurs can be regarded as composed of an entire line of unit

cubes, each of which is subjected to $(\Delta T)^H_{cr}$. Since the cubes near the ends x = 0 and x = L are constrained less than those in the center, the critical temperature for the end cubes will differ from that given by Equation 13. Nevertheless, for the middle third, the parallel strip can be validly represented by a line of unit cubes.

Now as the temperature change ΔT continues to increase, other strips (e.g., Strips 2 and 3 in Figure 41) also attain the value of $(\Delta T)^H_{cr}$ given by Equation 13. Finally the maximum temperature is reached, and $(\Delta T)_{max}$ along the line of intersection is attained. Then the strips exhibit various amounts of plastic strain given by Equation 15a. The T value to be used in Equation 15a is that corresponding to the ΔT for the strip in question. As the two panels are cooled, $(\Delta T)^C_{cr}$ given by Equation 18 is eventually reached in the center strips. Upon continued cooling, $(\Delta T)^C_{cr}$ is reached in some of the adjacent strips. Finally, reaching room temperature, there is some additional plastic strain in the strips. The σ_1 shown in Figure 40 can be computed for each strip and designated by σ_i. The equation form

$$\sigma_i = \left.\frac{E\alpha\Delta T}{1-\nu}\right|_{70^\circ} + \sigma_1^{PH}\Big|_{70^\circ} + \left.\frac{E\alpha\Delta T}{1-\nu}\right|_{T_{max}} + \sigma_1^{PC}\Big|_{T_{max}} \qquad (20)$$

In Equation 20, σ_1^{PH} and σ_1^{PC} are given by Equations 17 and 19, respectively. The vertical lines indicate the points from which T is to be measured. The distribution of σ_i over the panels is shown in Figure 42.

Of course, the panel does not behave like a series of independent strips. The stresses in one strip will cause strains in adjacent strips by virtue of the compatibility which must exist at the strip interfaces. This effect can be seen by assuming the panel behavior is like a beam on an elastic foundation. Thus, the residual stresses as calculated for the strips are $\sigma_{i_{STRIP}}$ where i = 1, 2, ..., n and n is the number of strips in a half panel. Converting these to strains, $\epsilon_{i_{STRIP}} = \frac{\sigma_{i_{STRIP}}}{E}$ and finally, since $\epsilon = \frac{\Delta L}{L}$, $\Delta L_i = \frac{L\sigma_{i_{STRIP}}}{E}$. Since $\sigma_{i_{STRIP}}$ is calculated from Equation 20, ΔL_i can be computed easily. If the panel is regarded as, in effect, a beam of unlimited length, some results from Reference 15 can be utilized. For instance, a uniformly applied load g causes a deflection y (at a location a units from the left end of the load) given by

$$y = \frac{g}{2k}\left[(1-e^{-\lambda a}\cos\lambda a) + (1-e^{-\lambda b}\cos\lambda b)\right] \qquad (21)$$

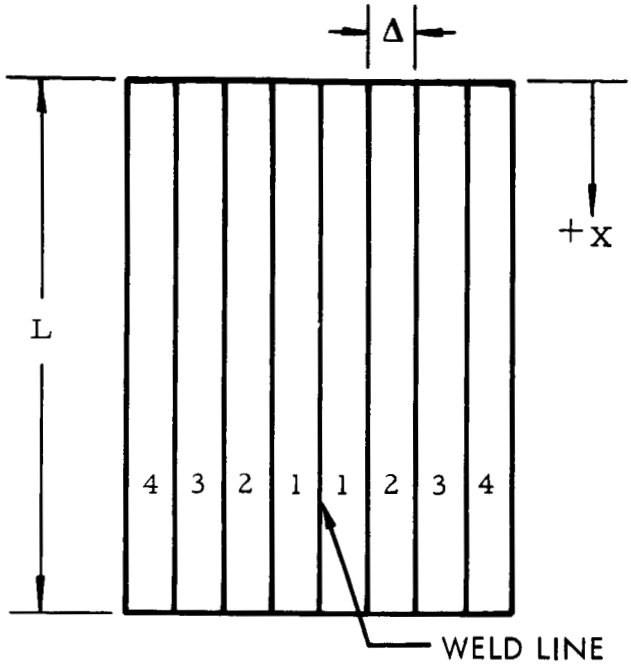

Figure 41. Parallel Strip Model

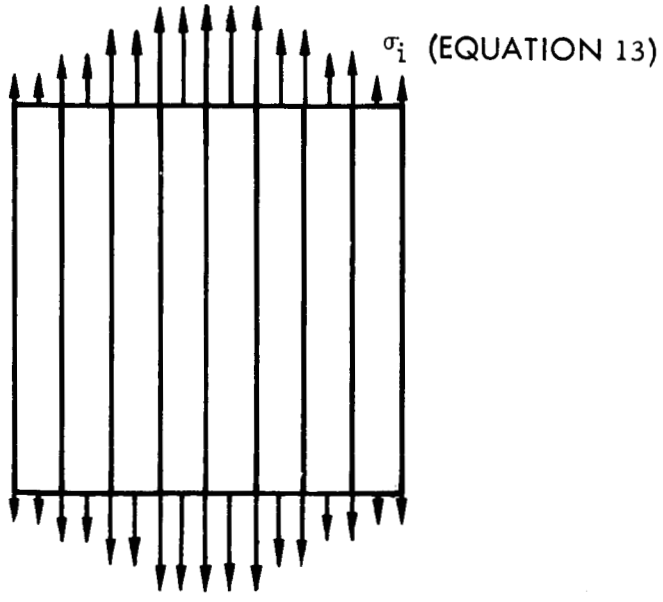

Figure 42. Distribution of σ_i Across Panel

where

b = distance from point in question to right end of load

k = the foundation modulus

$$\lambda = \sqrt[4]{\frac{k}{4EI}}$$

E = modulus of elasticity of beam

I = moment of inertia of beam

By virtue of the strip analogy, an approximate ΔL_i has been calculated, which enters the above equation as y. Hence, the magnitude of a uniform load g distributed over a length a + b could be calculated, which would produce a deflection ΔL_i at a location a units from the left end by using Equation 21. Then g could be divided easily by a reference width to determine σ_{iPANEL}. This, however, would predict a uniform residual stress pattern across the panel. Since this is foreign to experience, the correct expression to use is

$$y = \sum_{j=1}^{\infty} \frac{g_j}{2k} \left[(1 - e^{-\lambda a_j} \cos \lambda a_j) + (1 - e^{-\lambda b_j} \cos \lambda b_j) \right] \qquad (22)$$

Equation 22 indicates that the ΔL_i calculated is due to the superposition of a number of uniform loads g_j distributed over various lengths $a_j + b_j$. Use of Equation 22 would thus produce the familiar nonuniform residual stress pattern.

Unfortunately, Equation 22 is poorly suited for solving for $\sum_{j=1}^{\infty} g_j$, which is the quantity required for calculation of σ_{iPANEL}. There is no prior knowledge of the magnitudes of a_j and b_j, and hence, any results obtained using Equation 22 would depend on choice of the a's and b's.

In place of this procedure, an approximate method will be used which is in error in the web portion of the panel, but is sound in the region of interest, the weld land. This method, while approximate, is simple. To estimate the compatibility effect (that is, the fact that the strips are not distinct, but exert influences on one another), consider a similar problem of three equal loads applied to an elastic foundation, as described in

Reference 16, p. 199. There it is found that the maximum deflections (and hence, strains) under the middle load are 1.60 times the deflections caused by the middle load acting alone; hence, a load only $\frac{10}{16}$ times as large as actually existed would have caused the same deflections and strains as predicted using the middle load alone.

If this ratio $\frac{1}{1.6}$ is applied as a compatibility correction factor, it will have taken account in an approximate way of the actual physical continuity of the panel.

Hence

$$\sigma_{i_{PANEL}} = \frac{1}{1.6} \sigma_{i_{STRIP}} \tag{23}$$

where

$\sigma_{i_{STRIP}}$ is the quantity calculated in Equation 20.

Note that the panel originally considered (Figure 41) was completely free of stresses at the ends x = 0 and x = L. Hence the panel possessed no externally applied forces or moments. The panel of Figure 42 has no externally applied moment, but does possess an externally applied force. To bring the panel back to its original end conditions, a uniformly applied compressive stress must be imposed at the edges x = 0, and x = L. The additional applied stress must be uniform to preserve the pattern shown in Figure 42. The total external force P, existing at the edges x = 0 and x = L as shown in Figure 42, is

$$P = 2 \sum_{i=1}^{n} \sigma_{i_{PANEL}} \Delta_i t_i$$

where

n = number of strips in a half panel.

Consequently, the magnitude of the necessary uniform compressive stress to be applied is

$$\sigma_u = \sum_{i=1}^{n} \sigma_{i_{PANEL}} \Delta_i t_i \Big/ \sum_{i=1}^{n} \Delta_i t_i \tag{24}$$

The result of the superposition of the uniform stress σ_u on the panel residual stress σ_{iPANEL} is shown in Figure 43.

While the local picture near the ends is different for the cases illustrated in Figures 41 and 43, the macroscopic picture is the same. Hence, by invoking St. Venant's principle, the stresses existing in the interior of the panel at locations removed from the localized effects can be calculated adequately using the representation of Figure 43. The stresses so calculated would be the residual stresses due to the uniform heating and cooling operation.

Having devised a simple model to calculate the residual stresses existing in a uniformly heated panel, this analysis can be extended to the case of a welded panel.

A welded panel differs from a uniformly heated panel in that thermocouples at various values of x will report different temperatures at different times. Nevertheless, the moving heat source will create a temperature distribution of such a type that a thermocouple at any location x will, sooner or later, report the same temperature distribution as every other thermocouple in the same strip. A thermocouple located early in the weld pass will report a high temperature followed by a gradual decay, while simultaneously, a thermocouple farther down the weld axis is still reporting low temperatures. Later on however, the second thermocouple will essentially duplicate the behavior of the first one, and vice versa. Since the residual stresses are not measured until the entire weldment has cooled, the time-lag effect, as a first approximation, can be neglected and the procedure described above for the uniformly heated panel to be directly applied to the

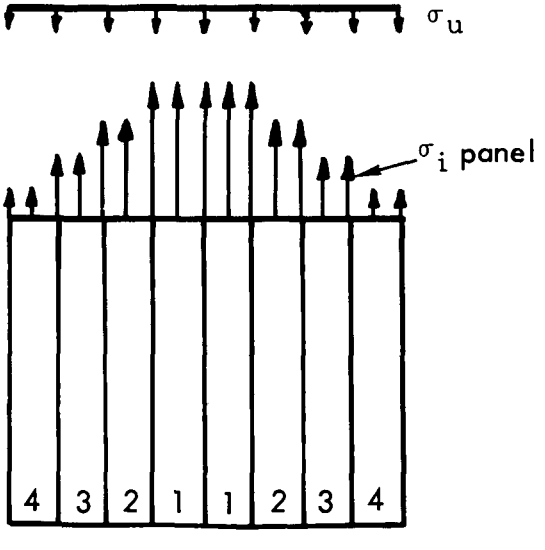

Figure 43. Superposition of σ_i Panel and σ_u

welded panel using the temperatures reported. But, as a practical restriction, the approach should be limited to the middle third of the panel to avoid excessive local effects. Thus, the analysis of the residual stresses existing in a welded panel (without pre-straining) can be reduced to the following equation

$$\sigma_{rs} = \sigma_{i_{PANEL}} - \sigma_u \tag{25}$$

where

$\sigma_{i_{PANEL}}$ is given by Equation 23

σ_u is given by Equation 24

PARALLEL STRIP MODEL - PRE-STRAINED PANEL

The analysis presented in the previous section states that the residual stresses existing in the middle third of the panel after welding (in a free panel) are given by Equation (25). Hence, a positive value for σ_{rs} denotes tension. Now, the residual stress can be tensile or compressive, depending upon the relative magnitudes of the two terms on the right-hand side of Equation 25. The introduction of an elastic pre-strain of the type described in this report will affect the residual stress pattern by superimposing some additional stresses on those given by Equation 25. To determine the magnitude and sign of the additional stresses due to pre-straining, it is essential to recall the order of the operations involved. The strain given by Equation 10 and the associated stress are imposed before welding. Hence, one could treat the pre-strained panel during welding as an entirely different panel, denoted by panel*. After the welding is completed and the panel cools, the pre-strain is removed. The effect is to introduce a compressive stress of magnitude P/A to panel*. In other words, a panel pre-strained by tension and then welded should behave very similarly to a panel welded without pre-strain and then subjected to a compressive stress P/A all during its service life. Hence, the final residual stress existing in a pre-strained panel is

$$\sigma_{rs} = \sigma_{i_{PANEL}} - \sigma_u - \sigma_{ps} \tag{26}$$

where

a positive sign denotes tension.

$\sigma_{i_{PANEL}}$ is given by Equation 23.

σ_u is given by Equation 24.

$$\sigma_{ps} = \frac{P}{A} = \frac{P}{2\,at + (b - 2a)\,2t} \tag{27}$$

CALCULATION OF RESIDUAL STRESSES AND COMPARISON WITH EXPERIMENTAL VALUES

The following is a trial and error calculation of $(\Delta T)^{H}_{cr}$. Using Equation 13 and charts of material properties (taking $\nu = 0.3$), try $(\Delta T)^{H}_{cr} = 300°$:

$$\frac{(44,000)\,(0.7)}{(1.3 \times 10^{-5})\,9.6 \times 10^{6}} = 247°$$

Try $(\Delta T)^{H}_{cr} = 400°$:

$$\frac{(28,000)\,(0.7)}{(1.325 \times 10^{-5})\,(8.95 \times 10^{6})} = 166°$$

Try $(\Delta T)^{H}_{cr} = 200°$:

$$\frac{(50,500)\,(0.7)}{(1.3 \times 10^{-5})\,(10^{7})} = 272°$$

Try $(\Delta T)^{H}_{cr} = 250°$:

$$\frac{(45,500)\,(0.7)}{(1.3 \times 10^{-5})\,(9.8 \times 10^{6})} = 250°$$

Hence $(\Delta T)^{H}_{cr} = 250°F$

Since the isotherms and material property curves are given in items of room temperature (70 degrees), $(\Delta T)^{H}_{cr}$ corresponds to an actual temperature of 320°F. By consulting the thermal profile curves (Figures 16 and 17), it can be seen that Thermocouples 5 and 6 never reach 320°F. Hence, according to Equation 20, σ_i is zero for all strips greater than

2 inches from the weld centerline. Also T_{max} for Thermocouple 4 is only 340 degrees, so we can sensibly restrict attention (as far as the σ_i calculation is concerned) to points $\leq$ 1.32 inches from the weld centerline. Thus, Figure 40, for all points > 1.32 inches from the weld centerline, reduces to Figure 44.

Four strips on the half panel can be constructed in such a manner that Thermocouples 1 through 4 are located on the strip centerlines. That is, the strips shown in Figure 45 are taken. Thus, σ_i for each strip can be calculated according to Equation 20 by using available curves. The results are summarized in Table 12. To illustrate a sample calculation for Strip 4, Column 5 is calculated as

$$E_{avg}\left[\frac{F_{cy}}{E}(1-\nu)-\alpha\Delta T\right]\Bigg|_{70^\circ} = 10.12\times10^6\left[\frac{(43,500)(0.7)}{9.75\times10^6} - (1.30)(270)\,10^{-5}\right] = 3940 \text{ psi}$$

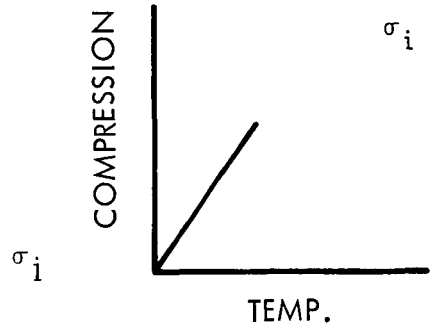

Figure 44. Elastic Behavior Only if ΔT $(\Delta T)^H_{CR}$

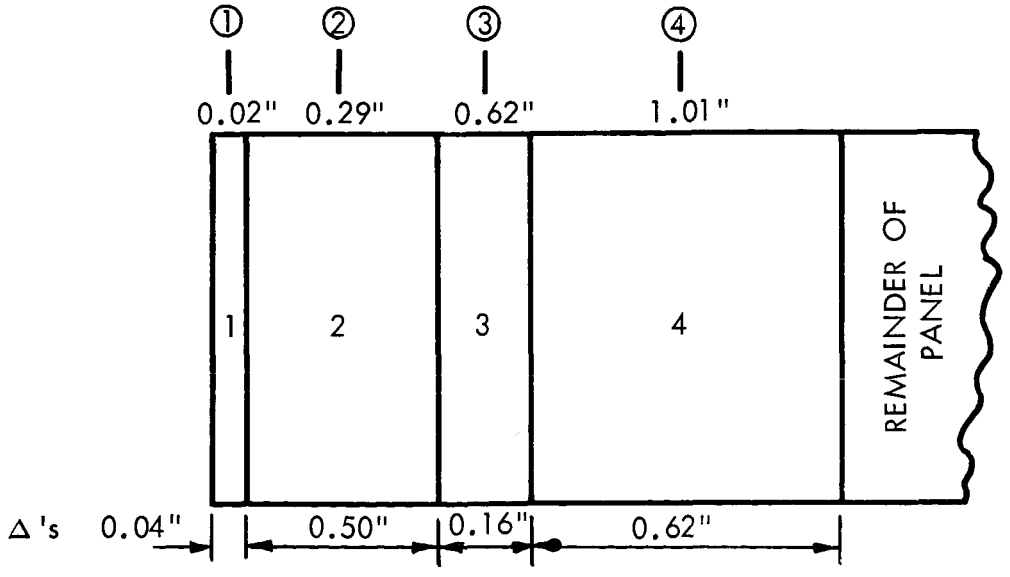

Figure 45. Strips with Thermocouples at Centerlines

Table 12. Mechanically Pre-Loaded Rectangular Panel Calculations

Strip	$(\Delta T)^{H}_{cr}$ Equation 13 °F	σ^{EH}_{1} Equation 12a psi	T_{max} °F	σ^{PH}_{1} Equation 17 psi	$\sigma^{EH}_{1} - \sigma^{PH}_{1}$ psi	$(\Delta T)^{C}_{cr}$ Equation 18 °F
1	250	45,000	1650	45,000	0	0
2	250	45,000	740	45,000	0	100
3	250	45,000	450	21,800	23,200	300°
4	250	45,000	340	3940	41,060	7270°

Strip	σ^{EC}_{1} Equation 12a psi	σ^{PC}_{1} Equation 19 psi	σ_i psi $= -\sigma_1^{EH} + \sigma_1^{PH} + \sigma_1^{EC} + \sigma_1^{PC}$ if $\sigma_1 \leq 25,000$ $= 25,000$ if $-\sigma_1^{EH} + \sigma_1^{PH} + \sigma_1^{EC} + \sigma_1^{PC} \geq 25,000$
1	0	63,000	+25,000
2	11,200	62,000	+25,000
3	+55,000	8800	+25,000
4	+50,700	0	+9640
The 25,000-psi level is taken as a yield cutoff in the thermally treated material.			

Since 3940 psi is less than 45,000 psi, we have for Column 6

$$\sigma_1^{EH} - \sigma_1^{PH} = 45,000 - 3940 = 41,060 \text{ psi}$$

We now have to solve for $(\Delta T)_{cr}^{H}$ by trial and error, using Equation 18. Since the material has experienced high temperatures during the welding process, the material properties (i.e., E, F_{ty}, F_{cy}, α, etc.) are not represented adequately by the prewelding curves. In particular, F_{ty} will be taken to have at room temperature a maximum value of 25,000 psi. For this feasibility study, the pre-welding curves are used, but a cutoff at F_{ty} = 25,000 psi is imposed. The choice of F_{ty} maximum as 25,000 psi is somewhat arbitrary. It should actually be a function of location on the cross-section, since the material located close to the weld is more strongly heated than material at the far end of the weld land. Thus, material located away from the weld line should have a higher yield stress than 25,000 psi. Preliminary investigations at S&ID have indicated that the 25,000-psi figure is representative. Proceeding then to evaluate Equation 18, we obtain

$$(\Delta T)_{cr}^{C} = \frac{(45,000 + F_{ty_{T_2}})\ 0.7}{E\alpha}$$

Try $(\Delta T)_{cr}^{C} = 300°$:

$$\frac{(45,000 + 25,000)\ 0.7}{10.1 \times 10^{6} \times 1.3 \times 10^{-5}} = 369°$$

Hence $(\Delta T)_{cr}^{C}$ is > 300 degrees and the entire unloading is elastic. So

$$\sigma_1^{EC} = \frac{E\alpha\Delta T}{1-\nu}\bigg|_{T_{max}} = \frac{10.1 \times 10^{6} \times 1.3 \times 10^{-5} \times 270°}{0.7} = 50,700 \text{ psi}$$

and for the fourth strip

$$\sigma_4 = \sigma_1^{EH} + \sigma_1^{PH} + \sigma_1^{EC} + \sigma_1^{PC}$$

$$= -45,000 + 3940 + 50,700$$

$$= 9640 \text{ psi (tensile)}$$

The results for the other three strips are also presented in Table 12. It should be noted that high stresses exist as far as one inch from the weld line

By virtue of Equation 23, the compatibility effect is incorporated as

$$\sigma_{1_{PANEL}} = \frac{1}{1.6}\sigma_{1_{STRIP}} = 25,000 \times \frac{1}{1.6} = 15,600 \text{ psi}$$

$$\sigma_{2_{PANEL}} = \sigma_{3_{PANEL}} = \sigma_{1_{PANEL}} = 15,600 \text{ psi}$$

$$\sigma_{4_{PANEL}} = \frac{1}{1.6}\sigma_{4_{STRIP}} = 6000 \text{ psi}$$

Now, Equation 24 yields (for t = 0.125 inch, a = 14.75 inches, b/2 = 16.00 inches)

$$\sigma_u = \frac{1368 + 517}{3.8787} = 500 \text{ psi}$$

Hence, for a panel without pre-strain, the following is obtained

$$\begin{aligned}
\sigma_{rs_1} &= \sigma_{1_{PANEL}} - \sigma_u = 15,100 \text{ psi} \\
\sigma_{rs_2} &= \sigma_{rs_1} = \sigma_{rs_3} = 15,100 \text{ psi} \qquad (28) \\
\sigma_{rs_4} &= \sigma_{4_{PANEL}} - \sigma_u = 5500 \text{ psi} \\
\sigma_{rs_5} &= -\sigma_u = -500 \text{ psi}
\end{aligned}$$

The results of Equation 28 are plotted in Figure 46 where a curve is faired in to represent the residual stresses existing in non-pre-strained panel.

Previous analysis has shown that the pre-straining effect should be calculated using Equation 7, which permits a variation of stress across the panel. The factor G(kL) in Equation 7 is a function of load, so the transverse effect may become more pronounced for some pre-strain levels than for others. Nevertheless, an approximate solution can be obtained by taking σ_{ps} to be given by Equation 27. The pre-strain load applied to the panel was approximately 37,500 pounds. Hence, using Equation 27

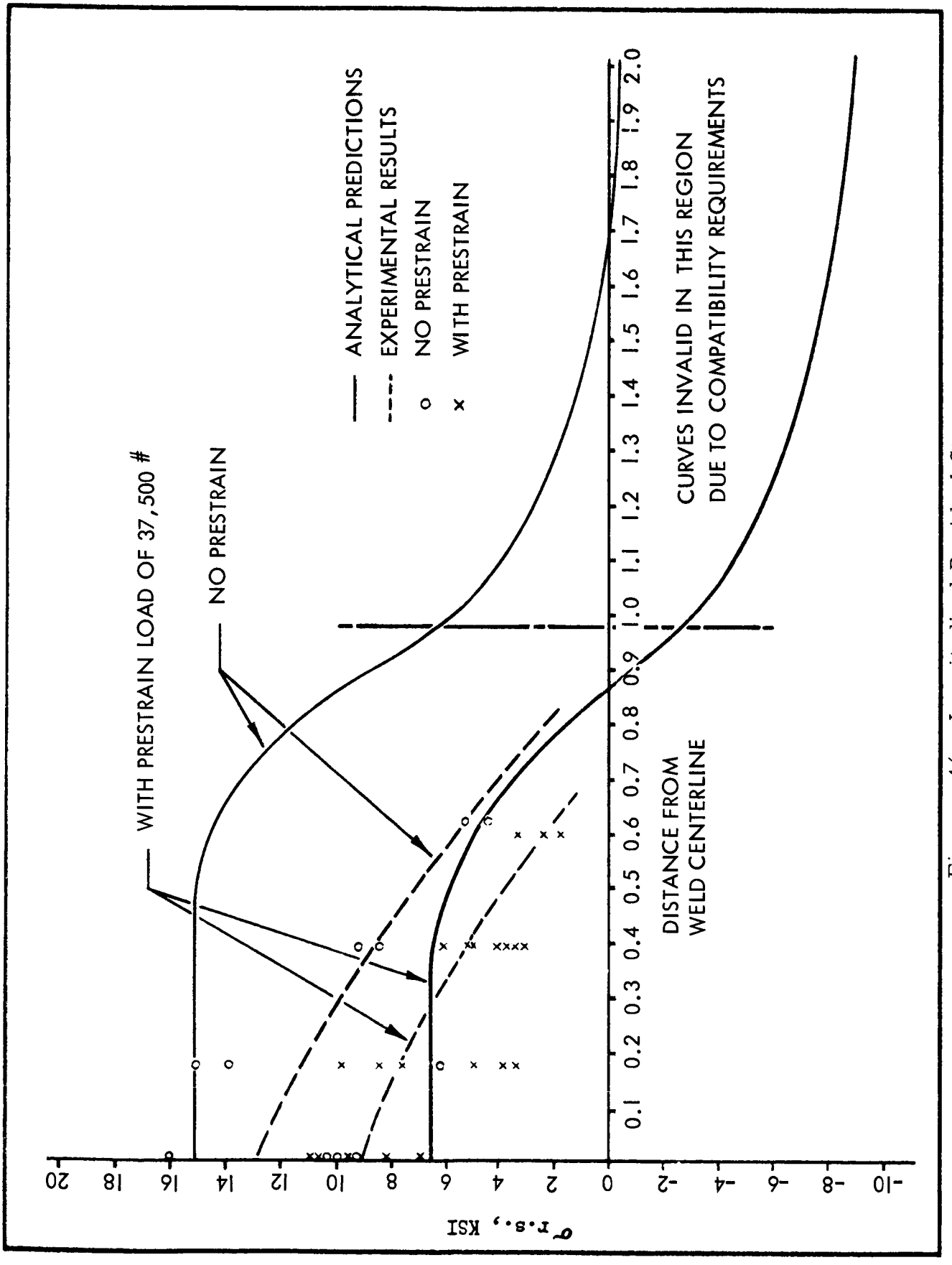

Figure 46. Longitudinal Residual Stress

$$\sigma_{ps} = \frac{37,500}{2\,(14.75)\,(0.125) + (2.50)\,(.250)} = 8600 \text{ psi}$$

Hence, Equation 26 yields $\sigma_{rs} = \sigma_i - \sigma_u - \sigma_{ps}$, and presents a curve concordant to the "no pre-strain" curve, but located 8600 psi below it. The result is shown in Figure

It should be pointed out that the procedure employed is capable of several refinements. The travel around the cycle of Figure 40 could be carried out more precisely by using a digital computer to do the work. Also the pre-straining effect could be more precisely given by using Equation 7. Nevertheless, the procedure employed is basically sound. The beneficial effects of pre-straining are evident from examination of Figure 46.

Note that the pre-strain applied in this feasibility study is not the optimum. A more effective pre-strain load would reduce σ_{rs} even more in the region $d \leqslant 1.0$ inch, but then die out quickly when $d \geqslant 1.7$ inch. Thus, a properly chosen pre-strain load (i. e., both optimum magnitude and distribution across the panel) could reduce, ideally, residual stress to zero.

Experimental points are shown on Figure 46. Fair correspondence is obtained in the region of interest. The optimum pre-strain in the middle third can be calculated from Figure 46, as follows:

$$\sigma_{rs} = 15 \text{ ksi} - \frac{7}{900}\epsilon$$

For σ_{rs} to vanish,

$$\epsilon = \frac{900 \times 15}{7} = 1930 \ \frac{\mu\text{in}}{\text{in}}$$

This corresponds to a stress in the middle third of $\sigma = 19,300$ psi, corresponding to about 32 percent of nominal yield strength, and an axial load of 84, 000 pounds.

In Figure 46, the experimental results were obtained by taking transverse effects into account (i. e., σ_x was calculated as $\sigma_x = [E/1 - \nu^2][\epsilon_x + \nu\epsilon_y]$). On the other hand, the analytical predictions disregarded transverse effects. Furthermore, the presence of the right half panel restraint on the left half panel really imposed pre-strain in the transverse direction. Despite all the complicating factors in this problem, agreement of analytical and experimental results indicates that the model employed in this study leads to specific, reasonable results.

CIRCULAR PANELS—NO PRE-STRAIN

In this section an analysis is performed to predict the residual stresses existing in a circular part that has been subjected to a thermally induced strain prior to welding.

Analytical Model

The model used for predicting residual stresses is similar to the unit-cube/parallel-strip model described elsewhere in this report; but in this instance, the model takes the form of concentric rings (Figure 47). As in the case of the rectangular panels, the radial distribution of temperature varies with circumferential angle θ; but eventually, the thermocouples at any circumferential station give the same results (nominally) as those given by the thermocouples at some other station. Because data regarding the residual effects existing after the entire piece has cooled are desired, the time effects may be disregarded; and work may be confined to the isotherms for an arbitrarily selected circumferential angle θ. In the absence of more definitive actual test results, for analytical purposes these isotherms are taken to be the same as those reported for the rectangular 0.250-inch weld-land thickness weldment.

The unit-cube/strip approach still holds where constraint is imposed in the radial and circumferential directions but not in the normal direction. Because the same isotherms are used, $(\Delta T)^{H}_{cr}$ as given by Equation 13 will apply in this case also. Note that transverse effects, insofar as they affect F_{cy}, are neglected in this analysis just as they were in the mechanical pre-strain analysis. Thus, in a more precise analysis, consideration should be given to yield loci such as those used in the Tresca or the Von Mises yield criterion. The elastic stress encountered during heating (in the circumferential direction) is given by Equation 12, and the plastic heating stresses are given by Equation 17. Cooling stresses and critical temperature for cooling are described adequately by Equations 18 and 19 also if the uniaxial yielding concept is retained. Equation 20, therefore, is a reasonable expression for the circumferential tensile stresses that exist after welding when no shrink-fitting is introduced in a member composed of circumferential strips. By an argument analogous to that presented in the case of the rectangular panels, the compatibility correlation factor 1/1.6 can be introduced to take account of the interaction of the strips; then, the results are identical with those given in the previous section; namely,

$$\sigma_1 = \sigma_2 = \sigma_3 = 15{,}600 \text{ psi}$$

and

$$\sigma_4 = 6000 \text{ psi}$$

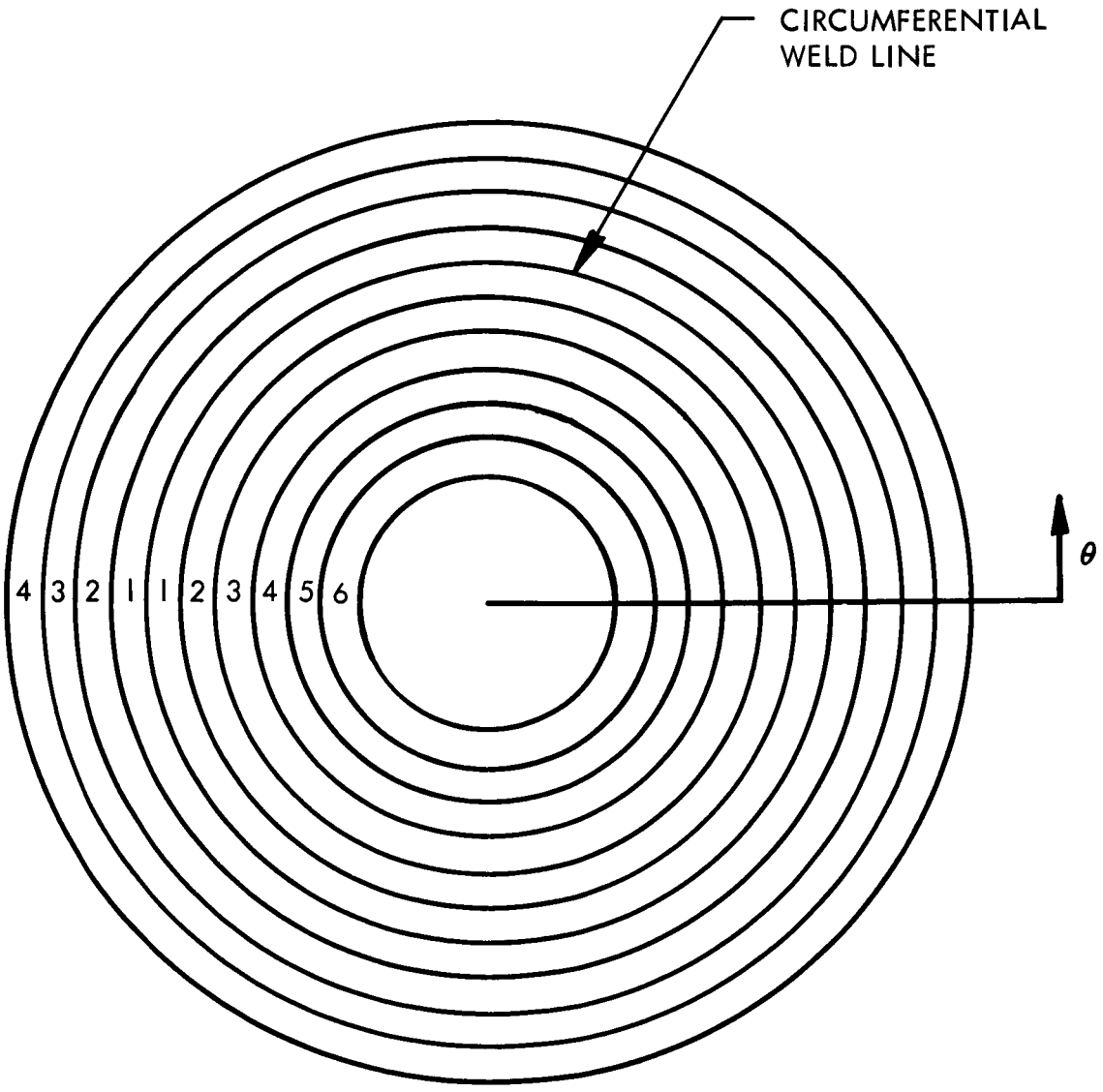

Figure 47. Circumferential Ring Model

where the subscripts denote the ring in question. If a horizontal line is passed through the equator, the σ_i are in moment equilibrium, but not in vertical force equilibrium; hence, it is necessary that a compressive uniform stress σ_u be imposed to restore vertical equilibrium. Using the dimensions given in Figure 48,

$$\sigma_u = \frac{15,600(1.40) + 6000(1.24)}{7.5} = 3900 \text{ psi.}$$

Hence, a simplified analysis would predict the stress distribution given by Equation (29)

$$\sigma_{r.s.} = \left\{ \begin{array}{ll} 15,600 - 3900 = 11,700 \text{ psi} & \leq 0.70'' \text{ from weld } \mathbb{C}_L \\ 6000 - 3900 = \quad 2100 \text{ psi} & > 0.70'' \text{ from weld } \mathbb{C}_L, \text{ but } \leq 1.32'' \\ -3900 \text{ psi} & > 1.32'' \text{ from weld } \mathbb{C}_L \end{array} \right\} \quad (29)$$

in a non-prestrained weldment. These stresses are presented graphically in Figure 48.

CIRCULAR PANELS WITH THERMAL PRE-STRAIN

An existing procedure is the thermal prestraining of fittings before welding, which is performed by cutting the blanks according to

$$D = d - f \quad (30)$$

where

D = diameter of hole

d = diameter of fitting

f = shrink factor

By a process of freezing the fitting, heating the combined assembly, and cooling to room temperature, the fitting can be "shrunk-fit" to the segment. By this technique, the diameter of the final interface falls somewhere between D and d. Because the material on opposite sides of the line of interface is under the same conditions, it is reasonable to assume that the final diameter is

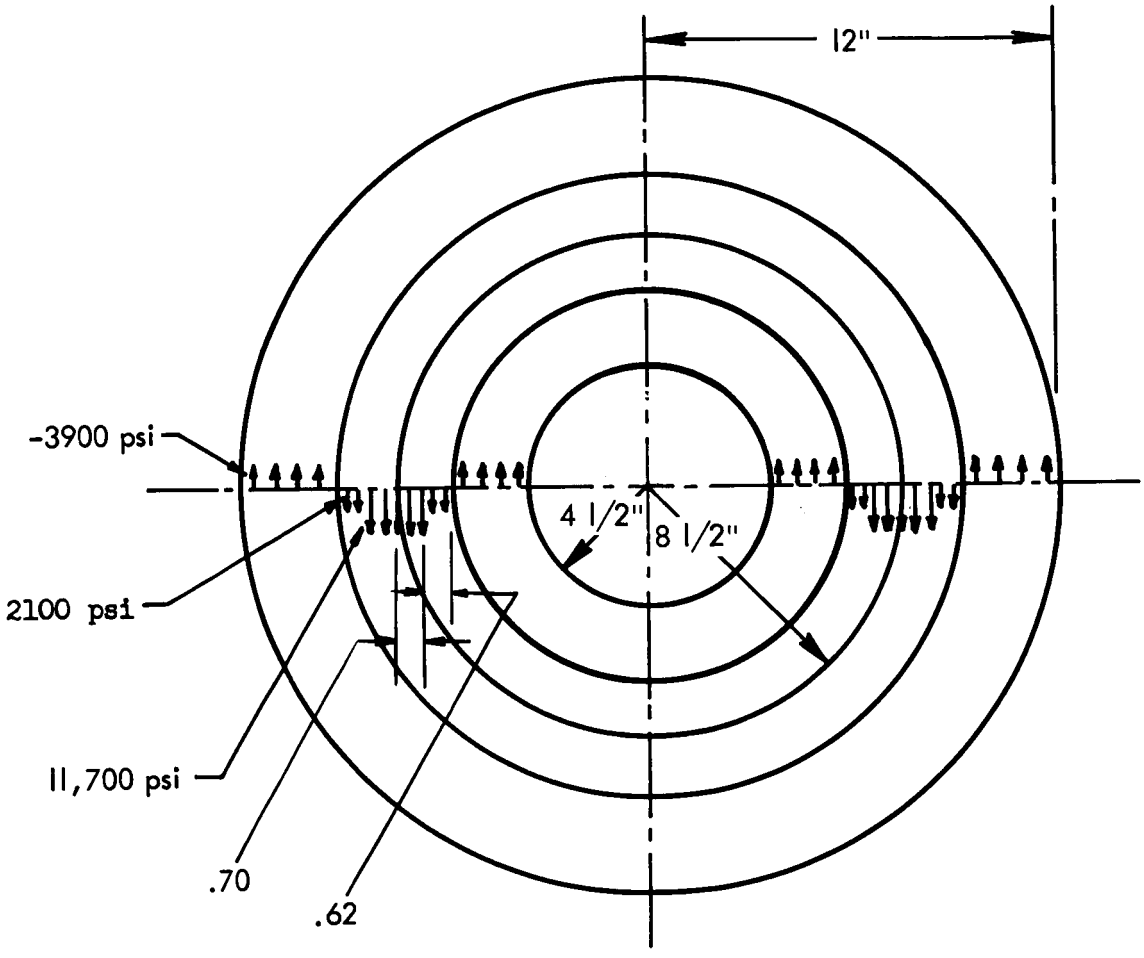

Figure 48. Residual Stresses in Non-Pre-Strained Circular Weldments

$$S = \frac{D + d}{2} \tag{31}$$

where

S = final diameter of composite.

Using Equation 30,

$$S = \frac{d}{2} - \frac{f}{2} + \frac{d}{2} = d - \frac{f}{2}, \tag{32}$$

so the strain of the fitting in the radial direction is

$$\epsilon_r = \frac{S - d}{d} = \frac{S}{d} - 1 = \frac{d}{d} - \frac{f}{2d} - 1 = -\frac{f}{2d} \tag{33}$$

Also, the circumferential strain ϵ_θ is

$$\epsilon_\theta = \frac{\pi(S - d)}{\pi d} = \epsilon_r = -\frac{f}{2d}, \tag{34}$$

so the fitting is under a biaxial state of strain such that $\epsilon_r = \epsilon_\theta = -f/2d$ (both compressive). To determine the equivalent stress existing prior to welding, the generalized Hooke's Law is used:

$$\sigma_{\theta_{ps}} = \frac{E}{1 - \nu^2}\left[\epsilon_\theta + \nu\epsilon_r\right] \tag{35}$$

and

$$\sigma_{r_{ps}} = \frac{E}{1 - \nu^2}\left[\epsilon_r + \nu\epsilon_\theta\right], \tag{36}$$

so in the inner annulus,

$$\sigma_{\theta_{ps}} = \sigma_{r_{ps}} = -7.15\left(\frac{f}{d}\right) \times 10^6 \text{ psi} \tag{37}$$

An analysis similar to that described in the preceding section shows that the outer annulus experiences strains due to the shrink-fitting operation given by

$$\epsilon_\theta = -\epsilon_r = +\frac{f}{2D} \approx \frac{f}{2d}$$

Using Equations (35) and (36)

$$\sigma_{\theta_{ps}} = -\sigma_{r_{ps}} = 3.85 \left(\frac{f}{d}\right) \times 10^6 \text{ psi} \qquad (38)$$

Equation (38) refers to the outer annulus.

Table 13 contains the results of analytical calculations based on the preceding equations for four weldments of interest. The weldments considered are —

1. One with no shrink fit
2. One with f/d = 0.001178 (designated as Panel No. 1)
3. One with f/d = 0.002825 (designated as Panel No. 2)
4. One with f/d = 0.003265 (designated as Panel No. 3)

For each of the four weldments, $\sigma_{\theta_{ps}}$ was calculated using Equation (37), for the inner annulus and Equation 38 for the outer annulus. The results appear in the table in Columns 3 and 4, respectively. With the circumferential stresses existing in the inner and outer annuli due to the shrink-fitting operation, the circumferential residual stresses can be predicted by superimposing the results of Equation 29, which gives the tensile welding stresses. The predictions for $\sigma_{\theta_{rs}}$ in the inner and outer annuli are given in table Columns 5 and 6, respectively. In the same manner, the residual stresses in the radial direction could be predicted. The pre-stress radial stresses can be calculated directly from Equations 37 and 38, but the welding stresses in the radial direction are more difficult to establish. To establish stresses in the radial direction properly, procedures analogous to those used in the determination of Equation 29 should be employed. Instead of performing the extensive calculations necessary, the analytical predictions are restricted to $\sigma_{\theta_{rs}}$ with the assumption that similar results would be obtained for $\sigma_{r_{rs}}$

Table 13. Circular Weldment Calculations

① Circular Weldment	② $\frac{f}{d}$ ($\times 10^{-3}$)	③ $\sigma_{\theta ps}$, psi Inner Annulus Equation y	④ $\sigma_{\theta ps}$, psi Outer Annulus Equation s	⑤ $\sigma_{\theta rs}$, psi Inner Annulus Equations j and r	⑥ $\sigma_{\theta rs}$, psi Outer Annulus Equations j and s	⑦ Experimental $\sigma_{\theta rs}$, psi Using Measured Strains	
No Interference Fit	0	0	0	+11,700	+11,700		
Panel No. 1	1.178	-8,420	+4,530	+3,280	+16,230	+2,270 +14,700	9:00 12:00
Panel No. 2	2.825	-20,200	+10,880	-8,500	+22,580	+11,400 +13,800	9:00 12:00
Panel No. 3	3.265	-23,400	+12,580	-11,700	+24,280	+13,700 +13,820	9:00 6:00

⑧ Circular Weldment	⑨ Experimental $\sigma_{r_{rs}}$, psi Using Measured Strains	⑩ Position	⑪ Analytical $\frac{\sigma_{\theta_{rs}} \text{ Inner Annulus} + \sigma_{\theta_{rs}} \text{ Outer Annulus}}{2}$ 1 psi
Panel No. 1	+15,300 +8,400	9:00 12:00	+9,755
Panel No. 2	+326 +1,665	9:00 12:00	+7,040
Panel No. 3	+8,750 +2,800	9:00 6:00	+6,290

Experimentally determined residual stresses are also presented in Table 13. The results for $\sigma_{\theta_{rs}}$ (experimental) and $\sigma_{r_{rs}}$ (experimental) appear in table Columns 7 and 9, respectively. $\sigma_{\theta_{rs}}$, for example, is calculated using

$$\sigma_{\theta_{rs}} = \frac{E}{1 - \nu^2}\left[\epsilon_{\theta_{MEAS}} + \nu\epsilon_{r_{MEAS}}\right] \tag{39}$$

In Equation 39, $\epsilon_{\theta_{MEAS}}$ is the average of the values reported in the circumferential direction on the upper and lower faces of the weldment. $\sigma_{r_{rs}}$ is calculated similarly. The strain gages used in obtaining input information for Equation 39 were located at two circumferential stations. Hence two experimental stresses are obtained for each of test Panels 1, 2, and 3, as indicated in table Column 10.

Several observations can be made at this stage of the investigation. At low values of f/d, the circumferential variation in $\sigma_{\theta_{rs}}$ is very apparent. As f/d increases, however, $\sigma_{\theta_{rs}}$, as given in Column 7, appears to be nearly axisymmetric. The results are not as conclusive for $\sigma_{r_{rs}}$, given in Column 9. Since this is a transverse effect, it is not surprising that the circumferential results are more meaningful.

The apparent lack of agreement between the theoretical predictions, Columns 5 and 6, and the experimental results of Column 7, should be noted. Because of financial considerations, a minimum number of strain gages were used. Thus the experimental results reported in Column 7 correspond to strain gages located right at the interface of the inner and outer annuli. In retrospect, a better procedure would have been to have at least two radial stations for each circumferential angle investigated, with one of the radial stations in the inner annulus and the other in the outer annulus. Experimental results then could be reported for the residual stress existing in the circumferential and radial directions for both annuli. It is expected that the results of such a procedure would check the predictions of Columns 5 and 6. Although the values in Column 7 present a clouded picture in that the contributions of the individual annuli cannot be segregated, in most cases the experimental results fall roughly between the theoretical predictions for the inner and outer annuli, thus indicating about equal contributions from each.

It is realized that a complete assessment of the beneficial effects of shrink-fitting should be based on the reduction in magnitude of the principal stresses in the inner and outer annuli. This could be done by using three-element strain rosettes in both the inner and outer annuli. In this way, shearing effects could be measured. Because funds were limited in the present program, a substitute criterion is to examine the average residual

circumferential stress at the several pre-strain levels. Column 11 presents the average of Columns 5 and 6. Since the sharp discontinuity must take place over a finite distance, it is reasonable to assume that the average value of circumferential stress gives some indication of the beneficial prestrain effect. Also notice that the radial residual stresses are lower in Panels 2 and 3 than in Panel 1. Hence, the optimum shrink-fit is probably not too far from that corresponding to Panel 3.

APPLICATION OF PRE-STRAIN CONCEPTS TO S-II PRODUCTION

MECHANICAL PRE-LOAD

Pre-strain welding techniques of a comparatively simple nature are currently being applied to the horizontal or circumferential welding accomplished in the vertical build-up of the S-II LH_2 cylinders. Initial attempts at horizontal welds without circumferential expansion at weld lands resulted in excessive inward peaking. Development and proofing exercises indicated that a circumferential increase would result in a safe and satisfactory metal strain necessary to meet low magnitude pre-stressed skin alignment requirements.

One possible method of creating an acceptable pre-loaded condition would require redesign and rework of the presently existing back-up bar, as illustrated in Figures 49 and 50. Loads required to expand the LH_2 cylinders to the desired level, as well as additional strength requirements on the tool to transmit these loads outward, would have to be considered in an actual redesign. The sketches shown do not necessarily reflect the ultimate structural rework of the tool, but rather the principle used to expand the LH_2 cylinder as required.

Application of the mechanical pre-strain concept to gore-to-gore weldments is presently under consideration. Conceptual plans have not progressed far enough, however, to warrant inclusion in this report. NAA will keep NASA advised of any future plans or developments.

THERMALLY APPLIED PRE-LOAD

One method of thermally applying a pre-load is already being used on S-II production assemblies. This method consists of freezing the systems plates and fuel line fittings in liquid nitrogen at -320 F prior to insertion into gore panels and LH_2 cylinder sections (Figures 51 and 52). This has made it possible to retain contour and has considerably reduced distortion, buckling, and warping.

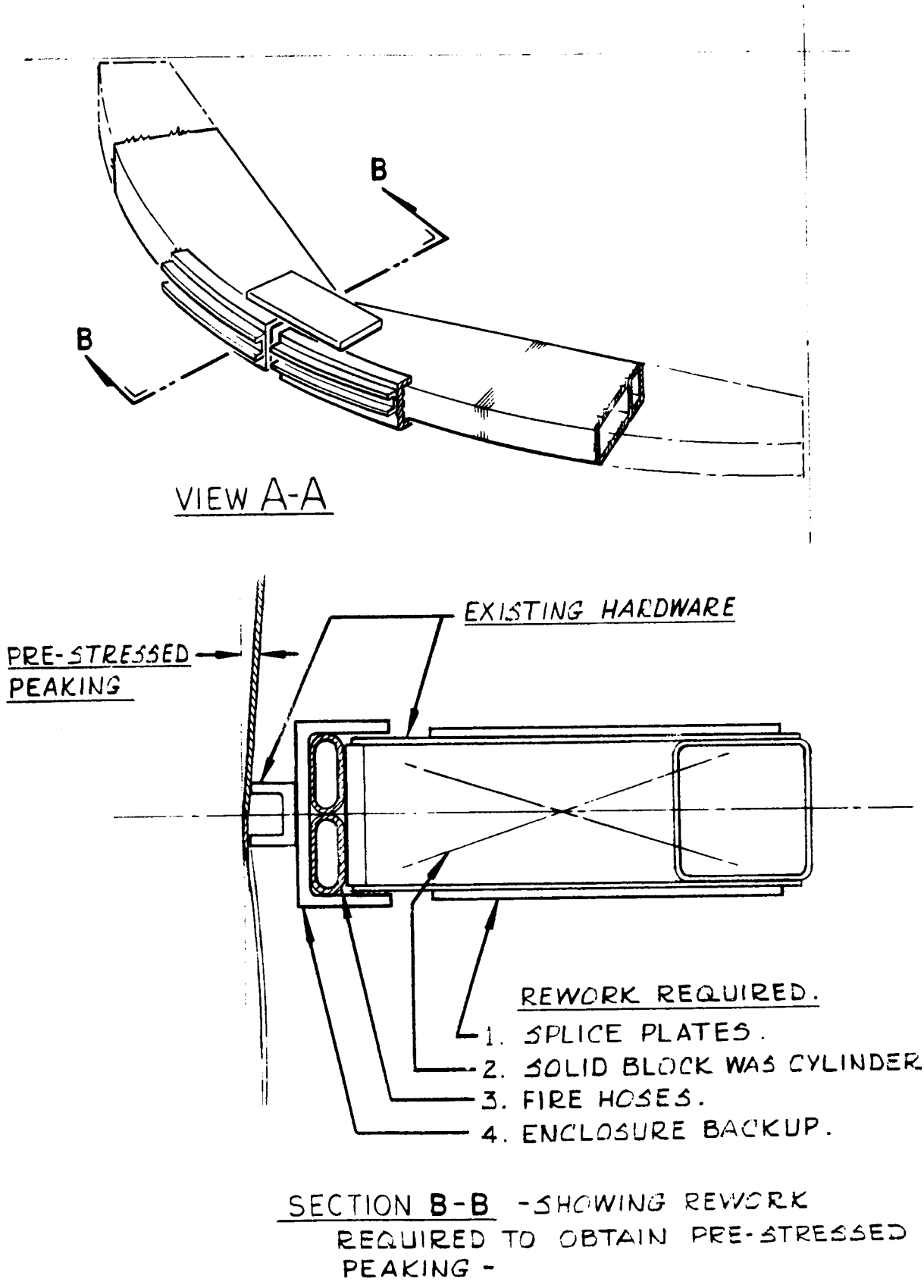

Figure 49. Pre-Strain Welding Design Concepts for S-II Production

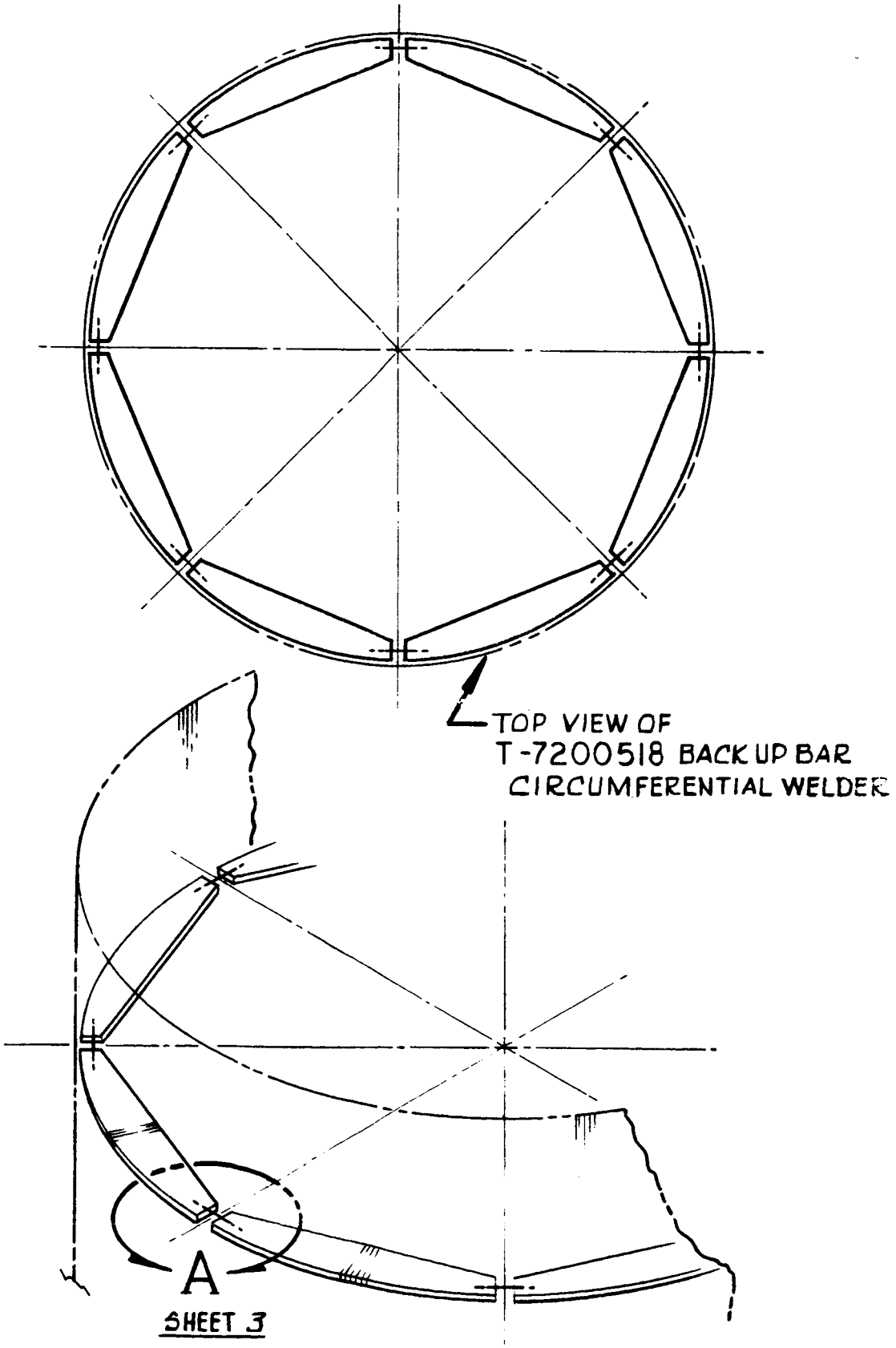

Figure 50. Application of Pre-Strain Welding Concept to S-II Production

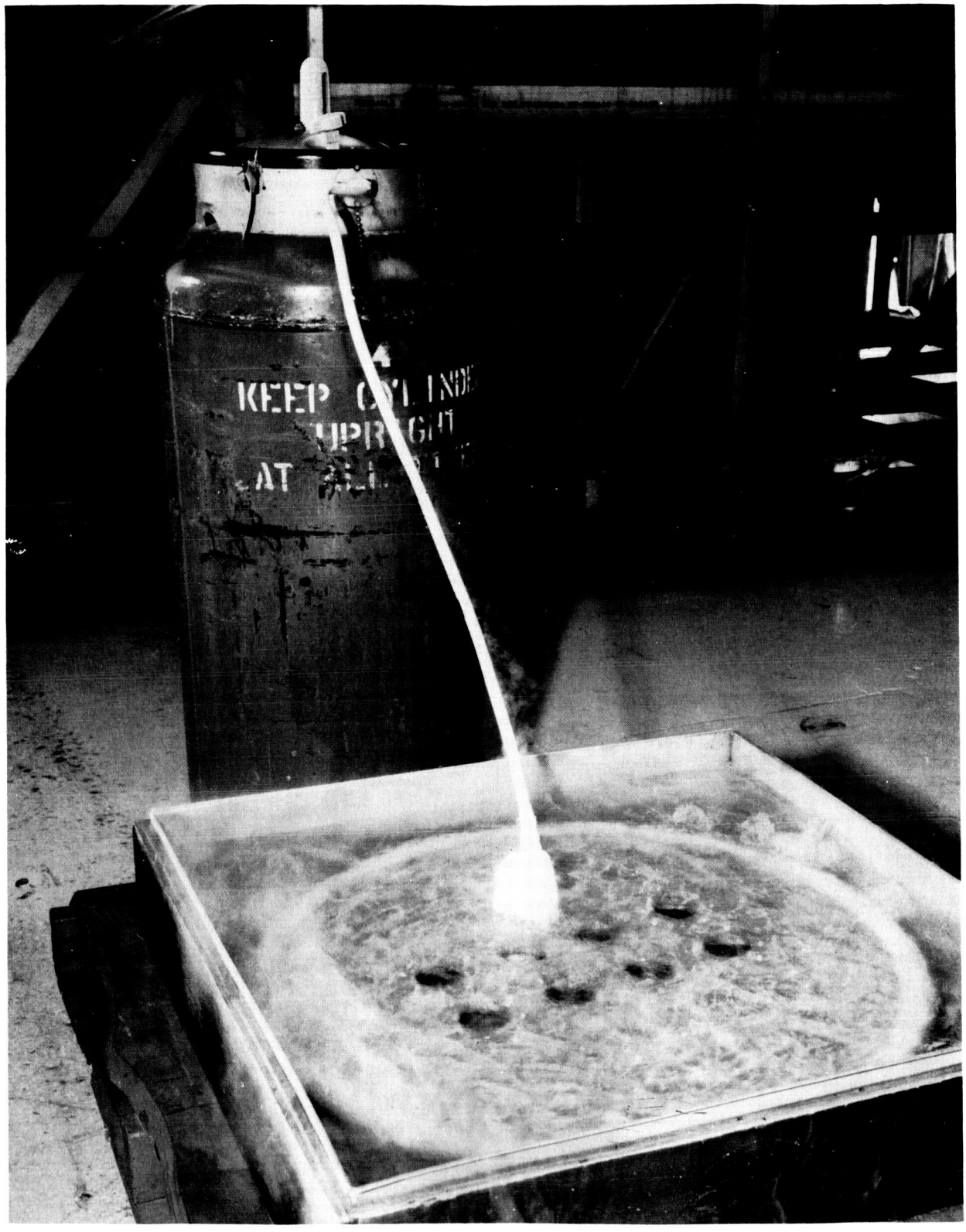

Figure 51. Production System Plate Being Chilled Prior to Insertion in Gore Panel

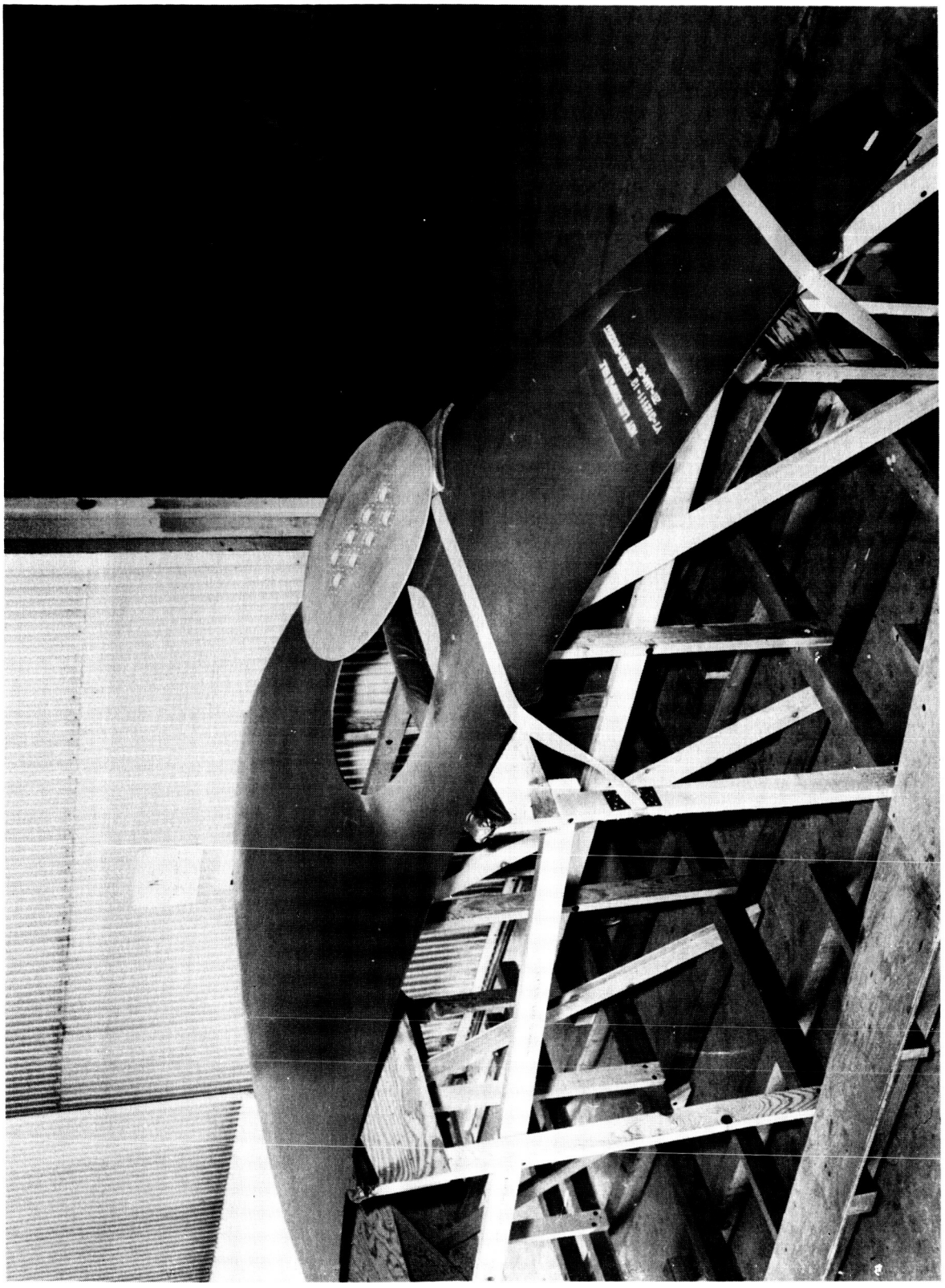

Figure 52. Production Gore Panel and System Plate

CONCLUSIONS AND RECOMMENDATIONS

The experimental program definitely supports the supposition that properly controlled pre-load application during fusion welding of aluminum alloy parts by mechanical or thermally induced shrink-fit means —the choice depending on suitability with respect to part geometry —will result in beneficial effects from the standpoint of reduced residual stress and/or distortion.

The mechanics analysis showed that the unit cube/parallel strip model chosen reasonably represents the thermophysical phenomena causing weld shrinkage. It also predicts the beneficial effect of pre-strain application to weldments and shows promise of becoming a useful tool for quantizing magnitude and pattern of pre-strain application. Its use in the latter case can result in a best compromise between desired benefits and maximum reduction of all residual stress components causing distortion.

The following additional work is recommended in order to provide a more substantial body of experimental facts in the range of pre-strain levels of main interest, and of weldment gages in which thermal gradients through the thickness of the material is appreciable enough to require consideration.

Recommended future work includes the following:

1. Refinement of the analytical method of taking into account effects of temperature gradients through the weldment thickness and use of more accurate valves for elastic modules reflecting dependence on stress and strain levels as well as temperature.
2. Rephrasing of mathematical expressions to adapt them to computer programming.
3. Performance of additional weld experiments on mechanically pre-loaded linear panels under conditions permitting application of higher pre-load levels in the relatively uniformly pre-loaded central portion of the specimen, thus isolating pre-load level from possible geometry effects and permitting more definitive conclusions as to optimum pre-load conditions.
4. Verification of mechanics analysis by comparison of analytical predictions with experimental results on additional mechanically preloaded linear weldments of different gages.
5. Inclusion of an investigation of angular pre-positioning of weldment details in future weld experiments.

REFERENCES

1. Phillips, W.J., Preweld Shrinkage Development Program, Saturn S-II Project. NAA, NA 64-1231 (23 Nov. 1964)

2. Metallic Materials and Elements for Flight Vehicle Structures. MIL-HDBK-5

3. Cryogenic Materials Data Handbook. ML-TDR-64-280 (Aug. 1964)

4. Air Weapons Materials Application Handbook, Metals and Alloys (Dec. 1959)

5. Thermophysical Properties of Solid Materials. WADC-TR 58-476, Vol. II - Alloys (Nov. 1960)

6. S&ID Structures Manual. NAA S&ID, 543-G-11

7. Material Properties Handbook. NAA LAD

8. Gottlieb, T., Thermal Expansion and Contraction of Various Materials. NAA Rocketdyne, R-3462 (31 Mar. 1962)

9. Perry, S., Coefficients of Thermal Expansion for Aircraft Alloys Over a Range of -100 F to 212 F. NAA LAD, CR-217 (11 July 1947)

10. Communication, T.S. Touloukian, Director of Thermophysical Properties Research Laboratory, Purdue University, to F.M. Zanella, NAA (22 Dec. 1964)

11. Communication, G.R. Hosner, Aluminum Company of America, to E. Margitan (23 Dec. 1964)

12. Ramsey, P.W., J.J. Aryle, J.N. Kuler, P.S. Myers, M. Weiss, and W. Groth, "Infrared Temperature Sensing Systems for Automatic Fusion Welding." Supplement to the Welding Journal (Aug. 1963)

13. Timoshenko, S., and J.N. Goodier, Theory of Elasticity. McGraw-Hill (1951)

14. Gatewood, B., Thermal Stresses. McGraw-Hill (1957)

15. Hetenyi, M., Beams of Elastic Foundation. University of Michigan Press (1946)

16. Seely, F., and J. Smith, Advanced Mechanics of Material. Wiley (1957)

BIBLIOGRAPHY

Kihara, A., M. Watanabe, K. Masubuchi, and K. Satoh, Researches on Welding Stress and Shrinkage Distortion in Japan. Society of Naval Architects in Japan, 60th Anniversary Series, Vol. 4 (1959)

Lackman, L. M., Relief of Residual Stresses from Fusion Welding. NAA, NA 62-326 (21 Mar. 1962)

Nagaraja Rao, R. N., and Lambert Tall, "Residual Stresses in Welded Parts." Welding Journal, Vol. 40 (1961)

Voorhees, H. R., and J. W. Freeman, "Report on the Elevated-Temperature Properties of Aluminum and Magnesium Alloys." ASTM Special Technical Publication No. 291 (Oct. 1960)